ELUCIDATING BIOLOGICAL MECHANISMS OF HOST RESPONSE TO NITRIC OXIDE-RELEASING GLUCOSE BIOSENSORS

James Bryan Taylor

A dissertation submitted to the faculty at the University of North Carolina at Chapel Hill in partial fulfillment of the requirements for the degree of Doctor of Philosophy in the Department of Chemistry (Analytical Chemistry)

Chapel Hill
2020

Approved by:

Mark H. Schoenfisch

Leslie M. Hicks

Matthew R. Lockett

Shannon M. Wallet

Timothy C. Nichols

ABSTRACT

JAMES BRYAN TAYLOR: Elucidating the Biological Mechanisms of Host Response to Nitric Oxide-Releasing Glucose Biosensors
(Under the direction of Mark H. Schoenfisch)

Despite the utility of continuous glucose monitors (CGM) in improving health outcomes for type I diabetic persons, these implants have a limited duration due to the foreign body response (FBR). Though nitric oxide (NO)-releasing glucose biosensors have been demonstrated to reduce the FBR and extend implant lifetime, the biological mechanisms impacted by NO release to trigger these therapeutic outcomes have not been explored in detail. Herein, NO's effects on phenotype and activity of biological systems were investigated to identify biomarkers and NO's mechanisms of actions.

As macrophages deplete enough local glucose from an implant site to create reductions in sensor accuracy, glucose consumption was analyzed as a function of both NO and inflammatory state. Using 2-NBDG uptake as a measure of glucose consumption, preliminary data demonstrated 500 μM SNAP causing increases in glucose consumption (~10% or ~60% increase in pro- or anti-inflammatory macrophages, respectively) and 5 μM SNAP resulting in a ~50% reduction in glucose consumption for pro-inflammatory macrophages and no change for the anti-inflammatory counterparts.

Using a euglycemic porcine model, mechanisms and biomarkers affected by NO release were evaluated through protein and gene expression analyses on tissue explanted from an NO-releasing implantation site. With NO release, chemokine levels were found to be reduced at 7-days post-implantation and pro-inflammatory mediators were found to be broadly reduced by NO exposure. Genetic analysis supported previously reported decreases

in leukocyte infiltration with NO and discovered variations in the leukocyte composition present at the implantation site.

The activity of matrix metalloproteinases (MMPs) was investigated as a function of both inflammatory state and NO release. Reductions in MMP activity were observed at lower NO doses, showing the potential of NO release to reduce inflammation associated with increased MMP levels. Significant increases were observed in macrophages exposed to 0.02 mg/mL DPTA/NO at endotoxin levels ≥ 2.5 μg/mL. As meaningful differences were not observed at 0.2 mg/mL DPTA/NO or from 0.02-0.2 mg/mL DETA/NO, a slower releasing NO donor, these data imply that there is a narrow therapeutic window for NO reducing MMP activity which merits further investigation.

ACKNOWLEDGEMENTS

The most important thing I want to stress in my PhD is that this was a gargantuan effort that involved so many different people. I was absurdly well supported throughout my PhD and though there are more people than I can name in this short section, I want it to be known that I am deeply grateful to everyone who has helped me make it to this point.

First, I would like to thank my parents, James and Aminata, who emigrated here from Sierra Leone, at one point the poorest country in the world, and have built so much in a foreign country, starting from scratch. Surely, you both did it without expecting to one day watch their son obtain a terminal degree, or maybe you were far more prescient than you let on. To you both I say: you did good. And I have so much family that these thanks extend to. So many aunts and uncles and friends whom all believed in me. A special thank you goes to my siblings. To Doris, Kevin, and mom's favorite, Nolan, thank you all for your steadfast support. Doris, it is no doubt rare to have a sibling going through a parallel experience, with you also trying to close your PhD and it has been priceless to be able to commiserate with a sibling trudging through the same ordeal. I am in awe of the scientist you were able to become, and boy am I proud. I would also like to give never-ending thanks to John Chavis III, Kwadwo Owusu-Boaitey, and Megha Kori for being such amazing friends from afar. Though there are several thousand miles between us, you three have been stellar support, personally and professionally, and I definitely would not have been able to finish this endeavor without you three dragging me through it. You guys among my strongest blessings.

My UNC journey started in the Soper lab and to them, I owe so much thanks. Thank you to Drs. Soper, Witek, Hupert, and Jackson for all your support during that initial project and for creating a lab environment where I was able to acclimate to grad school. I also want

to thank my lifelong friends and labmates, Kristina Herrera, Dr. Nicole Smiddy, Dr. Mike Schotzinger, and our labmom, Dr. Colleen O'Neil. Though we worked together only briefly, meeting you four was easily the best thing to come out of working in our lonely spire by the hospital. You all are some of the truest friends I have ever known.

Since leaving the Soper lab, I have been blessed to finish my PhD in the Schoenfisch lab. To Mark – I cannot ever thank you enough for all your patience and support. For me to sit in your office on two separate occasions and tell you that I'm quitting, and for you to have never thought less of me in doing so while continuing to support me is a true testament to you and your character. I am even still here, much less finishing this degree. I was initially going to join your lab but passed to explore the novelty of microfluidics. But sometimes life throws a curveball and you end up back where you ran from. Though it has been rocky at times, I am ultimately glad I got to end up back in your lab. And to all my amazing labmates, I am consistently in awe of you all and your ability. That I feel like I have always been the dumbest graduate student is saying more about you all. Especially because I joined the lab during an abrupt lab transition, I want to thank every single lab member I interacted with because you had never once made me feel like the stepchild I was. Special thanks to Drs. Robert Soto, Dakota Suchyta, and Micah Brown for helping get established when I showed up that January. A special heartfelt thanks to Micah, for he not only recruited me to UNC but has played double duty as a mentor and confidant. And to the rest of my labmates, it was my honor to share the stage with you all. Special thanks go to labmom and labdad, Sara Maloney and Jackson Hall (truly, thank you for all you did for us), the always fun to talk to friends: Dr. Lei Yang, Dr. Kaitlyn Rouillard, and Dr. Evan Feura, a frequent collaborator in Dr. Maggie Malone-Povolny, and a special thanks to Brian Tran. You may not know it, but working with you has definitely made me a better scientist. Believe in yourself and you'll be just fine. And finally, I was graced with a fantastic undergraduate researcher in Chenyang Wang and I have never met such a hardworking man in my life. I am fully confident you will go as far as you want to in this life.

I would also like to thank my many collaborators. Drs. Robert Maile and Shannon Wallet, thank you so much for all your help closing my PhD. It may not have been possible without you both. I would also like to thank Dr. Kelsey Miller for being a frequent co-commiserator and partner-in-crime. And also, thanks for linking me with my job at Nikon; very serendipitous but I truly couldn't have done it without you! Thanks for taking a chance on my crazy macrophage lipidomics excursion and I'm glad we got to bond because of it. And thanks for getting Thank you to all the people who have supported me at UNC, including Dr. Andreas Wierschen, Donnyell Batts, Dr. Susanna Harris, Jill Fallin, Kathy Wood, Ampson Hagan, Don Holmes, Rufai Ibrahim, Anginelle Alabanza, Dean Steve Matson, the staff of the Chancellor's Science Students who took me in like I was one of their own, Drs. Richard Watson, Noelle Romero, and Thomas Freeman. A heartfelt thanks to the Meyerhoff Scholars Program, and especially Mr. Keith Harmon. Without you all, I would never have even made it to the gate, much less the finish line. Thank you to the Morehead Planetarium and the NC Science Festival for providing an outlet for me in science outreach. Thank you especially to Tamara Poles for believing in me and for letting me be a part of so many cool initiatives and thank you to the Museum of Life and Science and my work supervisor, Tomara Gee, for all the fun I had working there Summer 2018. Thank you to the Triangle Comedy community for being a constant source of growth and support, with a special thank you to Dr. Andrew Aghapour, Dr. Tara Regan, Bryce Bowden, Joshua "Rowdy" Rowsey, Holly Schmidt, Dan DeSalva, and Wil Heflin. And one final shoutout to Mike and Ethel and Aidan's Pizza, by far the best pizza in the Triangle.

Though I've listed so many people here, there are indeed so many people who have helped me get to this point and who are not named here nor are coauthors on any of my work. Nevertheless, I can't give them enough thanks. And I'd also love to commemorate all the people I have lost and grieved over the course of my graduate school career. I hope I have made you all proud.

Finally, I'd like to give the most heartfelt thanks to Kate Kastelberg. Thank you so much for always believing in me. I am so grateful for your support through all my whining and I'm so excited for the future. Love you.

'If yu nɔ no usay yu de go, no usay yu kɔmɔt' –

If you don't know where you are going, know where you came from

TABLE OF CONTENTS

LIST OF TABLES

LIST OF FIGURES

CHAPTER 1 – HOST RESPONSE OF NITRIC OXIDE-RELEASING GLUCOSE MONITORS

1.1 Continuous Glucose Monitors in Diabetes Management

Diabetes mellitus is a family of diseases characterized by physiological resistance to or deficient production of insulin.[1,2] Insulin is a key steroid secreted by the pancreas and insulin resistance, any diminishment in insulin's effect, leads to decreased blood glucose regulation. In humans, blood glucose is maintained in a narrow range of 80-120 mg/dL (4.4 – 6.6 mM), providing the glucose required to drive the body's metabolic processes without incurring the adverse effects of increased glucose levels, including atherosclerosis.[2] Without blood glucose regulation, various adverse health outcomes may occur, including loss of eyesight, chronic wounds, ketoacidosis, and even death.[3,4] There is a specific need concerning Type I diabetes, a congenital disease where the pancreas produces atypically low amounts of insulin. Inadequate levels of insulin result in hyper- and hypoglycemic swings (extreme high or low levels of blood glucose, respectively), both of which can lead to the adverse health outcomes and morbidity. To control these swings in blood glucose, type I diabetic persons regularly monitor their blood glucose and inject of exogenously produced insulin.

For the management of type I diabetes, blood glucose is most commonly monitored via a finger-prick blood glucometer, an instrument that uses a lance to withdraw ≤ 1 μL of blood and determines a blood glucose concentration through electrochemical quantification.[5] Glucose management, with the finger-prick glucometer and corresponding treatment with insulin, has led to demonstrable improvements in diabetes survivability and health outcomes. However, these measurements are limited by the discrete nature of sampling. Because finger-

prick measurements require frequent and conscious action, they are prone to discontinuation due to pain or management issues, which in turn facilitates adverse health outcomes.[5,6] Furthermore, glucose readings become impossible to obtain if the individual cannot self-administer the finger-prick, most notably while asleep. Hyper- and hypoglycemic swings can happen rapidly, creating a unique problem when designing technology to assist in diabetes management.

A modern advancement in these technologies is the development of the implantable glucose monitor. In contrast to discrete measurements, continuous glucose monitors (CGMs) are designed to track glucose measurements in real time over extended periods to minimize adverse health outcomes borne from sampling error.[3,7,8] Though there are colorimetric and impedance-based CGMs available, electrochemical glucose detection is most commonly used. In electrochemical CGM, the enzyme glucose oxidase is immobilized onto an electrode surface or sensor. The process involves the oxidation of glucose to gluconolactone and the concomitant reduction of oxygen to hydrogen peroxide. It is the hydrogen peroxide that is electrochemically detectable, resulting in an electrical current that is proportional to the glucose concentration. The sensor is implanted transcutaneously to follow interstitial glucose concentrations that lag levels in blood by only a few minutes. The continuous nature of this measurement allows blood glucose tracking without requiring user input, producing an alarm alerting the patient to both hyper- and hypoglycemic swings. Electrochemistry-based CGMs are available by prescription and have led to significant improvements in health outcomes for type I diabetes patients.[9–15] Physicians have recently recognized the "time in range", or the amount of time spent at a healthy blood glucose level and is uniquely assessable only by CGM, is a more reliable predictor of health outcomes than the current standard, glycosylated hemoglobin levels (HbA1C).[16] Thus, CGM technologies represent a new frontier in medical devices. The diabetes technology community is working towards an implantable and

automated insulin pump that would be able to work in tandem with CGM, creating a closed-loop treatment for a diabetic individual, with minimal input on their end.[15]

1.2 Foreign Body Response

Though CGM holds great promise for diabetes management, it is not without drawbacks. The average sensor lifetime once implanted is perhaps the greatest. The sensor is implanted in the body, which then elicits a series of immune reactions known collectively as the foreign body response (FBR) (Figures 1.1 and 1.2),[17–21] with the sensor serving as a foreign body. Protein adsorption initiates the immune response cascade, both signaling neutrophil infiltration and attenuating the glucose sensor signal through biofouling (i.e., the passivation of the sensor surface). Neutrophils then arrive at the site of insult, primarily phagocytosing debris or pathogens in an attempt to clean the implant site.[22] Three to four days post-implantation, monocytes migrate towards the released proteins and are differentiated into macrophages, one of the most influential cells in the foreign body response.[18,23–25] These macrophages phagocytose like their neutrophil counterparts, but additionally release large levels of reactive oxygen and reactive nitrogen species (ROS and RNS, respectively) to destroy pathogens and the foreign body, leading to phagocytosis attempts on the damaged implant. Frustrated, the macrophages will fuse under their frustrated phagocytosis into polymorphonuclear cells, also known as foreign body giant cells (FBGCs).[24,26] FBGCs release a larger flux of reactive species including superoxide, hydrogen peroxide, and peroxynitrite, all leading to significant implant damage.[27–29] Upon insufficient removal of the foreign body at roughly 7 days, fibroblasts arrive and isolate the implant in a fibrous collagen capsule.

The foreign body response is damaging to the lifetime and function of any implant, but has particularly ramifications for continuous glucose sensors. The most serious is that the collagen capsule impedes glucose transport towards the sensing surface, which in turn confounds glucose measurement by increasing response time, ultimately leading to sensor

lag, loss of sensitivity, and decreases in sensor lifetime.[30,31] Understanding the biology of the inflammatory response and how sensor designs might mitigate the foreign body response are both of prime importance to develop better sensors. The following sections focus on the two major cell types, macrophages and fibroblasts, involved in the FBR as well as sensor design strategies to mitigate the foreign body response. In addition, there is evidence that mechanisms in the foreign body response are also dependent on other immune cells, including T cells[32], mast cells,[33] and dendritic cells,[34,35] although these will not be explored in great detail herein.

1.2.1 Macrophages

Macrophages are a class of leukocyte that play a vital role in the inflammation process. They are derived from monocytes and ultimately differentiate into macrophages upon stimulus from present cytokines. Macrophages have been identified as the primary drivers of inflammation, as cytokines released by the macrophages control the arrival and phenotype of other cells to the implant site, including keratinocytes, fibroblasts, and epithelial cells. Though several types of macrophages exist, including osteoclasts and glial cells, the discussion below will refer broadly to macrophages involved in the healing of dermal tissue.

1.2.2 Macrophage Effects on Implanted Sensors

The FBR is deleterious to sensor function in many ways. Though macrophages are important to the regulation and progression of the whole process, they can be detrimental to the function of an implanted device and need to be accounted for when designing longer-lasting, durable sensors. Of note, macrophages notably have a large native glucose consumption relative to other cells at the site of insult.[30,36–38] For example, Novak et al. employed a two-compartment diffusion model to simulate the glucose consumption of the various cells present at the implant site. They reported that macrophages consume a

disproportionate amount of glucose over time, eclipsing the consumption of other cell types.[30] This glucose depletion was also observed by Klueh et al. in an in vivo CGM model in which macrophages were injected into the implant site. Upon injection, a nearly immediate decrease in current was observed, in contrast to injected lymphocytes, which did not produce an observable change in current.[36]

1.2.3 Macrophage Polarization and Plasticity

Macrophages change their phenotypes in response to their microenvironment; this phenomenon is known as macrophage polarization or activation.[25,39,40] In the original theory, polarization states were used to distinguish pro-inflammatory from anti-inflammatory macrophages with binary modality.[41–43] Current research suggests that macrophage polarization is more spectral in nature. However, this dissertation will refer to activated macrophages as broadly pro- or anti-inflammatory unless otherwise noted.

Pro-inflammatory macrophages, also known as M1 or classically-activated macrophages, are the macrophages associated with pathogen and debris clearance. Removal of debris is mediated by the release of ROS and RNS species that are biocidal to pathogens and can damage larger foreign bodies. These reactive species include hydrogen peroxide (H_2O_2), superoxide ($O^{2-\cdot}$), and nitric oxide (NO), each recognized for their biocidal action. This phenotype can be induced via several cytogenic markers including interferon-gamma (IFNy), tumor necrosis factor (TNFa), and interleukin 6 (IL-6), which are released from cells, notably T-helper cells, to create an inflammatory environment. Additionally, macrophages can be induced to M1 phenotypes by pathogenic markers shed from bacteria, most notably lipopolysaccharides (LPS) shed from bacterial cell walls.

Anti-inflammatory macrophages, also known as M2 or alternatively-activated macrophages, are associated more closely to wound healing and cell signaling with 3 broad subtypes (M2a, M2b, and M2c).[44] For simplicity, this dissertation will refer to all anti-

inflammatory macrophages as being in the M2 phenotype. Broadly speaking, polarization can produce anti-inflammatory macrophages through cytokines, including interleukin 4 (IL-4) and interleukin 13 (IL-13). Anti-inflammatory supplements and drugs can also promote M2 character in macrophages. For example, the soybean extract genistein has been linked to anti-inflammatory character. It has been observed to reduce GLUT1 expression in macrophages, resulting in decreased glucose consumption.[45]

Of importance, not all macrophages are equally polarized. The nature of the stimulant plays a vital factor in their polarization. For example, macrophages stimulated solely with LPS differ in activity from those with stimulated with a combination of IFNy and LPS, even though they are both pro-inflammatory in nature. Murray et al. proposed a new identification scheme for polarized macrophages that account for this discrepancy whereby macrophages are represented by M(X), where X is the stimulant in question (e.g. M(LPS), M(IL-4), M(IFNy + LPS)), as an alternative to designating macrophages as M1 or M2.[46]

Others have theorized that M1 macrophages inhabit a wound site during the early acute phases of inflammation and then shift to an M2 phenotype during proper wound healing, implying that the ratio of M1 and M2 macrophages serves as an additional marker of wound healing progression, known as the M2:M1 ratio.[47–50] Badylak et al. implanted rats with either porcine small intestinal submucosa (SIS) or porcine submucosa subjected to carbodiimide crosslinking (CDI-SIS) to elicit an exaggerated inflammatory response.[50] Over the 16 week implantation, histology and immunohistochemistry were used to monitor the quality of the wound healing. The SIS model featured more favorable wound healing and a higher ratio of M2:M1 cells at every interrogated timepoint, compared to the CDI-SIS model, which had greater counts of M1 cells to M2 cells at every time point.[50] This study is one of several supporting the theory that the M2:M1 ratio is an important predictor of proper wound healing. When additionally considering that macrophage phenotypes are plastic and

modulated by changes in the microenvironment,[40,51,52] macrophage phenotyping and the M2:M1 ratio remain important and especially dynamic markers for wound healing status.

Of particular importance to implantable glucose sensors, the glucose consumption of macrophages has been linked to their polarization state. Pro-inflammatory macrophages consume greater levels of glucose to drive the release of reactive species. For example, the over-expression of the GLUT1 glucose transporter was observed with the addition of pro-inflammatory stimuli, compared to wild-type macrophages.[53–55] For the anti-inflammatory counterpart, preliminary evidence suggests higher rates of fatty acid oxidation drive the metabolic processes of anti-inflammatory macrophages instead of increased glucose consumption.[53,56]

To explore the role of polarization on glucose consumption, Novak et al. expanded on their previously published glucose transport model and devised a macrophage-embedded fibrin gel model, in which a CGM was inserted to simulate an implanted continuous glucose monitor.[57] They were able to use this model to interrogate a Medtronic CGM with unstimulated macrophages as a control and macrophages stimulated with 1 ug/mL LPS or 50 nM phorbol myristate acetate (PMA) to induce an M1 phenotype, or 100 μM Genistein, a soybean extract shown to have some anti-inflammatory character. Using the raw glucose consumption data from the sensor and extracted kinetic information, both M(PMA) and M(LPS) cells consumed more glucose and at larger rates, while M(Genistein) cells consumed less glucose at lower rates, all compared to unstimulated macrophages. As macrophages consume the most glucose of all the cells at the sensing site, controlling their polarization state to reduce confounding glucose consumption and may represent an ideal strategy for extending sensor lifetimes.

1.2.4 Fibroblasts

Another key class of cells in the foreign body response are the fibroblasts which orchestrate the collagen capsule that isolates the foreign body. Derived from the mesoderm, fibroblasts arrive to a wound site as proto-myofibroblasts to create cell contacts with the extracellular matrix (ECM). The proto-myofibroblasts subsequently differentiate into myofibroblasts that are responsible for the majority of collagen deposition at the site of insult. As the wound closes, anti-inflammatory mediators decrease in concentration with the resolution of inflammation, leading to apoptosis of the myofibroblasts and a ceasing of ECM deposition. With abnormal healing such as the FBR, chronic inflammation begets perpetual collagen deposition, leading to the formation of the collagenous capsule associated with sensor implantation. This layer is particularly deleterious for glucose sensors because it impedes glucose diffusion to the surface of the sensor and distorts sensor response.[31]

Along with wound reconstruction, fibroblasts are involved in inflammatory regulation by releasing inflammatory mediators such as TGFB1, GM-CSF, and PGE_2.[22,58,59] Much of this regulation occurs via both cross-talk with macrophages, which has been replicated both paracrine (i.e., indirect co-culture) and juxtacrine (i.e., direct co-culture) systems in vitro.[58,60,61] Cross-talk has also been observed between fibroblasts and mixed M1 and M2 macrophage populations within in the collagen capsule. Much like macrophages, fibroblasts are also inducible by similar inflammatory stressors. The inflammatory state of fibroblasts may be quantified by analysis of common inflammatory biomarkers similar to macrophages. One novel method of quantifying inflammation in fibroblasts is through their production of matrix metalloproteinases (MMPs).[60,62] MMPs are responsible both for degradation of ECM components and the regulation of various proteins like cytokines, chemokines, and MMPs themselves. Understanding how MMPs are affected by fibroblast inflammation provides more detailed insight into the immunomodulated pathways. This method of analysis has been explored using paracrine factors from M1 and M2 macrophages to examine fibroblast MMP

production. Ploeger et al. found that M1 paracrine factors result in higher MMP concentrations, and that the subsequent replacement with M2 factors in fact reversed some of the increases in MMP concentration, implying plasticity in the fibroblasts.[60] Bozkurt et al. later explored MMP concentration in gingival fibroblasts as a function of LPS concentration and also reported increasing concentrations of MMP-1, -2, and -3 with increasing inflammatory stress.[62] In addition, they noted that the increased MMP production correlated with a three- and five-fold increase in expression of IL-8 and IL-6, respectively.[62] Given the many roles fibroblasts play in inflammation, wound healing, and specifically the FBR, understanding the inflammation in fibroblasts is vital to advancing research into FBR mitigation.

1.2.5 Sensor Designs for Mitigating the Foreign Body Response

A number of strategies have emerged to maintain long-term sensor performance by mitigating the foreign body response. Active FBR-mitigation strategies involve the active release of pro-wound healing mediators (e.g., pro-angiogenic factors, anti-inflammatory agents) from the surface of the sensor that lessens the body's immune response at the implant site. In contrast, passive FBR-mitigation strategies involve manipulating the surface and topography of the sensor to control the phenotypes of cells adhered to the sensor surface to facilitate tissue reintegration.[63,64]

The above strategies rely on altering the phenotype and behavior of the infiltrating cells. Pores, micropatterning, and matting each affect wound healing progression by altering cell attachment to the implant.[63–65] Multiple studies appear to converge on ~35 μm pore sizes prompting a reconstructive macrophage phenotype and a lessened FBR.[63] Of note, this texturing appears to subtly alter the FBR rather than causing changes. For example, Singh et al. grew primary monocyte-derived human macrophages on microtextured surfaces (i.e., microgrooves or micropillars) to assess their influence on polarization. While the surface

texture did not result in notable differences in concentrations of various inflammatory biomarkers (i.e., IL-1β, IL-1RA, IL-12, CCL18, TNFα), differences in phagocytotic rates, transcription, translation, and in cell morphology were noted.[66] Wang et al. also reported that nanotexturing significantly impedes macrophage fusion, showing the promise of nanotexturing for lessening foreign body reactions.[67]

A number of chemical agents have been released from implants to induce anti-inflammatory effects. For example, dexamethasone, a corticosteroid, has been used to promote more favorable wound healing and a higher proportion of M2 macrophages.[68–73] Ward et al. developed an implantable glucose sensor featuring dexamethasone release using a low pressure osmotic pump.[74] These implants resulted in positive histological outcomes for wound healing when compared to controls. The release of dexamethasone in this manner was such that immune suppression was avoided upon accumulation in the implant pocket. Given that dexamethasone also suppresses angiogenesis, concurrent exposure to dexamethasone and an angiogenic agent (e.g., VEGF, TGFB) were also of interest.[75,76] However, the challenges of a dual release system currently preclude their usage for in vivo sensor systems.

1.3 Nitric Oxide

1.3.1. Nitric Oxide and Endogenous Activity

The use of nitric oxide in an active release strategy has shown promise for continuous glucose monitors.[77–79] Nitric oxide (NO) is a diatomic gas molecule that serves several biological roles including intercellular communication, neurotransmission, and both antibacterial and tumoricidal action. Most relevant to this dissertation, however, are NO's roles in angiogenesis, inflammation, and vasodilation. Importantly, these three physiological pathways are important to wound regulation and will be discussed herein.

Through the transformation of L-arginine, NO is produced endogenously (in the body) via one of three enzymes: the nitric oxide synthases (NOS). Two NOS enzymes are

constitutively expressed and continually produce nitric oxide (nNOS/NOS1, the neuronal nitric oxide synthase; and, eNOS/NOS3, the endothelial nitric oxide synthase). The third NOS enzyme, iNOS/NOS2, the inducible nitric oxide synthase, is expressed only in response to an inflammatory event. Of the NOS species, NOS2 is notable because it produces a much greater concentration of NO, in the nM-μM range, compared to a pM-nM range for NOS3. Additionally, it is most commonly expressed in pro-inflammatory macrophages which are released as part of their respiratory burst and meant to degrade local foreign bodies and pathogens.[18,80] Evolved NO can modify existing proteins in the environment through nitrosation, modifying free thiols on cysteine residues into RSNO moieties, creating S-nitrosothiols that spontaneously release NO with heat, light, Cu^{2+}, or via reduction by a free thiol. In this respect, the nitrosation acts as a form of post-translational modification and may alter protein activity, including enzyme kinetics and signal transduction, showing NO's influence in physiology.[81,82]

1.3.2. Exogenous Nitric Oxide Delivery

The simplest way to deliver NO exogenously is via a gas cylinder. Gaseous NO has been used in healthcare settings, such as in antipathogenic treatment in the lungs of cystic fibrosis patients.[83,84] However, this form of delivery necessitates a gas cylinder that precludes localized release (i.e., from the surface of an implanted sensor).[85] To circumvent this limitation, NO may be derived chemically using an NO donor. The two most promising NO donors for in situ applications include S-Nitrosothiols (RSNOs) and N-diazeniumdiolates (NONOates). The NONOates are formed by reacting secondary amines with high pressures of NO gas in basic conditions, creating a structure that releases two molar equivalents of NO via hydrolysis. Conversely, RSNOs are formed by the nitrosation of thiol groups. Nitric oxide is released upon cleavage of the S-N bond in the presence of heat, light, Cu^{2+}, or through a thiol-thiol linkage. The use of NO donors importantly grants tunable control over the NO-release flux. As NO is

released from both S-nitrosothiols and N-diazeniumdiolates via decomposition, altering the structure and stability of the molecule allows tuning of the kinetics of NO release.

Improving on small molecule NO donors, macromolecular scaffolds have been created and modified with NONOates or RSNOs to store and release NO. Macromolecular scaffolds improve NO release by allowing greater NO storage and more complexity in tuning release kinetics while retaining tunability of release. Examples include silica nanoparticles,[86–88] hyperbranched polymers,[89] and chemically modified biopolymers (e.g., polysaccharides).[90,91] The usage of biopolymers, in particular, allows for a biocompatible platform that can be readily degraded by the body (e.g. amylases degrading NO-releasing polysaccharides), preventing bioaccumulation and deleterious effects.

These NO-releasing molecules may then be decorated on implants through physical entrapment in polymer matrices. Kinetics of the nitric oxide release is modulated through parameters of the polymer including its hydrophobicity, thickness, and how much of the NO-releasing material it contains.[92,93] Choice of the polymer matrix may also improve biocompatibility or affect the leaching of entrapped macromolecules.[63,64,94,95]

1.3.3. Nitric Oxide in Wound Healing & Inflammation

Endogenous NO release is facilitated most commonly through NOS enzymes. Using inflammatory stimuli (e.g., LPS, IFNγ) results in iNOS expression, producing large fluxes of NO. An endogenous release may also be modulated through knockout experiments or the use of either NOS inhibitors or NO scavengers. In contrast, exogenous NO may be introduced within polymers using NO donors or from a gas cylinder. Either of these two strategies may enable the examination of the role of NO in a biological setting. For the scope of this dissertation, a brief look at NO's role in wound healing follows. In particular, both endogenous and exogenous NO release have been linked to altering the host angiogenic response, collagen deposition, and chemokinesis of various cell types.

The first observed endogenous effect of NO involved its discovery as the endothelium-derived relaxing factor, for which it was recognized as molecule of the year in 1992 and subsequently led to the 1998 Nobel Prize in physiology.[96,97] Since then, NO's role in angiogenesis has been the subject of many studies, most of which its positive feedback of other angiogenic factors, such as VEGF and TGFβ.[98,99] Another important pathway involves the regulation of cGMP, a known regulator of vasodilation.[100] Given that NO's most common target, soluble guanylyl cyclase (sGC), is a key intermediary in the cGMP cycle, NO has been observed to activate sGC, resulting in increased cGMP activity and increased angiogenic response.[101,102] The angiogenic response is modulated by angiostatin, an endogenously-produced inhibitor. Matsunaga et al. investigated the link between angiostatin production and NO formation.[103] Through testing with the NOS inhibitor L-NAME, they discovered a negative correlation between iNOS activity and the concentrations of angiostatin and the two MMPs responsible for angiostatin production, MMP-2 and MMP-9.[103]

Similarly, NO has also been found to inhibit wound collagen synthesis. Park et al. induced inflammation with turpentine in a wounded rat model and controlled NO release with an iNOS inhibitor.[104] By quantifying the production of hydroxyproline, an amino acid found primarily in collagen, it was observed that the inhibition of iNOS led to an increase in hydroxyproline concentration under inflammatory stress. Shukla et al. also observed increased collagen deposition in a wounded rat model when inhibiting iNOS, as observed by hydroxyproline concentration and histology.[105] They additionally probed the effect of increased NO concentrations, using either the NO donor sodium nitroprusside or a bolus of L-arginine to induce endogenous NO production. [105] Decreased collagen formation was observed, supporting a negative correlation between NO release and collagen deposition.[105] Both of these studies corroborate observations reported by Cao et al., who observed increased NO concentrations leading to lower hydroxyproline in a chondrocyte model but with both proline and methionine incorporation suggesting that the protein translation rate is

independent of NO.[106] This led to the hypothesis of a possible post-translational modification of hydroxyproline by NO as a cause for the observed collagen decreases in both histological and hydroxyproline-based investigations.

Given NO's roles in intercellular communication, work has been carried out to investigate NO's influence on proliferation and movement.[107–109] Generally, low concentrations of NO have been linked to cell proliferation and high doses to decreased cell density, apoptosis, cell toxicity. This behavior mirrors the low NO doses associated with anti-inflammatory action and eNOS as well as the high doses associated with increased inflammation and NO production by iNOS. Given the diversity of cells in a wound bed, a cell can have many responses as a result of NO exposure. For example, fibroblasts and T-cells are observed with reduced proliferation in response to NO whereas keratinocytes have been reported to proliferate with NO.[108,110] Importantly, NO promotes endothelial cell proliferation, linking NO's angiogenic response to its active recruitment of endothelial and smooth muscle tissue.[98,99,107] The expression of chemokines is also affected by NO. As chemokines directly influence cell homing towards a possible wound bed, this implicates NO in cell migration. The chemokine IL-8/CXCL8 in particular, mainly associated with neutrophil recruitment, has both been linked to the progression of inflammation and upregulated by NO. In one such study, Villarete and Remick examined the IL-8 production of whole blood exposed to DETA/NO or induced to produce NO through LPS exposure, and found a concomitant increase in IL-8 production.[111] Conversely, the use of L-NAME to inhibit NOS or DMSO to scavenge NO led to a decrease in IL-8 concentration.[111]

Though these studies explore the possible role of NO in wound healing, gaps still exist. Specifically, these studies were carried out in a binary fashion, interrogating with endogenous NO release or the addition of an NO donor, or without NO release, through knockout models or NOS inhibition. These methods of analysis leave unanswered questions regarding the appropriate NO dosage or the optimal NO-release kinetics needed to produce favorable wound

healing outcomes. For example, Seo et al. used either of two NO donors, DETA/NO ($t_{1/2}$ ~ 56 h) and SIN-1 ($t_{1/2}$ ~ 4 h), at the same concentrations to observe differences in the IL-8 production of gastric epithelial cells in response to NO.[112] While the Griess assay determined that the concentration of NO released had been statistically indistinguishable throughout the experiment, DETA/NO was shown to induce IL-8 expression earlier than SIN-1. After 24 h, DETA/NO also induced a two-fold upregulation of IL-8 compared to SIN-1, eluding to the importance of slower NO release for reducing inflammation.[112] This study highlights the need for further inquiries into the effects of NO-release kinetics and dosage on NO-induced immunomodulation.

1.3.4. Nitric Oxide Release in Implantable Technology

To exploit its pro-wound healing capabilities, exogenous NO release has been paired with implantable devices to reduce the FBR and improve device lifetimes.[77–79,113–116] The earliest such study was reported by Gifford et al., in which an implantable glucose sensor was impregnated a low molecular weight NO donor (dibutyldihexamine diazeniumdiolate; DBHD/N_2O_2) to release NO continuously at the sensor-tissue interface during the implantation.[77,117] Using histological analysis, it was discovered that NO led to an anti-inflammatory effect, particularly in the infiltration of inflammatory cells and less necrotic tissue at the site of insult. Three days post-implantation, NO-releasing sensors had fewer reported false negatives and false positives compared to control sensors, as shown by a Clark Grid Error Analysis.[77] However, this period of implantation indicated little about wound healing and sensor performance at timepoints beyond the limit of commercial CGMs.

Gifford's original studies have since been expanded upon. For example, the Schoenfisch lab has changing the composition of the polymer membrane and the NO donor allows for tunable NO release to levels that lessen the FBR, as monitored through the collagen capsule density, inflammatory cell density, and angiogenesis (Figure 1.3).[93,94,113,115] Research

to date supports that NO reduces FBR response and the effect is dependent on the NO-release duration, as demonstrated in Table 1.1. Although NO has been used to improve the biocompatibility of other implants, such as reducing thrombosis at a catheter surface and reducing catheter-associated urinary tract infections,[64,118–121] the rest of this dissertation will be focused on NO's application in glucose sensing.

Nichols et al. investigated NO's effect in an implantable system by using microdialysis in a murine model.[114] A microdialysis device was implanted subcutaneously with a saturated NO solution flowing out of the implant into tissue. Glucose was quantified in the collected dialysate to track how NO affected the developing collagen capsule, and specifically the corresponding glucose diffusion. Nichols et al. reported from 14-28 days, the glucose recovery in the system with NO was higher than that of the blank control. Supporting histology showed reduced leukocyte infiltration with NO release relative to controls.

In 2014, Soto et al. reported on the in vivo analytical performance of NO-releasing sensors versus controls in a swine model,[78] recognized for both similar wound healing properties and blood flow to humans.[122–124] By implanting control and NO-releasing sensors along the back of the swine, both histology and sensor performance data were simultaneously collected and correlated. Sensor performance, as represented by the mean absolute relative deviation (MARD) between measurements, was shown to be lower for NO-releasing sensors but only for as long as the NO release persisted.

With the effect of NO on glucose recovery established, Nichols et al. employed a porcine model in their next investigation to determine the effect of NO-release kinetics and duration on the foreign body response.[115] Implants were coated with polyurethanes impregnated with NO donors and in changing the identity of the NO donor, the FBR was evaluated over 6 weeks of implantation as a function of variable NO-release kinetics and duration. It was observed that NO release resulted in thinner collagen capsules and less inflammatory cell infiltration, compared to controls. Importantly, these pro-wound healing

outcomes were associated with extended NO-release durations, as implant outcomes approached the control FBR response after the exhaustion of the NO source, demonstrating the importance of slow and sustained NO release.[115]

This study was followed up with investigations in a hyperglycemic porcine model, employing streptozotocin to kill the insulin-producing beta cells in the pancreas, impeding insulin production to simulate diabetes physiology.[79,116,125] As wound healing can be impaired by disease state, a more aggressive inflammatory response, and decreased angiogenesis were anticipated and observed. Two independent studies have since supported NO's role in improving sensor analytical biocompatibility in more diabetic porcine tissue for as long as the NO is released, with a current maximum release length of 30 days (Figure 1.4).[79,116]

1.4 Scope of this Dissertation

Nitric oxide is clearly a promising active release agent for improving CGMs; however, current research has several gaps in understanding how NO influences the foreign body response at the cellular level. Specifically, while histology and sensor performance both support NO's anti-inflammatory role, the specific mechanisms by exogenous NO leading to lessened FBR is still largely unexplored. Additionally, an understanding of NO dosage and NO-release kinetics in producing these mechanisms remains vague. Most in vivo studies have focused on the effects of release duration in lessening inflammation. Other studies have employed a total inhibition or knockout of NOS, or a single NO donor, with no consideration given to the NO-release kinetics or NO payloads. Elucidating the markers immunomodulated by NO and related mechanisms at the implant site may enable greater understanding of the optimal NO-release kinetics and dosage for maximum sensor lifetime and performance, and possibly result in more useful and predictive in vitro assays for interrogating the same questions systematically.

My dissertation work presented in the following chapters all address methods to increase our understanding of NO's mechanisms. As macrophages and their relatively strong glucose consumption can confound glucose measurements, Chapter 2 investigates techniques for examining glucose consumption of macrophages as a function of both polarization state and NO. Chapter 4 investigates the effects of NO on macrophages and fibroblasts, the key players responsible for driving the wound healing process. Through the quantification of MMP activity, the relationships between MMP activity, inflammation state, and NO release are explored. Chapter 3 explores the use of genetic and protein analyses for supplementing historical histology data and providing deeper insight into what expression changes exogenous NO produces as a function of diabetes and implant period. Finally, Chapter 5 contains a summary of the dissertation work and suggests new directions for future studies.

1.5 Figures and Tables

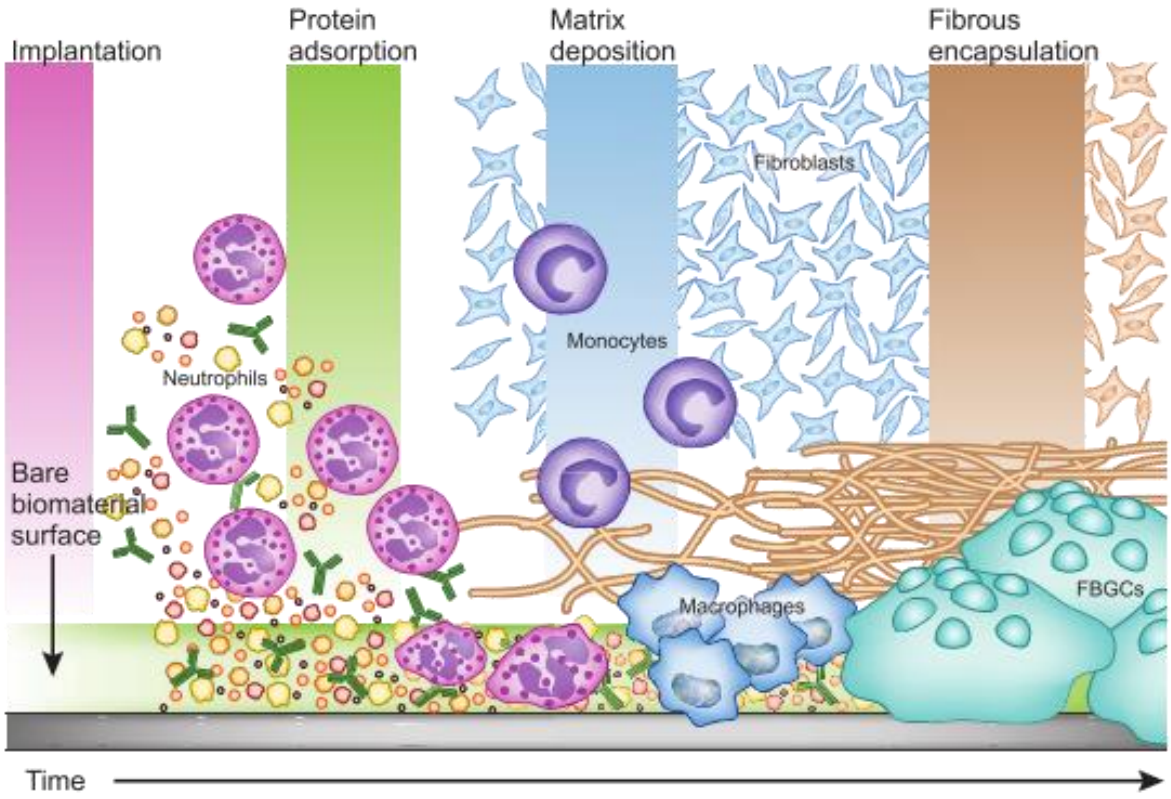

Figure 1.1. The foreign body response, wherein the proteins and cells hone to the surface of the implanted biomaterial over time. Reproduced with permission.[21] Copyright © 2013, Nature Publishing Group, a division of Macmillan Publishers Limited. All Rights Reserved.

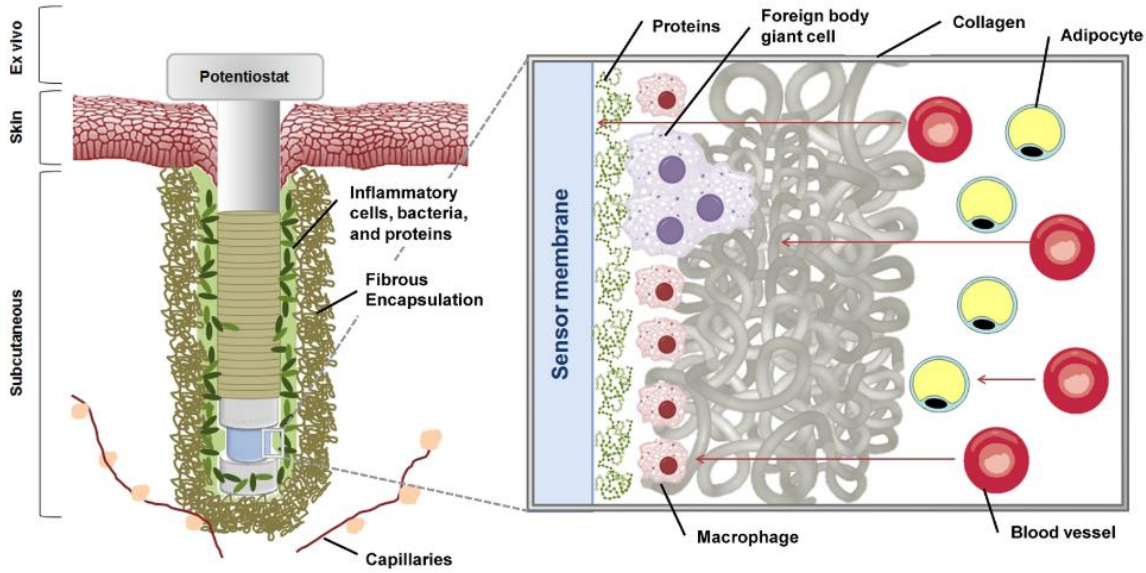

Figure 1.2. The foreign body response results in protein and leukocyte adhesion, and eventual encapsulation in an avascular collagen capsule unto the implant. Reprinted with permission from Nichols, S. P.; Koh, A.; Storm, W. L.; Shin, J. H.; Schoenfisch, M. H. Biocompatible Materials for Continuous Glucose Monitoring Devices. *Chem. Rev.* **2013**, *113* (4), 2528–2549. Copyright 2013 American Chemical Society.[63]

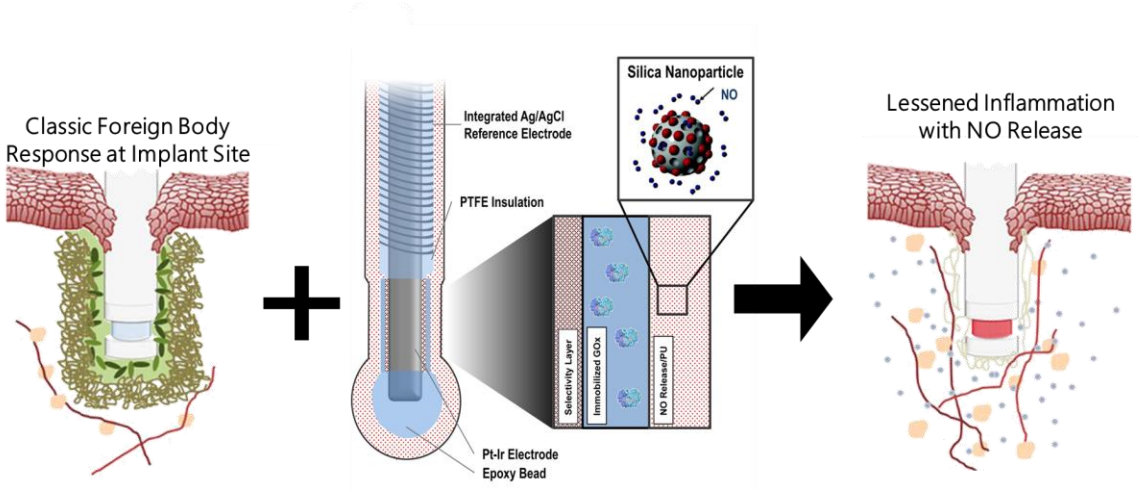

Figure 1.3. The foreign body response brings inflammatory cells to the surface of an implanted glucose sensor and will eventually isolate that implant in a collagen capsule, impeding glucose transport and thus detection. Using a glucose sensor decorated with NO-releasing macromolecules, a lessened foreign body response is observed, with increased vascularization, fewer inflammatory cells at the site of insult, and a thinner collagenous capsule. Adapted with permission from both [1] Soto, R. J.; Hall, J. R.; Brown, M. D.; Taylor, J. B.; Schoenfisch, M. H. In Vivo Chemical Sensors: Role of Biocompatibility on Performance and Utility. *Anal. Chem.* **2017**, *89* (1), 276–299. Copyright 2017 American Chemical Society.;[64] and [2] Nichols, S. P.; Koh, A.; Storm, W. L.; Shin, J. H.; Schoenfisch, M. H. Biocompatible Materials for Continuous Glucose Monitoring Devices. *Chem. Rev.* **2013**, *113* (4), 2528–2549. Copyright 2013 American Chemical Society.[63]

Table 1.1. A summary of in vivo investigations on the effect of NO-release duration on therapeutic outcomes of implanted sensors.

Study	Animal Model	t_d	$[NO]_{max}$ (pmol cm^{2-} s^{-1})	Measurement Times (days)	Analysis Method	Biological Outcomes of NO-Releasing Implants
Gifford et al. (2005)[77]	Euglycemic Rat	12 - 18 h	7.52	1 - 3	Histology & Glucose Monitoring	Improved sensor response and less leukocyte infiltration with NO release.
Nichols et al. (2012)[115]	Euglycemic Pig	6h - 14 d	41.78 - 3128	3, 7, 21, 42	Histology	Longer releasing NO systems promote reduced collagen capsule thicknesses over time.
Soto et al. (2014)[78]	Euglycemic Pig	16.0 and 74.6 h	685.8 and 551.4	0, 1, 3, 7, 10	Glucose Monitoring	Retained sensitivity and reduced sensor lag with extended NO release.
Soto et al. (2018)[116]	Eu- and Hyperglycemic Pigs	48 – 312 h	8.4 - 54.7*	3, 10, 25	Histology	Sustained NO release demonstrated increased angiogenesis and reduced collagen capsules and leukocyte infiltration in both models. 6+ days of NO release required for therapeutic benefits at day 35.
Malone-Povolny et al. (2019)[79]	Hyperglycemic Pig	14 and 28 d	3.36 and 6.28*	14, 28	Histology & Glucose Monitoring	Longer NO release promotes retention of sensor accuracy, less leukocyte infiltration and collagen deposition; 14-day release leads to reversal of therapeutic effects by day 28.

$[NO]_{max}$ – Maximum NO flux obtained
t_d – Reported NO release duration
* denotes $[NO]_{max}$ obtained from the day 1 NO flux

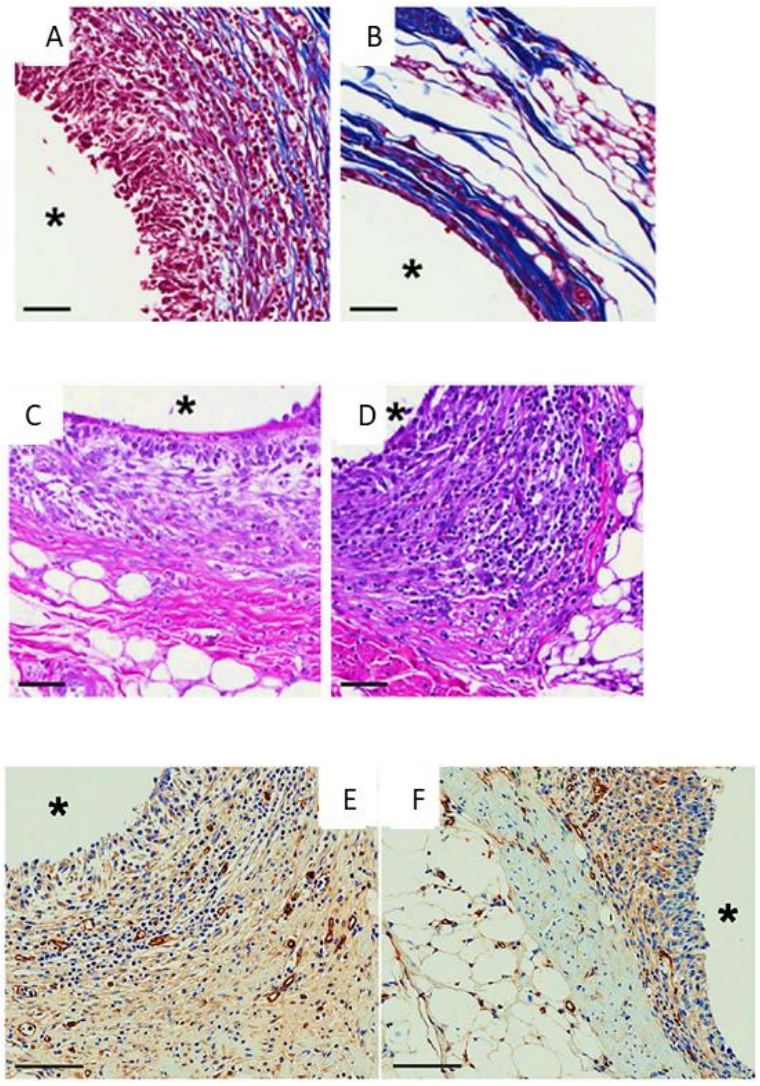

Figure 1.4. Histopathological images from a euglycemic porcine compares tissue response of NO- (A, C, and E) and non-releasing (B, D, and F) implants at 10 days post-implantation using Masson's trichrome to assess collagen capsule density (blue = collagen fibers; A and B), hematoxylin and eosin to quantify inflammatory cell infiltration (purple = inflammatory cell nuclei; C and D), and CD31 immunohistochemical staining to determine angiogenic response (brown open tubes = developing blood vessels; E and F). Asterisk denotes location of implant. Adapted with permission from work published by Soto et al.[116]

REFERENCES

(1) American Diabetes Association. National Diabetes Statistics Report , 2014 Estimates of Diabetes and Its Burden in the Epidemiologic Estimation Methods. *Natl. Diabetes Stat. Rep.* **2014**, 2009–2012.

(2) Association, A. D. Standards of Medical Care in Diabetes--2010. *Diabetes Care* **2010**, *33* (Supplement_1), S11–S61.

(3) Reach, G.; Wilson, G. S. Can Continuous Glucose Monitoring Be Used for the Treatment of Diabetes. *Anal. Chem.* **1992**, *64* (6), 381A-386A.

(4) Kirk, J. K.; Stegner, J. Self-Monitoring of Blood Glucose: Practical Aspects. *J. Diabetes Sci. Technol.* **2010**, *4* (2), 435–439.

(5) Grady, M.; Pineau, M.; Pynes, M. K.; Katz, L. B.; Ginsberg, B. A Clinical Evaluation of Routine Blood Sampling Practices in Patients with Diabetes: Impact on Fingerstick Blood Volume and Pain. *J. Diabetes Sci. Technol.* **2014**, *8* (4), 691–698.

(6) Burge, M. R. Lack of Compliance With Home Blood Glucose Monitoring Predicts Hospitalization in Diabetes. *Diabetes Care* **2001**, *24* (8), 1502–1503.

(7) Clarke, W. L.; Kovatchev, B. Continuous Glucose Sensors: Continuing Questions about Clinical Accuracy. *J. Diabetes Sci. Technol.* **2007**, *1* (5), 669–675.

(8) Bode, B. W.; Gross, T. M.; Thornton, K. R.; Mastrototaro, J. J. Continuous Glucose Monitoring Used to Adjust Diabetes Therapy Improves Glycosylated Hemoglobin: A Pilot Study. *Diabetes Res. Clin. Pract.* **1999**, *46* (3), 183–190.

(9) Farmer, A.; Balman, E.; Gadsby, R.; Moffatt, J.; Cradock, S.; McEwen, L.; Jameson, K. Frequency of Self-Monitoring of Blood Glucose in Patients with Type 2 Diabetes: Association with Hypoglycaemic Events. *Curr. Med. Res. Opin.* **2008**, *24* (11), 3097–3104.

(10) O'Connell, M. A.; Donath, S.; O'Neal, D. N.; Colman, P. G.; Ambler, G. R.; Jones, T. W.; Davis, E. A.; Cameron, F. J. Glycaemic Impact of Patient-Led Use of Sensor-Guided Pump Therapy in Type 1 Diabetes: A Randomised Controlled Trial. *Diabetologia* **2009**, *52* (7), 1250–1257.

(11) Miller, K. M.; Beck, R. W.; Bergenstal, R. M.; Goland, R. S.; Haller, M. J.; McGill, J. B.; Rodriguez, H.; Simmons, J. H.; Hirsch, I. B. Evidence of a Strong Association between Frequency of Self-Monitoringof Blood Glucose and Hemoglobin A1c Levels in T1D Exchange Clinic Registry Participants. *Diabetes Care* **2013**, *36* (7), 2009–2014.

(12) Deiss, D.; Bolinder, J.; Riveline, J. P.; Battelino, T.; Bosi, E.; Tubiana-Rufi, N.; Kerr, D.; Phillip, M. Improved Glycemic Control in Poorly Controlled Patients with Type 1 Diabetes Using Real-Time Continuous Glucose Monitoring. *Diabetes Care* **2006**, *29* (12), 2730–2732.

(13) Beck, R. W. Sustained Benefit of Continuous Glucose Monitoring on A1C, Glucose Profiles, and Hypoglycemia in Adults With Type 1 Diabetes. *Diabetes Care* **2009**, *32* (11), 2047–2049.

(14) Beck, R. W.; Hirsch, I. B.; Laffel, L.; Tamborlane, W. V; Bode, B. W.; Buckingham, B.; Chase, P.; Clemons, R.; Fiallo-Scharer, R.; Fox, L. A.; Gilliam, L. K.; Huang, E. S.; Kollman, C.; Kowalski, A. J.; Lawrence, J. M.; Lee, J.; Mauras, N.; O'Grady, M.; Ruedy, K. J.; Tansey, M.; Tsalikian, E.; Weinzimer, S. A.; Wilson, D. M.; Wolpert, H.; Wysocki, T.; Xing, D. The Effect of Continuous Glucose Monitoring in Well-Controlled Type 1 Diabetes. *Diabetes Care* **2009**, *32* (8), 1378–1383.

(15) Peters, A. L.; Ahmann, A. J.; Battelino, T.; Evert, A.; Hirsch, I. B.; Murad, M. H.; Winter, W. E.; Wolpert, H. Diabetes Technology—Continuous Subcutaneous Insulin Infusion Therapy and Continuous Glucose Monitoring in Adults: An Endocrine Society Clinical Practice Guideline. *J. Clin. Endocrinol. Metab.* **2016**, *101* (11), 3922–3937.

(16) Battelino, T.; Danne, T.; Bergenstal, R. M.; Amiel, S. A.; Beck, R.; Biester, T.; Bosi, E.; Buckingham, B. A.; Cefalu, W. T.; Close, K. L.; Cobelli, C.; Dassau, E.; DeVries, J. H.; Donaghue, K. C.; Dovc, K.; Doyle, F. J.; Garg, S.; Grunberger, G.; Heller, S.; Heinemann, L.; Hirsch, I. B.; Hovorka, R.; Jia, W.; Kordonouri, O.; Kovatchev, B.; Kowalski, A.; Laffel, L.; Levine, B.; Mayorov, A.; Mathieu, C.; Murphy, H. R.; Nimri, R.; Nørgaard, K.; Parkin, C. G.; Renard, E.; Rodbard, D.; Saboo, B.; Schatz, D.; Stoner, K.; Urakami, T.; Weinzimer, S. A.; Phillip, M. Clinical Targets for Continuous Glucose Monitoring Data Interpretation: Recommendations From the International Consensus on Time in Range. *Diabetes Care* **2019**, *42* (8), 1593–1603.

(17) Anderson, J. M. Biological Responses to Materials. *Annu. Rev. Mater. Res.* **2001**, *31* (1), 81–110.

(18) Sheikh, Z.; Brooks, P.; Barzilay, O.; Fine, N.; Glogauer, M. Macrophages, Foreign Body Giant Cells and Their Response to Implantable Biomaterials. *Materials (Basel).* **2015**, *8* (9), 5671–5701.

(19) Chandorkar, Y.; Krishnamurthy, R.; Basu, B.; Ravikumar, K.; Basu, B. The Foreign Body Response Demystified. *ACS Biomater. Sci. Eng.* **2019**, *5* (1), 19–44.

(20) Kastellorizios, M.; Tipnis, N.; Burgess, D. J. Immune Responses to Biosurfaces. In *Advances in Experimental Medicine and Biology*; Lambris, J. D., Ekdahl, K. N., Ricklin, D., Nilsson, B., Eds.; Advances in Experimental Medicine and Biology; Springer International Publishing: Cham, 2015; Vol. 865, pp 812–823.

(21) Grainger, D. W. All Charged up about Implanted Biomaterials. *Nat. Biotechnol.* **2013**, *31* (6), 507–509.

(22) Mariani, E.; Lisignoli, G.; Borzì, R. M.; Pulsatelli, L. Biomaterials: Foreign Bodies or Tuners for the Immune Response? *Int. J. Mol. Sci.* **2019**, *20* (3), 636.

(23) Van Putten, S. M.; Ploeger, D. T. A.; Popa, E. R.; Bank, R. A. Macrophage Phenotypes in the Collagen-Induced Foreign Body Reaction in Rats. *Acta Biomater.* **2013**, *9* (5), 6502–6510.

(24) Anderson, J. M.; Rodriguez, A.; Chang, D. T. Foreign Body Reaction to Biomaterials. *Semin. Immunol.* **2008**, *20* (2), 86–100.

(25) Brown, B. N.; Ratner, B. D.; Goodman, S. B.; Amar, S.; Badylak, S. F. Macrophage Polarization: An Opportunity for Improved Outcomes in Biomaterials and Regenerative Medicine. *Biomaterials* **2012**, *33* (15), 3792–3802.

(26) McNally, a K.; Anderson, J. M. Interleukin-4 Induces Foreign Body Giant Cells from Human Monocytes/Macrophages. Differential Lymphokine Regulation of Macrophage Fusion Leads to Morphological Variants of Multinucleated Giant Cells. *Am. J. Pathol.* **1995**, *147* (5), 1487–1499.

(27) Quinn, M. T.; Schepetkin, I. A. Role of NADPH Oxidase in Formation and Function of Multinucleated Giant Cells. *J. Innate Immun.* **2009**, *1* (6), 509–526.

(28) Ischiropoulos, H.; Zhu, L.; Beckman, J. S. Peroxynitrite Formation from Macrophage-Derived Nitric Oxide. *Arch. Biochem. Biophys.* **1992**, *298* (2), 446–451.

(29) Enelow, R. I.; Sullivan, G. W.; Carper, H. T.; Mandell, G. L. Cytokine-Induced Human Multinucleated Giant Cells Have Enhanced Candidacidal Activity and Oxidative Capacity Compared with Macrophages. *J. Infect. Dis.* **1992**, *166* (3), 664–668.

(30) Novak, M. T.; Reichert, W. M. Modeling the Physiological Factors Affecting Glucose Sensor Function in Vivo. *J. Diabetes Sci. Technol.* **2015**, *9* (5), 993–998.

(31) Novak, M. T.; Yuan, F.; Reichert, W. M. Modeling the Relative Impact of Capsular Tissue Effects on Implanted Glucose Sensor Time Lag and Signal Attenuation. *Anal. Bioanal. Chem.* **2010**, *398* (4), 1695–1705.

(32) Rodriguez, A.; MacEwan, S. R.; Meyerson, H.; Kirk, J. T.; Anderson, J. M. The Foreign Body Reaction in T-Cell-Deficient Mice. *J. Biomed. Mater. Res. - Part A* **2009**, *90* (1), 106–113.

(33) Tang, L.; Jennings, T. A.; Eaton, J. W. Mast Cells Mediate Acute Inflammatory Responses to Implanted Biomaterials. *Proc. Natl. Acad. Sci.* **1998**, *95* (July), 8841–8846.

(34) Keselowsky, B. G.; Lewis, J. S. Dendritic Cells in the Host Response to Implanted Materials. *Semin. Immunol.* **2017**, *29* (November 2016), 33–40.

(35) Leifer, C. A. Dendritic Cells in Host Response to Biologic Scaffolds. *Semin. Immunol.* **2017**, *29*, 41–48.

(36) Klueh, U.; Qiao, Y.; Frailey, J. T.; Kreutzer, D. L. Impact of Macrophage Deficiency and Depletion on Continuous Glucose Monitoring Invivo. *Biomaterials* **2014**, *35* (6), 1789–1796.

(37) Klueh, U.; Frailey, J. T.; Qiao, Y.; Antar, O.; Kreutzer, D. L. Cell Based Metabolic Barriers to Glucose Diffusion: Macrophages and Continuous Glucose Monitoring. *Biomaterials* **2014**, *35* (10), 3145–3153.

(38) Novak, M. T.; Yuan, F.; Reichert, W. M. Predicting Glucose Sensor Behavior in Blood

Using Transport Modeling: Relative Impacts of Protein Biofouling and Cellular Metabolic Effects. *J. Diabetes Sci. Technol.* **2013**, *7* (6), 1547–1560.

(39) Ivanova, E. A.; Orekhov, A. N. Monocyte Activation in Immunopathology: Cellular Test for Development of Diagnostics and Therapy. *J. Immunol. Res.* **2016**, *2016*.

(40) Mosser, D. M.; Edwards, J. P. Exploring the Full Spectrum of Macrophage Activation. *Nat. Rev. Immunol.* **2008**, *8* (12), 958–969.

(41) Mackaness, G. B. CELLULAR RESISTANCE TO INFECTION. *J. Exp. Med.* **1962**, *116* (3), 381–406.

(42) Stein, M.; Keshav, S.; Harris, N.; Gordon, S. Interleukin 4 Potently Enhances Murine Macrophage Mannose Receptor Activity: A Marker of Alternative Immunologic Macrophage Activation. *J. Exp. Med.* **1992**, *176* (1), 287–292.

(43) Nathan, C. F.; Murray, H. W.; Wlebe, I. E.; Rubin, B. Y. Identification of Interferon-γ, as the Lymphokine That Activates Human Macrophage Oxidative Metabolism and Antimicrobial Activity. *J. Exp. Med.* **1983**, *158* (3), 670–689.

(44) Mantovani, A.; Sica, A.; Sozzani, S.; Allavena, P.; Vecchi, A.; Locati, M. The Chemokine System in Diverse Forms of Macrophage Activation and Polarization. *Trends Immunol.* **2004**, *25* (12), 677–686.

(45) Vera, J. C.; Reyes, A. M.; Cárcamo, J. G.; Velásquez, F. V; Rivas, C. I.; Zhang, R. H.; Strobel, P.; Iribarren, R.; Scher, H. I.; Slebe, J. C.; Golde, D. W. Genistein Is a Natural Inhibitor of Hexose and Dehydroascorbic Acid Transport through the Glucose Transporter, GLUT1. *J. Biol. Chem.* **1996**, *271* (15), 8719–8724.

(46) Murray, P. J.; Allen, J. E.; Biswas, S. K.; Fisher, E. A.; Gilroy, D. W.; Goerdt, S.; Gordon, S.; Hamilton, J. A.; Ivashkiv, L. B.; Lawrence, T.; Locati, M.; Mantovani, A.; Martinez, F. O.; Mege, J.-L.; Mosser, D. M.; Natoli, G.; Saeij, J. P.; Schultze, J. L.; Shirey, K.; Sica, A.; Suttles, J.; Udalova, I.; van Ginderachter, J. A.; Vogel, S. N.; Wynn, T. A. Macrophage Activation and Polarization: Nomenclature and Experimental Guidelines. *Immunity* **2014**, *41* (1), 14–20.

(47) Brown, B. N.; Londono, R.; Tottey, S.; Zhang, L.; Kukla, K. A.; Wolf, M. T.; Daly, K. A.; Reing, J. E.; Badylak, S. F. Macrophage Phenotype as a Predictor of Constructive Remodeling Following the Implantation of Biologically Derived Surgical Mesh Materials. *Acta Biomater.* **2012**, *8* (3), 978–987.

(48) Wang, N.; Liang, H.; Zen, K. Molecular Mechanisms That Influence the Macrophage M1-M2 Polarization Balance. *Front. Immunol.* **2014**, *5* (NOV), 1–9.

(49) Mills, C. D. M1 and M2 Macrophages: Oracles of Health and Disease. *Crit. Rev. Immunol.* **2012**, *32* (6), 463–488.

(50) Badylak, S. F.; Valentin, J. E.; Ravindra, A. K.; McCabe, G. P.; Stewart-Akers, A. M. Macrophage Phenotype as a Determinant of Biologic Scaffold Remodeling. *Tissue Eng. Part A* **2008**, *14* (11), 1835–1842.

(51) Sica, A.; Mantovani, A. Macrophage Plasticity and Polarization: In Vivo Veritas. *J.*

Clin. Invest. **2012**, *122* (3), 787–795.

(52) Mai, N.-C.; Beryl, L.-B.; Christian, J.; Djouad, F. Deciphering the Complexity of Macrophage Biology and Function with the Zebrafish Model. *Macrophage* **2016**, *3* (0), 1–8.

(53) Freemerman, A. J.; Johnson, A. R.; Sacks, G. N.; Milner, J. J.; Kirk, E. L.; Troester, M. A.; Macintyre, A. N.; Goraksha-Hicks, P.; Rathmell, J. C.; Makowski, L. Metabolic Reprogramming of Macrophages: Glucose Transporter 1 (GLUT1)-Mediated Glucose Metabolism Drives a Proinflammatory Phenotype. *J. Biol. Chem.* **2014**, *289* (11), 7884–7896.

(54) Palmer, C. S.; Anzinger, J. J.; Zhou, J.; Gouillou, M.; Landay, A.; Jaworowski, A.; McCune, J. M.; Crowe, S. M. Glucose Transporter 1–Expressing Proinflammatory Monocytes Are Elevated in Combination Antiretroviral Therapy–Treated and Untreated HIV+ Subjects. *J. Immunol.* **2014**, *193* (11), 5595–5603.

(55) Palmer, C. S.; Ostrowski, M.; Gouillou, M.; Tsai, L.; Yu, D.; Zhou, J.; Henstridge, D. C.; Maisa, A.; Hearps, A. C.; Lewin, S. R.; Landay, A.; Jaworowski, A.; McCune, J. M.; Crowe, S. M. Increased Glucose Metabolic Activity Is Associated with CD4+ T-Cell Activation and Depletion during Chronic HIV Infection. *Aids* **2014**, *28* (3), 297–309.

(56) Vats, D.; Mukundan, L.; Odegaard, J. I.; Zhang, L.; Smith, K. L.; Morel, C. R.; Greaves, D. R.; Murray, P. J.; Chawla, A. Oxidative Metabolism and PGC-1β Attenuate Macrophage-Mediated Inflammation. *Cell Metab.* **2006**, *4* (1), 13–24.

(57) Novak, M. T.; Yuan, F.; Reichert, W. M. Macrophage Embedded Fibrin Gels: An in Vitro Platform for Assessing Inflammation Effects on Implantable Glucose Sensors. *Biomaterials* **2014**, *35* (36), 9563–9572.

(58) Witherel, C. E.; Abebayehu, D.; Barker, T. H.; Spiller, K. L. Macrophage and Fibroblast Interactions in Biomaterial-Mediated Fibrosis. *Adv. Healthc. Mater.* **2019**, *8* (4), 1–16.

(59) Broughton 2nd, G.; Janis, J. E.; Attinger, C. E. The Basic Science of Wound Healing. *Plast. Reconstr. Surg.* **2006**, *117* (7 Suppl), 12S-34S.

(60) Ploeger, D. T. A.; Hosper, N. A.; Schipper, M.; Koerts, J. A.; Rond, S. De; Bank, R. A. Cell Plasticity in Wound Healing : Paracrine Factors of M1 / M2 Polarized Macrophages Influence the Phenotypical State of Dermal Fibroblasts. *Cell Commun. Signal.* **2013**, *11* (29), 1–17.

(61) Zhou, G.; Liedmann, A.; Chatterjee, C.; Groth, T. In Vitro Study of the Host Responses to Model Biomaterials via a Fibroblast/Macrophage Co-Culture System. *Biomater. Sci.* **2017**, *5* (1), 141–152.

(62) Bozkurt, S. B.; Hakki, S. S.; Hakki, E. E.; Durak, Y.; Kantarci, A. Porphyromonas Gingivalis Lipopolysaccharide Induces a Pro-Inflammatory Human Gingival Fibroblast Phenotype. *Inflammation* **2017**, *40* (1), 144–153.

(63) Nichols, S. P.; Koh, A.; Storm, W. L.; Shin, J. H.; Schoenfisch, M. H. Biocompatible Materials for Continuous Glucose Monitoring Devices. *Chem. Rev.* **2013**, *113* (4),

2528–2549.

(64) Soto, R. J.; Hall, J. R.; Brown, M. D.; Taylor, J. B.; Schoenfisch, M. H. In Vivo Chemical Sensors: Role of Biocompatibility on Performance and Utility. *Anal. Chem.* **2017**, *89* (1), 276–299.

(65) Thevenot, P.; Hu, W.; Tang, L. Surface Chemistry Influences Implant Biocompatibility. *Curr. Top. Med. Chem.* **2008**, *8* (4), 270–280.

(66) Singh, S.; Awuah, D.; Rostam, H. M.; Emes, R. D.; Kandola, N. K.; Onion, D.; Htwe, S. S.; Rajchagool, B.; Cha, B.-H.; Kim, D.; Tighe, P. J.; Vrana, N. E.; Khademhosseini, A.; Ghaemmaghami, A. Unbiased Analysis of the Impact of Micropatterned Biomaterials on Macrophage Behavior Provides Insights beyond Predefined Polarization States. *ACS Biomater. Sci. Eng.* **2017**, *3* (6), 969–978.

(67) Wang, J.; Loye, A. M.; Ketkaew, J.; Schroers, J.; Kyriakides, T. R. Hierarchical Micro- and Nanopatterning of Metallic Glass to Engineer Cellular Responses. *ACS Appl. Bio Mater.* **2018**, *1* (1), 51–58.

(68) Keeler, G. D.; Durdik, J. M.; Stenken, J. A. Localized Delivery of Dexamethasone-21-Phosphate via Microdialysis Implants in Rat Induces M(GC) Macrophage Polarization and Alters CCL2 Concentrations. *Acta Biomater.* **2015**, *12* (1), 11–20.

(69) Wang, Y.; Papadimitrakopoulos, F.; Burgess, D. J. Polymeric "Smart" Coatings to Prevent Foreign Body Response to Implantable Biosensors. *J. Control. Release* **2013**, *169* (3), 341–347.

(70) Gratchev, A.; Kzhyshkowska, J.; Utikal, J.; Goerdt, S. Interleukin-4 and Dexamethasone Counterregulate Extracellular Matrix Remodelling and Phagocytosis in Type-2 Macrophages. *Scand. J. Immunol.* **2005**, *61* (1), 10–17.

(71) Keeler, G. D.; Durdik, J. M.; Stenken, J. A. Effects of Delayed Delivery of Dexamethasone-21-Phosphate via Subcutaneous Microdialysis Implants on Macrophage Activation in Rats. *Acta Biomater.* **2015**, *23*, 27–37.

(72) Ao, X.; Sellati, T. J.; Stenken, J. A. Enhanced Microdialysis Relative Recovery of Inflammatory Cytokines Using Antibody-Coated Microspheres Analyzed by Flow Cytometry. *Anal. Chem.* **2004**, *76* (13), 3777–3784.

(73) Vallejo-Heligon, S. G.; Klitzman, B.; Reichert, W. M. Characterization of Porous, Dexamethasone-Releasing Polyurethane Coatings for Glucose Sensors. *Acta Biomater.* **2014**, *10* (11), 4629–4638.

(74) Ward, W. K.; Hansen, J. C.; Massoud, R. G.; Engle, J. M.; Takeno, M. M.; Hauch, K. D. Controlled Release of Dexamethasone from Subcutaneouslyimplanted Biosensors in Pigs: Localized Anti-Inflammatory Benefit without Systemic Effects. *J. Biomed. Mater. Res. - Part A* **2010**, *94* (1), 280–287.

(75) Price, C. F.; Burgess, D. J.; Kastellorizios, M. L-DOPA as a Small Molecule Surrogate to Promote Angiogenesis and Prevent Dexamethasone-Induced Ischemia. *J. Control. Release* **2016**, *235*, 176–181.

(76) Patil, S. D.; Papadmitrakopoulos, F.; Burgess, D. J. Concurrent Delivery of Dexamethasone and VEGF for Localized Inflammation Control and Angiogenesis. *J. Control. Release* **2007**, *117* (1), 68–79.

(77) Gifford, R.; Batchelor, M. M.; Lee, Y.; Gokulrangan, G.; Meyerhoff, M. E.; Wilson, G. S. Mediation of in Vivo Glucose Sensor Inflammatory Response via Nitric Oxide Release. *J. Biomed. Mater. Res. Part A* **2005**, *75A* (4), 755–766.

(78) Soto, R. J.; Privett, B. J.; Schoenfisch, M. H. In Vivo Analytical Performance of Nitric Oxide-Releasing Glucose Biosensors. *Anal. Chem.* **2014**, *86* (14), 7141–7149.

(79) Malone-Povolny, M. J.; Merricks, E. P.; Wimsey, L. E.; Nichols, T. C.; Schoenfisch, M. H. Long-Term Accurate Continuous Glucose Biosensors via Extended Nitric Oxide Release. *ACS Sensors* **2019**, *4* (12), 3257–3264.

(80) Yu, T.; Tutwiler, V.; Spiller, K. L. The Role of Macrophages in the Foreign Body Response to Biomaterials. *Biomater. Regen. Med. Immune Syst.* **2015**, 17.

(81) Hogg, N. The Biochemistry and Physiology of S-Nitrosothiols. *Annu. Rev. Pharmacol. Toxicol.* **2002**, *42*, 585–500.

(82) Kolesnik, B.; Palten, K.; Schrammel, A.; Stessel, H.; Schmidt, K.; Mayer, B.; Gorrenn, A. C. F. Efficient Nitrosation of Glutathione by Nitric Oxide. *Free Radic. Biol. Med.* **2013**, *63*, 51–64.

(83) Deppisch, C.; Herrmann, G.; Graepler-Mainka, U.; Wirtz, H.; Heyder, S.; Engel, C.; Marschal, M.; Miller, C. C.; Riethmüller, J. Gaseous Nitric Oxide to Treat Antibiotic Resistant Bacterial and Fungal Lung Infections in Patients with Cystic Fibrosis: A Phase I Clinical Study. *Infection* **2016**, *44* (4), 513–520.

(84) Bentur, L.; Gur, M.; Ashkenazi, M.; Livnat-Levanon, G.; Mizrahi, M.; Tal, A.; Ghaffari, A.; Geffen, Y.; Aviram, M.; Efrati, O. Pilot Study to Test Inhaled Nitric Oxide in Cystic Fibrosis Patients with Refractory Mycobacterium Abscessus Lung Infection. *J. Cyst. Fibros.* **2020**, *19* (2), 225–231.

(85) Hall, J. R.; Rouillard, K. R.; Suchyta, D. J.; Brown, M. D.; Ahonen, M. J. R.; Schoenfisch, M. H. Mode of Nitric Oxide Delivery Affects Antibacterial Action. *ACS Biomater. Sci. Eng.* **2020**, *6* (1), 433–441.

(86) Riccio, D. A.; Nugent, J. L.; Schoenfisch, M. H. Stöber Synthesis of Nitric Oxide-Releasing S-Nitrosothiol-Modified Silica Particles. *Chem. Mater.* **2011**, *23* (7), 1727–1735.

(87) Soto, R. J.; Yang, L.; Schoenfisch, M. H. Functionalized Mesoporous Silica via an Aminosilane Surfactant Ion Exchange Reaction: Controlled Scaffold Design and Nitric Oxide Release. *ACS Appl. Mater. Interfaces* **2016**, *8* (3), 2220–2231.

(88) Malone-Povolny, M. J.; Schoenfisch, M. H. Extended Nitric Oxide-Releasing Polyurethanes via S-Nitrosothiol-Modified Mesoporous Silica Nanoparticles. *ACS Appl. Mater. Interfaces* **2019**, *11* (13), 12216–12223.

(89) Yang, L.; Wang, X.; Suchyta, D. J.; Schoenfisch, M. H. Antibacterial Activity of Nitric

Oxide-Releasing Hyperbranched Polyamidoamines. *Bioconjug. Chem.* **2018**, *29* (1), 35–43.

(90) Ahonen, M. J. R.; Suchyta, D. J.; Zhu, H.; Schoenfisch, M. H. Nitric Oxide-Releasing Alginates. *Biomacromolecules* **2018**, *19* (4), 1189–1197.

(91) Jin, H.; Yang, L.; Ahonen, M. J. R.; Schoenfisch, M. H. Nitric Oxide-Releasing Cyclodextrins. *J. Am. Chem. Soc.* **2018**, *140* (43), 14178–14184.

(92) Koh, A.; Nichols, S. P.; Schoenfisch, M. H. Glucose Sensor Membranes for Mitigating the Foreign Body Response. *J. Diabetes Sci. Technol.* **2011**, *5* (5), 1052–1059.

(93) Koh, A.; Riccio, D. a.; Sun, B.; Carpenter, A. W.; Nichols, S. P.; Schoenfisch, M. H. Fabrication of Nitric Oxide-Releasing Polyurethane Glucose Sensor Membranes. *Biosens. Bioelectron.* **2011**, *28* (1), 17–24.

(94) Soto, R. J.; Schofield, J. B.; Walter, S. E.; Malone-Povolny, M. J.; Schoenfisch, M. H. Design Considerations for Silica-Particle-Doped Nitric-Oxide-Releasing Polyurethane Glucose Biosensor Membranes. *ACS Sensors* **2017**, *2* (1), 140–150.

(95) Shin, J. H.; Marxer, S. M.; Schoenfisch, M. H. Nitric Oxide-Releasing Sol-Gel Particle/Polyurethane Glucose Biosensors. *Anal. Chem.* **2004**, *76* (15), 4543–4549.

(96) Jornvall, H. *Nobel Lectures in Physiology or Medicine 1996 – 2000*; WORLD SCIENTIFIC, 2003.

(97) Ignarro, L. J.; Buga, G. M.; Wood, K. S.; Byrns, R. E.; Chaudhuri, G. Endothelium-Derived Relaxing Factor Produced and Released from Artery and Vein Is Nitric Oxide. *Proc. Natl. Acad. Sci.* **1987**, *84* (24), 9265–9269.

(98) Morbidelli, L.; Donnini, S.; Ziche, M. Role of Nitric Oxide in the Modulation of Angiogenesis. *Curr. Pharm. Des.* **2003**, *9*, 521–530.

(99) Cooke, J. P.; Losordo, D. W. Nitric Oxide and Angiogenesis. *Circulation* **2002**, *105* (18), 2133–2135.

(100) Witte, K.; Jacke, K.; Stahrenberg, R.; Arlt, G.; Reitenbach, I.; Schilling, L.; Lemmer, B. Dysfunction of Soluble Guanylyl Cyclase in Aorta and Kidney of Goto-Kakizaki Rats: Influence of Age and Diabetic State. *Nitric Oxide - Biol. Chem.* **2002**, *6* (1), 85–95.

(101) Montfort, W. R.; Wales, J. A.; Weichsel, A. Structure and Activation of Soluble Guanylyl Cyclase, the Nitric Oxide Sensor. *Antioxid. Redox Signal.* **2017**, *26* (3), 107–121.

(102) Friebe, A.; Koesling, D. Regulation of Nitric Oxide-Sensitive Guanylyl Cyclase. *Circ. Res.* **2003**, *93* (2), 96–105.

(103) Matsunaga, T.; Weihrauch, D. W.; Moniz, M. C.; Tessmer, J.; Warltier, D. C.; Chilian, W. M. Angiostatin Inhibits Coronary Angiogenesis during Impaired Production of Nitric Oxide. *Circulation* **2002**, *105* (18), 2185–2191.

(104) Park, J. E.; Abrams, M. J.; Efron, P. A.; Barbul, A. Excessive Nitric Oxide Impairs

Wound Collagen Accumulation. *J. Surg. Res.* **2013**, *183* (1), 487–492.

(105) Shukla, A.; Rasik, A. M.; Shankar, R. Nitric Oxide Inhibits Wound Collagen Synthesis. *Mol. Cell. Biochem.* **1999**, *200*, 27–33.

(106) Cao, M.; Westerhausen-Larson, A.; Niyibizi, C.; Kavalkovich, K.; Georgescu, H. I.; Rizzo, C. F.; Hebda, P. A.; Stefanovic-Racic, M.; Evans, C. H. Nitric Oxide Inhibits the Synthesis of Type-II Collagen without Altering Col2A1 MRNA Abundance: Prolyl Hydroxylase as a Possible Target. *Biochem. J.* **1997**, *324* (1), 305–310.

(107) Villalobo, A. Nitric Oxide and Cell Proliferation. *FEBS J.* **2006**, *273* (11), 2329–2344.

(108) Frank, S.; Kämpfer, H.; Wetzler, C.; Pfeilschifter, J. Nitric Oxide Drives Skin Repair: Novel Functions of an Established Mediator. *Kidney Int.* **2002**, *61* (3), 882–888.

(109) Luo, J. D.; Chen, A. F. Nitric Oxide: A Newly Discovered Function on Wound Healing. *Acta Pharmacol. Sin.* **2005**, *26* (3), 259–264.

(110) Bogdan, C. Regulation of Lymphocytes by Nitric Oxide. In *Suppression and Regulation of Immune Responses - Methods in Molecular Biolgoy vol. 677*; 2010; pp 375–393.

(111) Villarete, L. H.; Remick, D. G. Nitric Oxide Regulation of Interleukin-8 Gene Expression. *Shock* **1997**, *7* (1), 29–35.

(112) Seo, J. Y.; Yu, J. H.; Lim, J. W.; Mukaida, N.; Kim, H. Nitric Oxide-Induced IL-8 Expression Is Mediated by NF-KappaB and AP-1 in Gastric Epithelial AGS Cells. *J. Physiol. Pharmacol.* **2009**, *60 Suppl 7* (26), 101–106.

(113) Hetrick, E. M.; Prichard, H. L.; Klitzman, B.; Schoenfisch, M. H. Reduced Foreign Body Response at Nitric Oxide-Releasing Subcutaneous Implants. *Biomaterials* **2007**, *28* (31), 4571–4580.

(114) Nichols, S. P.; Le, N. N.; Klitzman, B.; Schoenfisch, M. H. Increased In Vivo Glucose Recovery via Nitric Oxide Release. *Anal. Chem.* **2011**, *83* (4), 1180–1184.

(115) Nichols, S. P.; Koh, A.; Brown, N. L.; Rose, M. B.; Sun, B.; Slomberg, D. L.; Riccio, D. A.; Klitzman, B.; Schoenfisch, M. H. The Effect of Nitric Oxide Surface Flux on the Foreign Body Response to Subcutaneous Implants. *Biomaterials* **2012**, *33* (27), 6305–6312.

(116) Soto, R. J.; Merricks, E. P.; Bellinger, D. A.; Nichols, T. C.; Schoenfisch, M. H. Influence of Diabetes on the Foreign Body Response to Nitric Oxide-Releasing Implants. *Biomaterials* **2018**, *157*, 76–85.

(117) Frost, M. C.; Batchelor, M. M.; Lee, Y.; Zhang, H.; Kang, Y.; Oh, B.; Wilson, G. S.; Gifford, R.; Rudich, S. M.; Meyerhoff, M. E. Preparation and Characterization of Implantable Sensors with Nitric Oxide Release Coatings. *Microchem. J.* **2003**, *74* (3), 277–288.

(118) Ren, H.; Colletta, A.; Koley, D.; Wu, J.; Xi, C.; Major, T. C.; Bartlett, R. H.; Meyerhoff, M. E. Thromboresistant/Anti-Biofilm Catheters via Electrochemically Modulated

Nitric Oxide Release. *Bioelectrochemistry* **2015**, *104*, 10–16.

(119) Schoenfisch, M. H.; Mowery, K. A.; Rader, M. V.; Baliga, N.; Wahr, J. A.; Meyerhoff, M. E. Improving the Thromboresistivity of Chemical Sensors via Nitric Oxide Release: Fabrication and in Vivo Evaluation of NO-Releasing Oxygen-Sensing Catheters. *Anal. Chem.* **2000**, *72* (6), 1119–1126.

(120) Pant, J.; Goudie, M. J.; Chaji, S. M.; Johnson, B. W.; Handa, H. Nitric Oxide Releasing Vascular Catheters for Eradicating Bacterial Infection. *J. Biomed. Mater. Res. Part B Appl. Biomater.* **2018**, *106* (8), 2849–2857.

(121) Homeyer, K. H.; Goudie, M. J.; Singha, P.; Handa, H. Liquid-Infused Nitric-Oxide-Releasing Silicone Foley Urinary Catheters for Prevention of Catheter-Associated Urinary Tract Infections. *ACS Biomater. Sci. Eng.* **2019**, *5* (4), 2021–2029.

(122) Malone-Povolny, M. J.; Maloney, S. E.; Schoenfisch, M. H. Nitric Oxide Therapy for Diabetic Wound Healing. *Adv. Healthc. Mater.* **2019**, *8* (12), 1–18.

(123) Soto, R. J.; Schoenfisch, M. H. Preclinical Performance Evaluation of Percutaneous Glucose Biosensors: Experimental Considerations and Recommendations. *J. Diabetes Sci. Technol.* **2015**, *9* (5), 978–984.

(124) Seaton, M.; Hocking, A.; Gibran, N. S. Porcine Models of Cutaneous Wound Healing. *ILAR J.* **2015**, *56* (1), 127–138.

(125) Bellinger, D. A.; Merricks, E. P.; Nichols, T. C. Swine Models of Type 2 Diabetes Mellitus: Insulin Resistance, Glucose Tolerance, and Cardiovascular Complications. **2006**, *47* (3), 243–258.

CHAPTER 2 – ASSESSING GLUCOSE CONSUMPTION OF POLARIZED MACROPHAGES EXPOSED TO EXOGENOUS NITRIC OXIDE

2.1 Introduction

Implantable glucose sensors for continuous glucose monitoring (CGM) are a promising technology for diabetes management, with numerous clinical trials demonstrating improved health outcomes for type 1 diabetic patients utilizing CGM technology.[1–5] However, a consistent barrier to more widespread implementation of CGM is the foreign body response (FBR), an irregular wound healing response mounted to remove foreign objects from the body. The FBR begins with protein adhesion to the implant surface, leading to the recruitment of inflammatory cells (e.g., neutrophils, macrophages) to the implant site, the release of inflammatory mediators and reactive oxygen and nitrogen species (ROS and RNS, respectively), and ending in the eventual collagenous encapsulation and isolation of the implanted sensor from surrounding tissue.[6–8] A combination of the physical destruction of the sensor from ROS and RNS exposure, the impediment of glucose transport by the collagen capsule, and its biofouling by proteins and surrounding cells all contribute to a reduction in sensor sensitivity and overall efficacy, rendering the sensor analytically nonviable (i.e., >10% daily sensitivity change) within weeks. To increase the effectiveness of CGM technology, researchers have explored how to minimize the effects of the FBR – from changing the topography or composition of the implant to the release of anti-inflammatory agents from the implant surface.[9–13]

A uniquely attractive method for reducing the FBR at the implantation site is through the release of nitric oxide (NO) from the implant surface. An endogenously produced

gasotransmitter, NO has been implicated in numerous biological processes, such as intercellular signaling, angiogenesis, and inflammation.[14–18] Molecules engineered for the spontaneous release of NO (NO donors) can be doped into polymer membranes and released from the surface of an implantable glucose sensor, including both small molecule NO donors (e.g., DETA/NO, SNAP, S-nitrosoglutathione) and macromolecular scaffolds (e.g., NO-releasing nanoparticles, dendrimers, hyperbranched polymers). The released NO promotes the reduction of inflammation, demonstrated by outcomes such as a decreased inflammatory cell count, decreased collagen thickness, and increased angiogenesis, [19,20] Due to NO's short *in vivo* half-life and subsequent travel distance, these effects are also uniquely localized to the area of release.[21] Importantly, NO release has also been linked to improved sensor performance, with observable improvements in both glucose recovery and sensitivity retention.[20,22–24]

Though NO release has been a beneficial addition to implantable sensors, little research has been done on the effect of exogenous NO on the phenotypes of the cells present at the implantation site. Macrophages are of particular interest due to their varied roles in controlling the FBR process, including pathogen destruction and removal, the release of regulatory cytokines, and the recruitment of fibroblasts to the implant site for collagen deposition in the FBR's resolution. Macrophage versatility stems from their phenotypic plasticity and depending on the microenvironmental stimuli present, macrophage phenotype can be polarized between pro-inflammatory (M1) and anti-inflammatory (M2) extremes. Pro-inflammatory phenotypes are known to be induced by specific cytokines, including interferon gamma (IFNγ) and tumor necrosis factor alpha (TNFα), and pathogenic markers, such as lipopolysaccharides (LPS) derived from bacterial cell walls. The response from M1 macrophages consists primarily of the release of ROS and RNS for pathogen removal and the degradation of the foreign body. M2 macrophages perform diverse functions more generally associated with wound healing and proliferation, such as promoting angiogenesis and

modulating T-cell activity.[25,26] While the literature suggests that a spectrum of activated states exists between the M1 and M2 phenotypes, as opposed to discrete states, and differential stimulant-dependent polarization states,[25,27,28] the following discussion will refer to macrophage polarization using the M1/M2 activation dichotomy to simplify the complex relationships macrophages have with their environment.

Besides having a critical role in the regulation of the FBR, macrophages also are unique barriers to CGM due to their high native glucose consumption. Novak et al. reported that the main contributor to signal decline in implanted glucose sensors over time is macrophage presence at the implant site.[29] Macrophages have high metabolic requirements and thus readily consume local glucose, resulting in significantly larger signal declines when compared to the resultant decline from bulk erythrocytes. Klueh et al. supported this claim by showing that the addition of macrophages to the sensor environment produces a significant reduction in signal, while the addition of lymphocytes showed almost no signal change.[30] Furthermore, implanted glucose sensors were characterized as having more stable signals over time in macrophage-deficient and macrophage-depleted mouse models compared to the wild-type.[31]

To elucidate the processes behind deleterious macrophage effects on implants, we investigated macrophage polarization, particularly the effect of the ratio of M1/M2 cells at the implantation site. It has been demonstrated that macrophage polarization is linked with the expression of glucose transporters, wherein M1 macrophages show increased expression of GLUT1 and GLUT3 transporters.[32–34] On the other hand, M2 macrophages show increased expression of genes associated with fatty acid oxidation and consume less glucose than M1 macrophages.[35,36] This allows polarization states to be differentiated via glucose consumption. With rational sensor design in mind, designing materials that reduce the count of M1 cells would minimize macrophage glucose consumption as a confounding factor in the sensor measurement, leading to improved sensor accuracy. Preliminary research suggests that implants with higher ratios of M2 to M1 cells at the implantation site show more favorable

wound reconstruction over time,[37,38] supporting the idea that promoting an anti-inflammatory macrophage phenotype at the implant site will lead to the reductions in the FBR and the resultant negative sensor outcomes.

Reports concerning NO-releasing glucose sensors have been primarily focused on the sensor accuracy and local histology, as opposed to NO's effect on interfering glucose depletion.[20,23,24,39–41] The first study to probe this question was reported by Nichols et al., who used a rat model in which a saturated solution of NO was flowed into an implanted dialysis probe, to ascertain NO's effect on the interstitial glucose able to be detected at the sensor.[22] Compared to control probes, with NO exposure the glucose recovered in the dialysate was significantly higher from 7 days post-implantation onward, and the inflammatory cell density was nearly halved at 14 days post-implantation.[22] These data together imply that NO likely produces higher glucose recovery by altering the local cell density. However, there remains a paucity of studies on NO's effect on macrophage polarization and the associated changes in glucose consumption.

To address this lack of clarity, we developed two different assays to monitor macrophage glucose consumption with the intention of elucidating the combined effects of NO exposure and macrophage polarization. The first was the use of a macrophage-embedded fibrin gel as a scaffold for continuous glucose monitoring. As reported by Novak et al., using a 3D macrophage scaffold allows the simulation of an implant site and through the use of an intrascaffold CGM, glucose consumption of macrophages can be monitored in real-time, with the goal of monitoring macrophages using an NO-releasing sensor to monitor NO-affected glucose consumption.[42] The second assay utilizes the fluorescent tracer 2-NBDG, a glucose molecule tagged with a fluorescent 7-nitrobenzofurazan moiety that has been previously used to monitor glucose uptake in both bacteria and mammalian cells.[42–46] Using fluorescence measurement, we can observe differential accumulation of 2-NBDG, as a function of NO dose and polarization state.

2.2 Materials and Methods

2.2.1 Materials

Sodium nitrite, lipopolysaccharides derived from E. Coli 055:B5 (LPS), dexamethasone (Dex), N-acetyl-D-penicillamine (NAP), diethylenetriamine (DETA), glucose oxidase (GOx; type VII from Aspergillus niger, > 100,000 units g^{-1}), and Antifoam B Emulsion were purchased from Sigma Aldrich. A cylinder of nitric oxide gas (99.5%) was purchased from Airgas. Hydrochloric acid, 10% neutral buffered formalin, 200 proof ethanol, and dimethylsulfoxide (DMSO) were purchased from Fisher Scientific. The murine macrophage-like cell line, RAW 264.7, was obtained from the American Type Culture Collection (ATCC). The glucose tracer 2-NBDG was purchased from Cayman Chemical and stored as a solution of 15 mg/mL in ethanol. Silver wires (0.005" diameter) and platinum-iridium wires (Pt-Ir; 0.005" diameter with 0.003" PTFE coating) were purchased from A-M Systems. Macrophages were cultured in either 1X DMEM (4.5 g/L glucose; Gibco) or glucose-free 1X DMEM (Gibco), both supplemented with 10% fetal bovine serum, 100 IU/mL penicillin, and 100 µg/mL streptomycin, at 37 °C and 5% CO_2 in a fully humidified incubator. Only macrophages at passages 5-15 were used in the following experiments. All chemicals were used as received unless otherwise stated. All other materials were obtained from commercial vendors and used without further purification.

2.2.2 Synthesis and Characterization of NO Donors

S-Nitroso-N-acetylpenicillamine (SNAP) was used as an NO donor, releasing NO primarily through heat-initiated decomposition. The synthesis was adapted from work done by Chipinda and Simoyi.[47] Briefly, 0.478 g of NAP was added to a stirring solution of 10 mL H_2O and 0.5 mL 5M HCl in a round bottom flask on ice. To the mixture, 0.176 g of $NaNO_2$ was added (1:1 molar ratio) and left to react in the dark for 40 minutes. After 40 minutes, 5 mL of

acetone were then added to the solution, which was then left another ten minutes to react. The product was recovered after the reaction via vacuum filtration, where it was washed twice with ice-cold water and twice with ice-cold acetone, and then dried under vacuum in the dark for 2 hours. Product was then stored at -20 °C until use.

Alongside SNAP, DETA was diazeniumdiolated to DETA/NO, adapting previously reported protocols. Briefly, DETA was dissolved in acetonitrile at 33 mg/mL and placed into a Parr stainless steel bomb. The bomb was purged with argon gas to remove dissolved oxygen and the mixture was left stirring under 145 psi NO gas for 3 days. Following the 3 days, the NO gas was purged from the reaction vessel with six argon flushes to remove residual NO. The product was then isolated through vacuum filtration, washed twice with cold diethyl ether, dried under vacuum overnight, and stored at -20 °C until used.

The NO-release kinetics for SNAP were characterized with a Zysense Nitric Oxide Analyzer (NOA). Briefly, 30 mL of 10% FBS in PBS were added to a reaction vessel and purged for at least 30 minutes with nitrogen gas. A bolus of the NO donor was added to the reaction vessel, wherein the NO donor would release NO spontaneously. Using nitrogen as a carrier gas, the liberated NO is carried into the NOA, where it is reacted with ozone in a reaction chamber, creating an activated species that liberates a photon to a photomultiplier tube for detection. This chemiluminescence signal serves as the transducer for NO release. For the measurement of the SNAP, the round bottom flask was kept at 37 °C with a water bath and covered with aluminum foil to prevent unwanted NO release. In addition, 30 mL of Antifoam B Emulsion were added to the round bottom to reduce foaming associated with the addition of FBS.

2.2.3 Electrochemical Sensor Fabrication and Characterization

Glucose sensors were adapted from the Wilson laboratory's original design for subcutaneous needle-based sensors, as previously reported by members of the Schoenfisch lab (Figure 2.1).[23,48,49] Briefly, 400 mm of silver wire was coiled and then incubated in a saturated solution of $FeCl_3$ to catalytically convert the surface to AgCl, allowing for use as an Ag/AgCl reference electrode. A platinum-iridium (Pt-Ir) wire was fed through the coiled reference. The exposed Pt-Ir wire serves as the working electrode. An epoxy bead was then deposited on the tip to improve the rigidity of the sensor for insertion into the hydrogel for the assay.

To functionalize the sensor for glucose detection, a sol-gel was made by mixing 25 μL methyltrimethoxysilane (MTMOS) and 100 μL ethanol with 50 μL of a solution of 9 mg of glucose oxidase (GOx) in 75 μL of water. The sol was then aged for at least 5 minutes before dip-coating the sensors in the solution through 15 dips (5 seconds submerged in sol-gel, 10 seconds in between dips). Once coated, the GOx at the sensing surface is capable of oxidizing glucose and reducing oxygen, yielding hydrogen peroxide. Hydrogen peroxide is then detected amperometrically at +0.6 V, as an indirect measure of glucose concentration. Glucose sensors are often limited by the high concentration of glucose relative to the low concentration of dissolved oxygen, leading to saturation in the activity of the enzyme. To circumvent this limitation, a polyurethane layer was coated onto the sensor atop the GOx layer to differentially control the diffusion of oxygen and glucose to the sensor surface. The polyurethane composition used was a loop-casted 50 mg/mL Tecophilic (HP-93A-100) for a total of 7 coats, followed by a topcoat of 30 mg/mL 3:1 Carbothane (PC3585A):Tecophilic in 3:1 THF:DMF applied via a single dip-coat. Each layer applied to the sensor was dried for at least 1 hour before application of subsequent layers. All electrochemical characterization discussed herein was performed using a CH Instruments potentiostat, measuring current continuously with a

static applied potential of +0.6 V vs Ag|AgCl. Sensors were calibrated in 1X PBS with glucose challenges. Sensitivity retention was characterized by daily glucose calibrations and storing electrodes in 10% FBS at room temperature overnight in between calibrations.

2.2.4 Continuous Glucose Monitoring in a Macrophage-Embedded Fibrin Gel

The creation of the 3D gel scaffold was adopted by the report from Novak et al.[42] Briefly, macrophages were plated in a culture flask and were either grown unstimulated or stimulated with either 1 μg/mL LPS, 0.1 μM dexamethasone, or 10 ng/mL IL-4. After 24 hours, RAW 264.7 macrophages were suspended in 1X DMEM at 4.2 x 10^6 cells/mL. 480 μL of the macrophage suspension (or 480 μL 1X DMEM for the acellular gel) were mixed with 100 μL Matrigel, 200 μL of 10 mg/mL fibrinogen in PBS, 200 μL of 2X DMEM, and 20 μL of 10 U/mL thrombin. The mixture was left uncovered at 37 °C for at least 45 minutes to solidify, yielding a cell scaffold with a macrophage density of 2 x 10^6 cells/mL, simulating the density of recruited macrophages at an implant site. This gel was submerged in a petri dish containing 3 mL of low glucose 1X DMEM and a sensor was inserted into the gel scaffold for continuous glucose measurement. Of note, the first 4 hours of measurement were taken as the electrode polarization time. The change in current is reported for all gel experiments as the instantaneous current relative to the current at the 4-hour time point.

2.2.5 Measuring Glucose Consumption with 2-NBDG

Macrophages were plated overnight on a 24-well plate at 0.5 x 10^6 cells/well. The wells were then co-incubated for 24 h with a combination of either 1 μg/mL LPS or 0.1 μM dexamethasone and either an NO donor or its corresponding non-releasing scaffold. For this study, 5/50/500 μM SNAP or NAP, or 0.02/0.2/2 mg/mL DETA/NO or DETA were used. Wells with no scaffold served as either the M(-) control (i.e., unstimulated), the M1 control (i.e., LPS), or the M2 control (i.e., dexamethasone). Following stimulation, macrophage

cultures were washed with 1X PBS and incubated in glucose-free DMEM for 30 minutes. After removing the glucose-free DMEM, a solution of 100 μM 2-NBDG in glucose-free DMEM was added to the experimental wells for a 10-minute incubation. Control wells of each stimulation condition were made by omitting the 2-NBDG and re-incubating for 10 minutes in blank glucose-free media. Following the incubation, the cells were washed with 1X PBS and fixed with 10% formalin for 15 minutes, to prevent enzymatic degradation of 2-NDBG. The formalin solution was exchanged with PBS and cells were either imaged on an Olympus IX81 inverted microscope or were mechanically removed from the plate for analysis on a Thermo Fisher Attune NxT flow cytometer.

2.3 Results and Discussion

2.3.1 Electrode Characterization

Glucose biosensors were fabricated to serve as the glucose consumption transducer in the assay. To function appropriately, biosensors were required to detect glucose reproducibly in a linear dynamic range that exceeds 6 mM glucose, as the low glucose media that the system would be submerged in has a glucose concentration of 5.6 mM. Sensors were calibrated in PBS against glucose injections (Figure 2.2). Polyurethane compositions were evaluated, identifying an optimal seven layers of HP-93A-100, which provided a glucose sensitivity of 5.14 ± 3.51 nA/mM and a linear dynamic range of from 0-7.8 ± 2.6 mM glucose. Another important parameter for these sensors was their sensitivity retention (Figure 2.3). As the measurement would take place over the course of at least 24 hours, it was important to assess that the sensitivity of the sensor would not decline dramatically during electrochemical measurement. After 3 days of incubation in proteinaceous media, it was found that the daily sensitivity change was less than 10%, falling in line with current ISO standards concerning CGM technology.[50]

2.3.2 Intrascaffold Analysis of Polarized Macrophages

Initial testing of macrophages compared glucose consumption of M(-) macrophages and the sensor response in an acellular gel (Figure 2.4A). As expected, the signal change was greater with the macrophages consuming glucose, with a relative current of ~0.4 for the macrophage containing gel. Importantly, this relative current matches closely with what was observed by Novak et al. for unstimulated macrophages.[42] The signal from the acellular gel was ~0.6. This change in current from baseline implies either glucose consumption or a higher baseline for our platform, compared to Novak et al., who found a relative current of ~0.9.[42]

Having distinguished the glucose consumption between the acellular gel and unpolarized macrophages, we explored the use of polarized macrophages in the scaffold, expecting a decrease in glucose consumption for anti-inflammatory macrophages and vice-versa. First, both dexamethasone and IL-4 were used to induce M2 phenotypes in the macrophages (Figure 2.4B) and dexamethasone in particular was shown to reduce the glucose consumption of macrophages to a current output matching that of the acellular gel. When surveying the M1 macrophages, however, the glucose consumption of the M(LPS) macrophages only reported a relative current of ~0.4 (Figure 2.5). This reported current is at the same level as the M(-) system, showing that our platform was not able to differentiate between M(-) and M1 macrophages. A macrophage pre-incubation of 1 μg/mL LPS and 50 μM SNAP was also not able to elicit a significant difference to the M(LPS) cells and thus the M(-) cells.

2.3.3 Fluorescence Measurement of 2-NBDG

Parallel to the *in situ* glucose monitoring, in vitro assays were developed to assess the glucose consumption of cultured macrophages using 2-NBDG, a fluorescent glucose analog used through the literature to assess glucose uptake.[43–46] Indeed, the study by Novak et al. also used 2-NBDG to corroborate the trends observed with their sensing platform.[42] Though 2-

NBDG interacts differently with the GLUT1 glucose transporter in comparison to native glucose,[44] quantifying how its transport is affected by NO and macrophage polarization would allow inference on the transport of glucose. For this series of experiments, SNAP was used to deliver NO to the cells, rapidly liberating NO in proteinaceous media likely due to interactions between SNAP and the free cysteine residues on the proteins, compared to its slow liberation of NO in PBS. Quantification via the NOA showed NO doses of 300 μM NO for 500 μM SNAP, 30 μM NO for 50 μM SNAP, and 3 μM for 5 μM SNAP in proteinaceous media.

Initial studies of 2-NDBG relied on fluorescence microscopy to visually confirm 2-NBDG buildup in the macrophages (Figure 2.6). Fluorescence intensity was quantified from the micrographs using pixel analysis, wherein light intensity from the pixel is a direct representation of fluorescence. A mean fluorescence intensity (MFI) would then be calculated to represent the glucose consumption of the macrophage population. It was found that using 5 μM SNAP could reduced the glucose consumption of M1 macrophages by as much as half, implying a reduction in pro-inflammatory behavior. Fluorescence microscopy however was prone to poor reproducibility due to background from the well plates and user variance during manual identification of cells. This issue of reproducibility, paired with the large number of cells, prompted us to employ flow cytometry as another semi-quantitative technique for assessing uptake of 2-NBDG.

The assay was initialized on the flow cytometer by comparing the MFIs of the M(-), M1, and M2 controls (Figure 2.7). A clear ~2.5-fold increase in glucose consumption is observed between the M1 cells and both the M2 and M(-) populations while no difference was observed between the M(-) and M2 cells, agreeing with data collected by Novak et al.[42] and shows that the assay was able to detect large differences in glucose consumption. After validating with controls, experiments studying the glucose uptake in the presence of exogenous NO were conducted. Interrogation of M1 and M2 cells co-stimulated with SNAP or NAP then showed that though SNAP was able to alter the glucose consumption of

macrophages, a significant difference between SNAP and NAP was not observed (Figures 2.8 and 2.9). In particular, M1 + 5 μM SNAP had ~60% less glucose consumption than the M1 population and M2 + 500 μM SNAP was able to increase glucose consumption by ~60%, relative to the M2 population, agreeing with the available literature on NO's effects on inflammation, wherein higher concentrations of NO (μM-nM) are associated with the inducible nitric oxide synthase and pro-inflammatory conditions.

As an alternative data analysis procedure, we also explored using the mode fluorescence intensity to characterize differences between populations. Using the mode as our measure of central tendency allowed us to use the maximum fluorescence signal of our population, which led to higher signal-to-noise ratios. Preliminary testing showed that with the mode fluorescence intensity, M2 + 500 μM SNAP cells showed a significant difference between the M2 control and the M2 + 5 μM SNAP (Figure 2.10). Additionally, when comparing the M2 + 500 μM SNAP cells and M2 cells, using the mode fluorescence intensity showed a similar increase to the relative MFI, showing the promise of this new analysis method in elucidating differences in glucose consumption.

2.4 Conclusions and Future Directions

Both of the assays described in this chapter attempted to elucidate the role of inflammation on macrophage glucose consumption. The 2-NBDG assay showed preliminary evidence supporting NO's possible therapeutic and inflammatory effects and continuous glucose monitoring in a 3D scaffold was able to differentiate M(-), M(IL-4), and M(Dex). Nonetheless, both assays can be improved to better quantify the relationship between NO exposure, macrophage polarization, and glucose consumption. First, a more robust characterization of the cells is imperative for correlating the glucose consumption to NO's effect on inflammation. Viability testing should occur on both platforms after exposure to NO, and after the sensing period on the 3D sensor platform, to correct for any changes in the cell

count that NO would produce, as the glucose consumption is proportional to the total number of cells. For viability measurements in the 3D gel specifically, while fluorescence live/dead staining (e.g., Calcein AM/Ethidium Homodimer) can be used for broad measurements, the gel can also be submerged in media to conduct a plate-based assay such as MTT/MTS or the lactase dehydrogenase assay, provided any incubation times are modified to account for diffusion through the scaffold. Lastly, inflammation and polarization markers (e.g., TNFα, IFNγ, CD163) should be surveyed alongside glucose consumption via gene or protein expression. Identifying NO-dose-dependent changes in the macrophage polarization state through expression changes of well-characterized biomarkers would aid in identifying concentrations at which glucose consumption is more likely to change and these data would elucidate the link between polarization state and glucose consumption.

The intrascaffold glucose monitoring system can specifically be improved in a number of additional ways. Ultimately, the goal for the platform would be to use NO-releasing sensors to assess in real-time how NO release affects the glucose consumption of differently polarized macrophages. However, prior to analysis with NO, the sensing platform should be made to be more reproducible and in particular, should be able to better differentiate between dramatically polarized macrophages. Once the assay has been fully validated, modeling could allow us to extract more quantitative information from the interrogation of macrophages. Novak et al. have used two-compartment diffusion models to simulate glucose transport from bulk (i.e., blood), through the collagen capsule, and to the sensor surface.[29,42,51,52] Using such a model with our system would allow determination of kinetic information for macrophage glucose consumption (e.g., V_{max}, K_M) and would allow us to support any conclusions of NO's effect on macrophage glucose consumption with recognized kinetic parameters and how they change in response to NO. Lastly, as this platform is currently unable to differentiate M1 and M(-), identifying any saturation in the sensitivity or shrinking of the dynamic range over time could provide insights to the discrepancy we observed. For example, preliminary data shows

that the phenol red from the DMEM is a significant interferent in the electrochemical measurement and experiments done using PBS supplemented with 10% FBS can reduce the interfering background current.

Assaying with 2-NBDG can also be made more robust. First, while 2-NBDG is a well-characterized glucose tracer, others have been synthesized and reported on.[53,54] Though they are considerably larger than 2-NBDG and would likely have more divergent transport through the glucose transporters compared to native glucose, these other tracers have much better quantum yields and are red-shifted relative to 2-NBDG, and thus will be less susceptible to biological autofluorescence.[53] The resultant increase in signal-to-noise would allow for more precise quantitation of glucose uptake. Another improvement to be made is the transfer of cells from the well-plate to the flow cytometer. Due to the high adhesion of RAW 264.7 cells to the well plates, they were subject to either scraping or high hydraulic pressure to remove them from the plate surface. Such methods can cause damage to the cell membrane, allowing potential leakage of 2-NBDG. Using gentler removal techniques, such as well plates with thermally-activated cell release, will allow for better interrogation.

Finally, it is critical that multiple NO-release kinetics be explored with this system to properly characterize NO's role in glucose consumption. Given that existing reports confirm different phenotypical outcomes when using different NO-release profiles,[24,40,41,55,56] it is likely that macrophage polarization would also be affected by varying the release kinetics. Preliminary data with using the relative MFIs of M1 + DETA/NO populations showed no statistical difference between the NO-releasing DETA/NO and the non-releasing DETA, similar to the measurements done with SNAP (Figure 2.11). However, again the glucose consumption with DETA/NO is being modulated compared to the M1 control, with decreasing glucose consumption observed at 5 μg/mL DETA/NO and increasing glucose consumption observed at 50 μg/mL. As DETA/NO has a much longer NO-release half-life, compared to the concentrations of SNAP surveyed in proteinaceous media, identifying whether the differences

in release kinetics are responsible for the different glucose consumptions between the SNAP- and DETA/NO-stimulated populations will help inform NO-release properties needed in vivo to specifically reduce the glucose depletion associated with macrophages at the CGM implant site.

In conclusion, the analysis of NO-affected macrophage polarization is still a promising area of research. Given both the role of macrophages in directing the FBR and their variable depletion of local glucose, identifying which NO fluxes lead to either pro- or anti-inflammatory behavior is essential to the rational design of NO-releasing sensors. Especially if NO affects the polarization state of the macrophage, using NO release to reduce any interfering glucose consumption from cells present at the implantation site will allow for extended sensor lifetimes and improved accuracy in vivo.

2.5 Figures and Tables

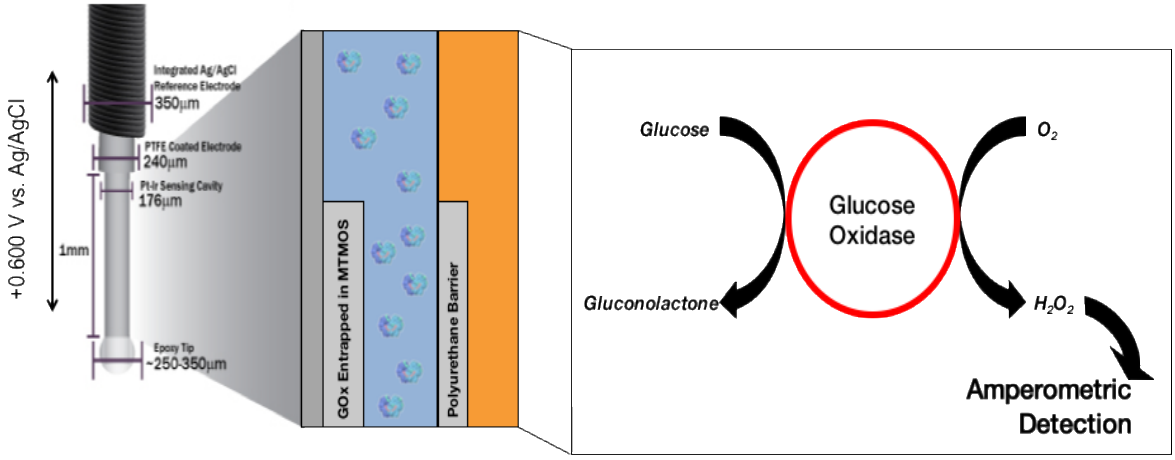

Figure 2.1. A schematic of our sensor set up. GOx is set on the electrode surface via an MTMOS sol-gel and a polyurethane barrier is set on top of it. Glucose and oxygen will diffuse through the polyurethane barrier to the enzyme layer where H_2O_2 is produced and detected at +0.6 V vs Ag|AgCl.

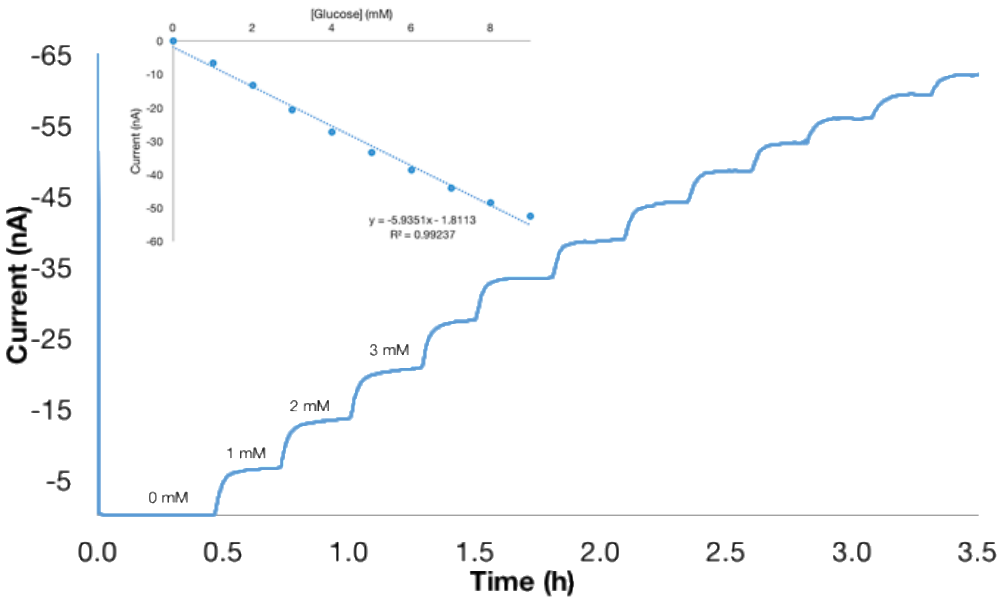

Figure 2.2. Representative calibration of a glucose sensor. After signal stabilization, glucose is injected. The current at that time point and glucose concentration is used for a calibration curve (glucose concentration (mM) vs current (nA)), as seen in the inset.

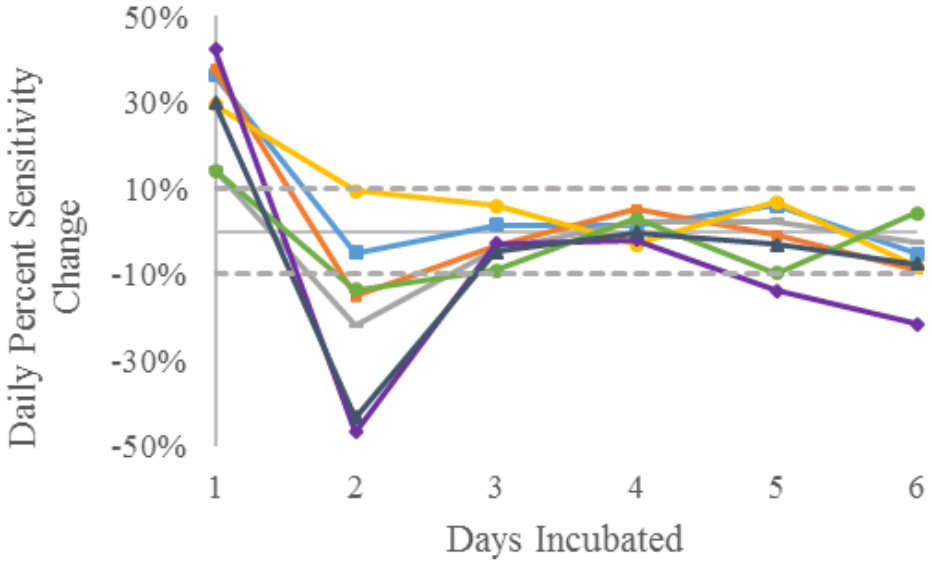

Figure 2.3. Sensitivity retention experiments were conducted by monitoring sensitivities of seven sensors incubated in 1X DMEM over a week, with each line represented a unique sensor. By the third day, sensitivity changes between consecutive days dropped to <10% a day for all but one sensor.

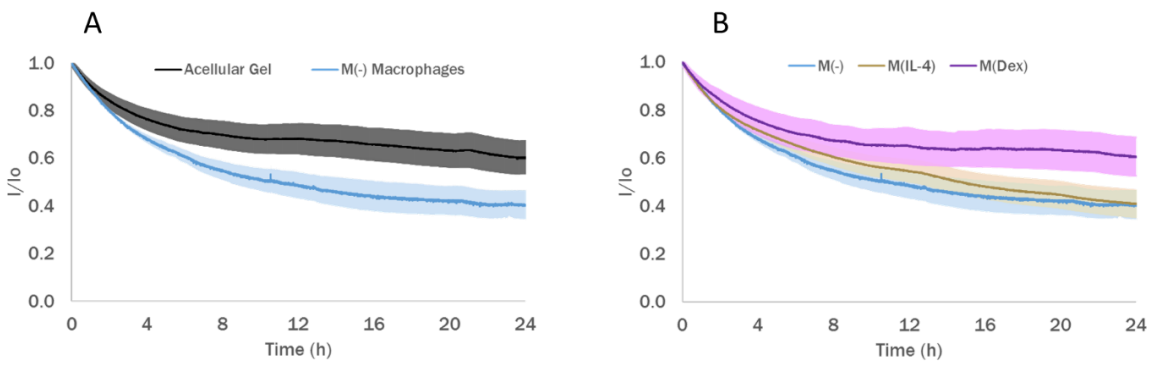

Figure 2.4. Sensors monitored glucose consumption in hydrogels containing different macrophage populations, with the average decline from the original signal plotted against time, shaded area representing standard error for N ≥ 3 sensors. A) M(-)-seeded hydrogels show a larger glucose consumption than acellular hydrogels. B) M(IL-4) and M(Dex)-seeded hydrogels show a possible decrease in both total glucose consumption and the rate of consumption.

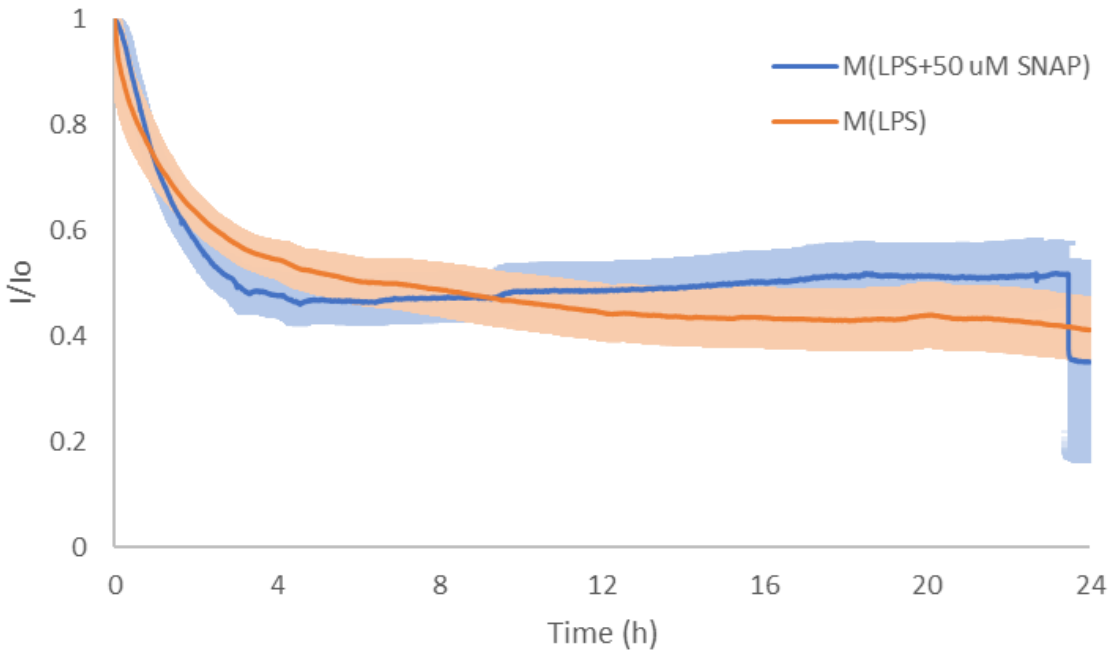

Figure 2.5. Sensors monitored glucose consumption in hydrogels containing macrophages stimulated with either 1 μg/mL LPS or 1 μg/mL LPS and 50 μM SNAP, with the average decline from the original signal plotted against time and the shaded area representing standard error for N ≥ 3 sensors.

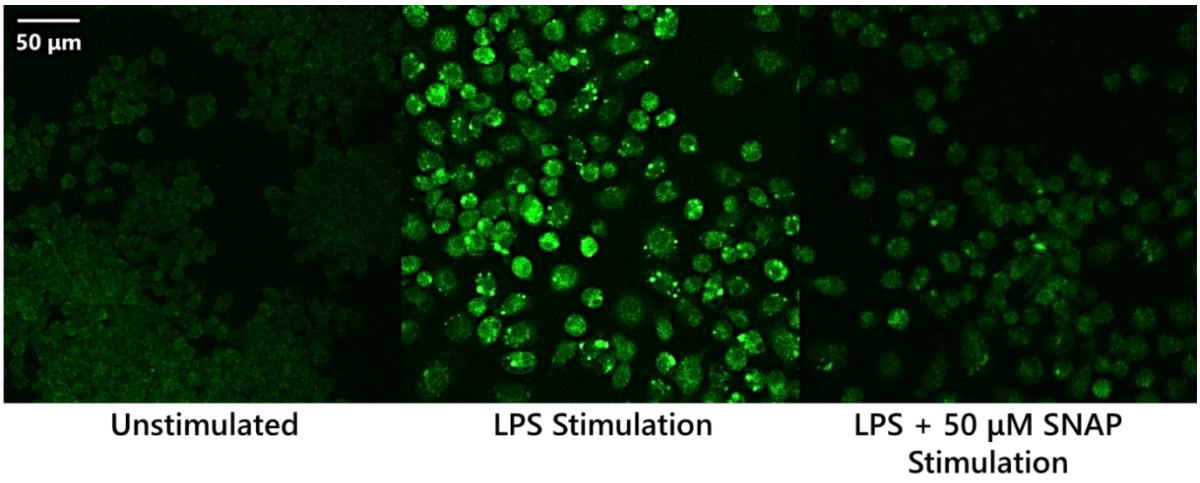

Figure 2.6. Fluorescence micrographs displaying differential 2-NBDG accumulation in macrophages as a function of polarization conditions. All images were acquired using the same exposure time.

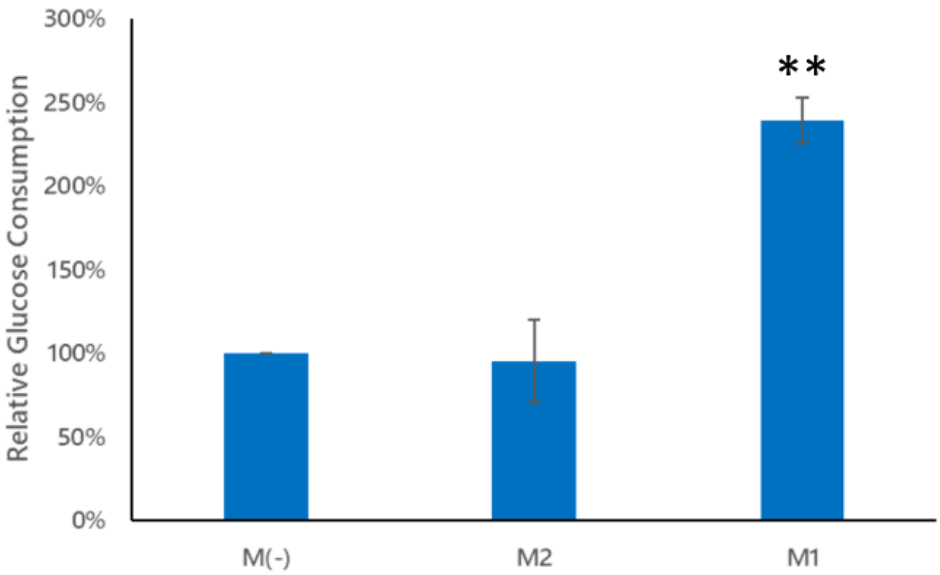

Figure 2.7. Macrophages in M(-), M2, and M1 phenotypes were analyzed for 2-NBDG accumulation using the Attune NxT flow cytometer. Glucose consumption was measured relative to the M(-) population. Error bars represent standard error, N ≥ 4 trials. Statistical significance was calculated using 2-tailed heteroscedastic t-tests. ** = $p < 0.005$, compared to M(-)

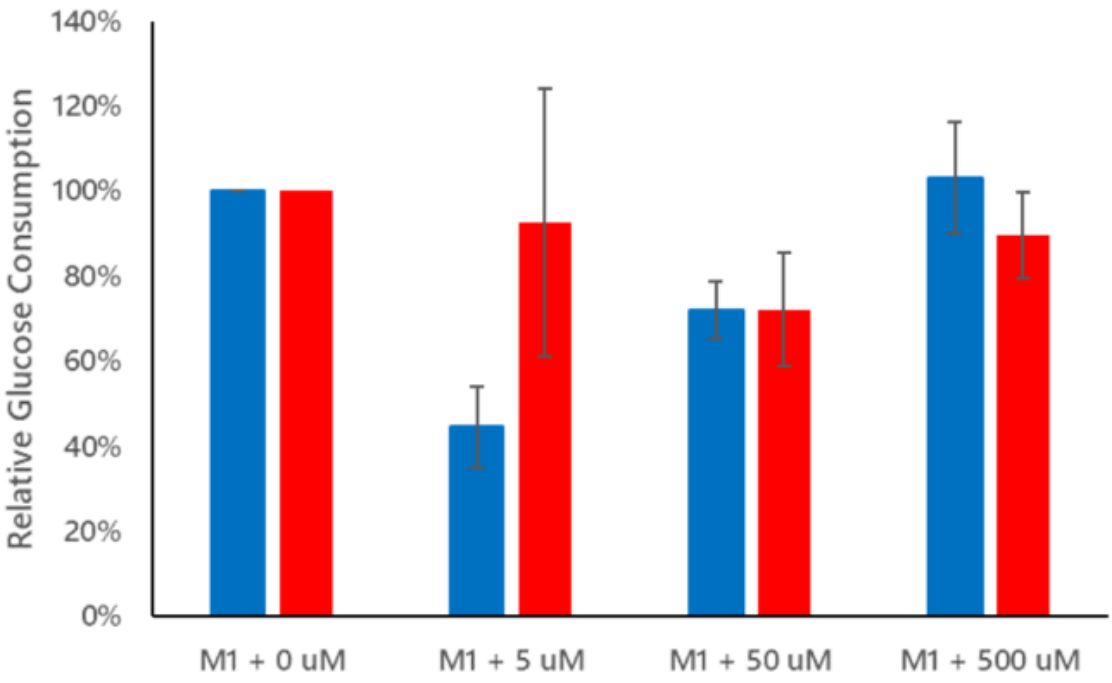

Figure 2.8. Macrophages were co-stimulated with 0–500 μM SNAP (blue) or NAP (red), in addition to 1 μg/mL LPS were analyzed for 2-NBDG accumulation using the Attune NxT flow cytometer. Glucose consumption was measured relative to M1 without the addition of SNAP or NAP. Error bars represent standard error, N ≥ 4 trials.

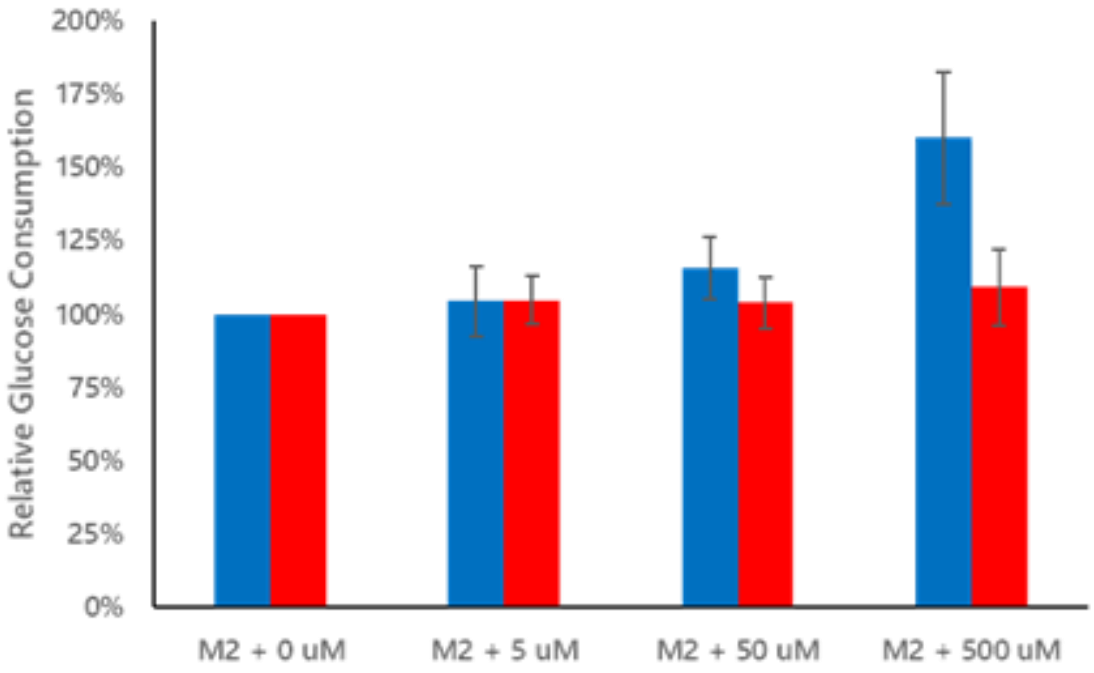

Figure 2.9. Macrophages were co-stimulated with 0–500 μM SNAP (blue) or NAP (red), in addition to 0.1 μM dexamethasone were analyzed for 2-NBDG accumulation using the Attune NxT flow cytometer. Glucose consumption was measured relative to M2 without the addition of SNAP or NAP. Error bars represent standard error, N ≥ 4 trials.

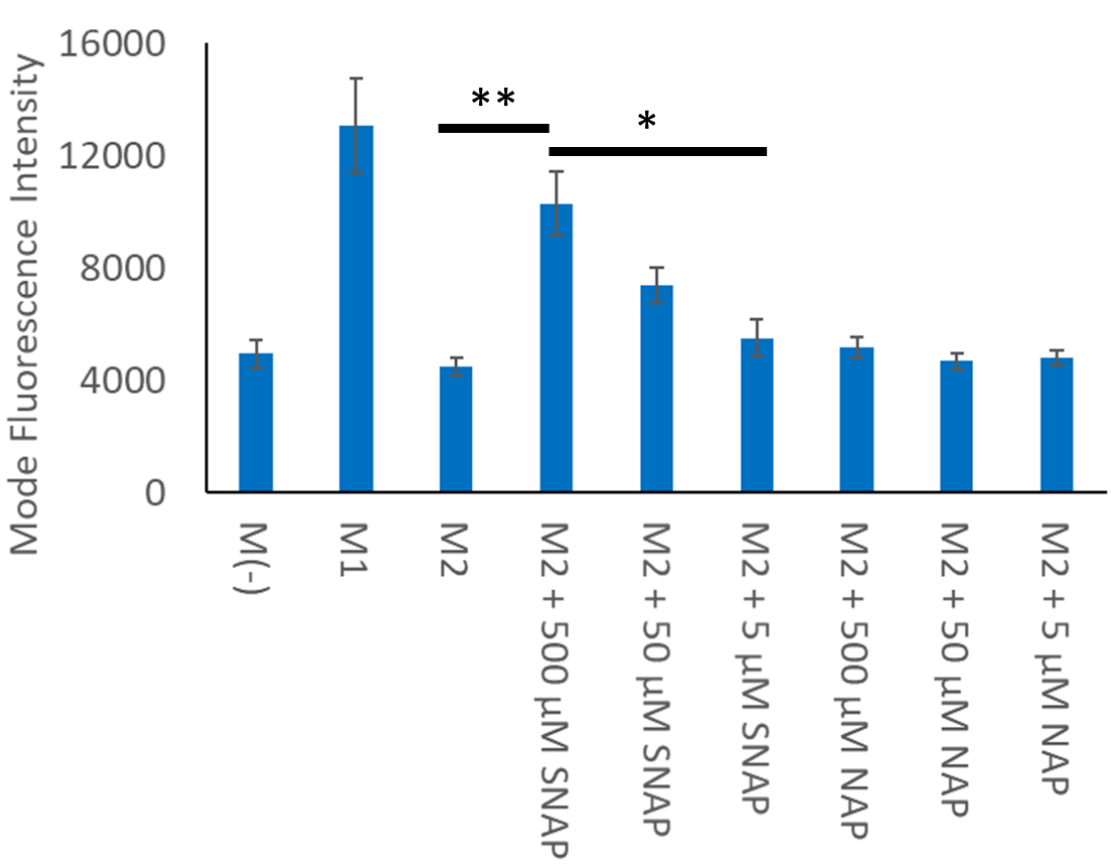

Figure 2.10. M2 macrophages were co-stimulated with 0–500 µM SNAP or NAP, and were analyzed for 2-NBDG accumulation using the Attune NxT flow cytometer and plotted according to their average mode fluorescence intensities ± standard error of the mean for N ≥ 3 trials. Statistical significance was calculated using 2-tailed heteroscedastic t-tests. * = $p < 0.05$, ** = $p < 0.005$

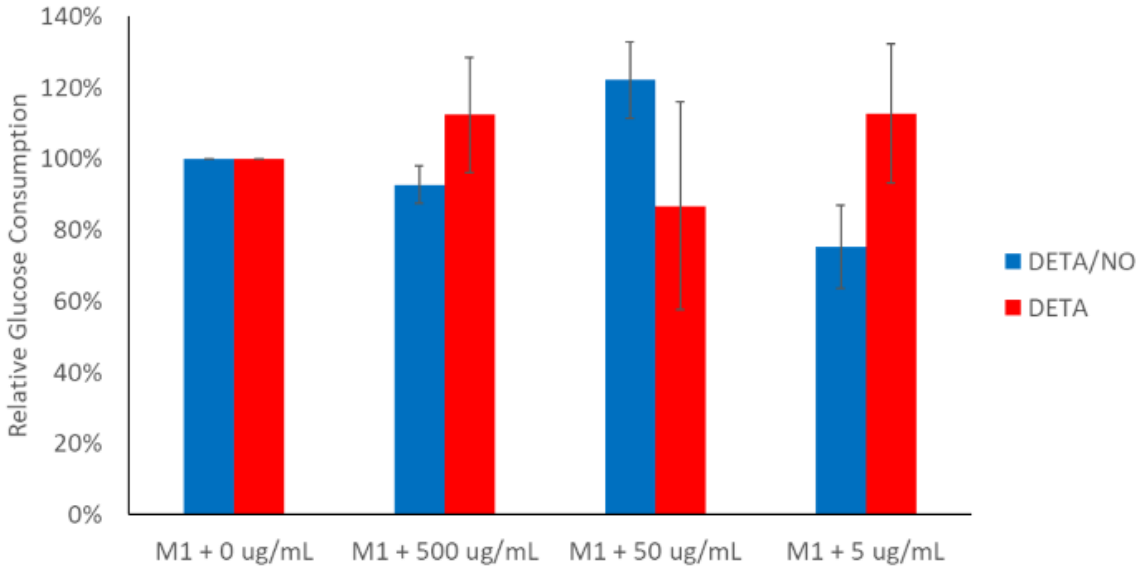

Figure 2.11. Macrophages were co-stimulated with 0–500 μg/mL DETA/NO (blue) or DETA (red), in addition to 1 μg/mL LPS for 2-NBDG accumulation using the Attune NxT flow cytometer. Glucose consumption was measured relative to M(LPS), both without the addition of DETA/NO or DETA. Error bars represent standard error, N ≥ 4 trials.

REFERENCES

(1) Farmer, A.; Balman, E.; Gadsby, R.; Moffatt, J.; Cradock, S.; McEwen, L.; Jameson, K. Frequency of Self-Monitoring of Blood Glucose in Patients with Type 2 Diabetes: Association with Hypoglycaemic Events. *Curr. Med. Res. Opin.* **2008**, *24* (11), 3097–3104.

(2) Miller, K. M.; Beck, R. W.; Bergenstal, R. M.; Goland, R. S.; Haller, M. J.; McGill, J. B.; Rodriguez, H.; Simmons, J. H.; Hirsch, I. B. Evidence of a Strong Association between Frequency of Self-Monitoringof Blood Glucose and Hemoglobin A1c Levels in T1D Exchange Clinic Registry Participants. *Diabetes Care* **2013**, *36* (7), 2009–2014.

(3) Beck, R. W. Sustained Benefit of Continuous Glucose Monitoring on A1C, Glucose Profiles, and Hypoglycemia in Adults With Type 1 Diabetes. *Diabetes Care* **2009**, *32* (11), 2047–2049.

(4) Deiss, D.; Bolinder, J.; Riveline, J. P.; Battelino, T.; Bosi, E.; Tubiana-Rufi, N.; Kerr, D.; Phillip, M. Improved Glycemic Control in Poorly Controlled Patients with Type 1 Diabetes Using Real-Time Continuous Glucose Monitoring. *Diabetes Care* **2006**, *29* (12), 2730–2732.

(5) O'Connell, M. A.; Donath, S.; O'Neal, D. N.; Colman, P. G.; Ambler, G. R.; Jones, T. W.; Davis, E. A.; Cameron, F. J. Glycaemic Impact of Patient-Led Use of Sensor-Guided Pump Therapy in Type 1 Diabetes: A Randomised Controlled Trial. *Diabetologia* **2009**, *52* (7), 1250–1257.

(6) Kastellorizios, M.; Tipnis, N.; Burgess, D. J. Immune Responses to Biosurfaces. In *Advances in Experimental Medicine and Biology*; Lambris, J. D., Ekdahl, K. N., Ricklin, D., Nilsson, B., Eds.; Advances in Experimental Medicine and Biology; Springer International Publishing: Cham, 2015; Vol. 865, pp 812–823.

(7) Anderson, J. M.; Rodriguez, A.; Chang, D. T. Foreign Body Reaction to Biomaterials. *Semin. Immunol.* **2008**, *20* (2), 86–100.

(8) Sheikh, Z.; Brooks, P.; Barzilay, O.; Fine, N.; Glogauer, M. Macrophages, Foreign Body Giant Cells and Their Response to Implantable Biomaterials. *Materials (Basel).* **2015**, *8* (9), 5671–5701.

(9) Wang, Y.; Papadimitrakopoulos, F.; Burgess, D. J. Polymeric "Smart" Coatings to Prevent Foreign Body Response to Implantable Biosensors. *J. Control. Release* **2013**, *169* (3), 341–347.

(10) Luu, T. U.; Gott, S. C.; Woo, B. W. K.; Rao, M. P.; Liu, W. F. Micro- and Nanopatterned Topographical Cues for Regulating Macrophage Cell Shape and Phenotype. *ACS Appl. Mater. Interfaces* **2015**, *7* (51), 28665–28672.

(11) Nichols, S. P.; Koh, A.; Storm, W. L.; Shin, J. H.; Schoenfisch, M. H. Biocompatible Materials for Continuous Glucose Monitoring Devices. *Chem. Rev.* **2013**, *113* (4), 2528–2549.

(12) Veiseh, O.; Doloff, J. C.; Ma, M.; Vegas, A. J.; Tam, H. H.; Bader, A. R.; Li, J.; Langan, E.; Wyckoff, J.; Loo, W. S.; Jhunjhunwala, S.; Chiu, A.; Siebert, S.; Tang, K.; Hollister-

Lock, J.; Aresta-Dasilva, S.; Bochenek, M.; Mendoza-Elias, J.; Wang, Y.; Qi, M.; Lavin, D. M.; Chen, M.; Dholakia, N.; Thakrar, R.; Lacík, I.; Weir, G. C.; Oberholzer, J.; Greiner, D. L.; Langer, R.; Anderson, D. G. Size- and Shape-Dependent Foreign Body Immune Response to Materials Implanted in Rodents and Non-Human Primates. *Nat. Mater.* **2015**, *14* (6), 643–651.

(13) Soto, R. J.; Hall, J. R.; Brown, M. D.; Taylor, J. B.; Schoenfisch, M. H. In Vivo Chemical Sensors: Role of Biocompatibility on Performance and Utility. *Anal. Chem.* **2017**, *89* (1), 276–299.

(14) Kiss, J. P. Role of Nitric Oxide in the Regulation of Monoaminergic Neurotransmission. *Brain Res. Bull.* **2000**, *52* (6), 459–466.

(15) Hickok, J. R.; Thomas, D. D. Nitric Oxide and Cancer Therapy: The Emperor Has NO Clothes. *Curr. Pharm. Des.* **2010**, *16* (4), 381–391.

(16) Schairer, D. O.; Chouake, J. S.; Nosanchuk, J. D.; Friedman, A. J. The Potential of Nitric Oxide Releasing Therapies as Antimicrobial Agents. *Virulence* **2012**, *3* (3), 271–279.

(17) Broughton 2nd, G.; Janis, J. E.; Attinger, C. E. The Basic Science of Wound Healing. *Plast. Reconstr. Surg.* **2006**, *117* (7 Suppl), 12S-34S.

(18) Morbidelli, L.; Donnini, S.; Ziche, M. Role of Nitric Oxide in the Modulation of Angiogenesis. *Curr. Pharm. Des.* **2003**, *9*, 521–530.

(19) Nablo, B. J.; Prichard, H. L.; Butler, R. D.; Klitzman, B.; Schoenfisch, M. H. Inhibition of Implant-Associated Infections via Nitric Oxide Release. *Biomaterials* **2005**, *26* (34), 6984–6990.

(20) Gifford, R.; Batchelor, M. M.; Lee, Y.; Gokulrangan, G.; Meyerhoff, M. E.; Wilson, G. S. Mediation of in Vivo Glucose Sensor Inflammatory Response via Nitric Oxide Release. *J. Biomed. Mater. Res. Part A* **2005**, *75A* (4), 755–766.

(21) Lancaster, J. R. A Tutorial on the Diffusibility and Reactivity of Free Nitric Oxide. *Nitric Oxide* **1997**, *1* (1), 18–30.

(22) Nichols, S. P.; Le, N. N.; Klitzman, B.; Schoenfisch, M. H. Increased In Vivo Glucose Recovery via Nitric Oxide Release. *Anal. Chem.* **2011**, *83* (4), 1180–1184.

(23) Soto, R. J.; Privett, B. J.; Schoenfisch, M. H. In Vivo Analytical Performance of Nitric Oxide-Releasing Glucose Biosensors. *Anal. Chem.* **2014**, *86* (14), 7141–7149.

(24) Malone-Povolny, M. J.; Merricks, E. P.; Wimsey, L. E.; Nichols, T. C.; Schoenfisch, M. H. Long-Term Accurate Continuous Glucose Biosensors via Extended Nitric Oxide Release. *ACS Sensors* **2019**, *4* (12), 3257–3264.

(25) Mosser, D. M.; Edwards, J. P. Exploring the Full Spectrum of Macrophage Activation. *Nat. Rev. Immunol.* **2008**, *8* (12), 958–969.

(26) Tobergte, D. R.; Curtis, S. Macrophages: A Review of Their Role in Wound Healing and Their Therapeutic Use Title. *J. Chem. Inf. Model.* **2013**, *53* (9), 1689–1699.

(27) Murray, P. J.; Allen, J. E.; Biswas, S. K.; Fisher, E. A.; Gilroy, D. W.; Goerdt, S.; Gordon, S.; Hamilton, J. A.; Ivashkiv, L. B.; Lawrence, T.; Locati, M.; Mantovani, A.; Martinez, F. O.; Mege, J.-L.; Mosser, D. M.; Natoli, G.; Saeij, J. P.; Schultze, J. L.; Shirey, K.; Sica, A.; Suttles, J.; Udalova, I.; van Ginderachter, J. A.; Vogel, S. N.;

Wynn, T. A. Macrophage Activation and Polarization: Nomenclature and Experimental Guidelines. *Immunity* **2014**, *41* (1), 14–20.

(28) Mantovani, A.; Sica, A.; Sozzani, S.; Allavena, P.; Vecchi, A.; Locati, M. The Chemokine System in Diverse Forms of Macrophage Activation and Polarization. *Trends Immunol.* **2004**, *25* (12), 677–686.

(29) Novak, M. T.; Yuan, F.; Reichert, W. M. Predicting Glucose Sensor Behavior in Blood Using Transport Modeling: Relative Impacts of Protein Biofouling and Cellular Metabolic Effects. *J. Diabetes Sci. Technol.* **2013**, *7* (6), 1547–1560.

(30) Klueh, U.; Frailey, J. T.; Qiao, Y.; Antar, O.; Kreutzer, D. L. Cell Based Metabolic Barriers to Glucose Diffusion: Macrophages and Continuous Glucose Monitoring. *Biomaterials* **2014**, *35* (10), 3145–3153.

(31) Klueh, U.; Qiao, Y.; Frailey, J. T.; Kreutzer, D. L. Impact of Macrophage Deficiency and Depletion on Continuous Glucose Monitoring Invivo. *Biomaterials* **2014**, *35* (6), 1789–1796.

(32) Johnson, A. R.; Qin, Y.; Cozzo, A. J.; Freemerman, A. J.; Huang, M. J.; Zhao, L.; Sampey, B. P.; Milner, J. J.; Beck, M. A.; Damania, B.; Rashid, N.; Galanko, J. A.; Lee, D. P.; Edin, M. L.; Zeldin, D. C.; Fueger, P. T.; Dietz, B.; Stahl, A.; Wu, Y.; Mohlke, K. L.; Makowski, L. Metabolic Reprogramming through Fatty Acid Transport Protein 1 (FATP1) Regulates Macrophage Inflammatory Potential and Adipose Inflammation. *Mol. Metab.* **2016**, *5* (7), 506–526.

(33) Freemerman, A. J.; Johnson, A. R.; Sacks, G. N.; Milner, J. J.; Kirk, E. L.; Troester, M. A.; Macintyre, A. N.; Goraksha-Hicks, P.; Rathmell, J. C.; Makowski, L. Metabolic Reprogramming of Macrophages: Glucose Transporter 1 (GLUT1)-Mediated Glucose Metabolism Drives a Proinflammatory Phenotype. *J. Biol. Chem.* **2014**, *289* (11), 7884–7896.

(34) Palmer, C. S.; Anzinger, J. J.; Zhou, J.; Gouillou, M.; Landay, A.; Jaworowski, A.; McCune, J. M.; Crowe, S. M. Glucose Transporter 1–Expressing Proinflammatory Monocytes Are Elevated in Combination Antiretroviral Therapy–Treated and Untreated HIV+ Subjects. *J. Immunol.* **2014**, *193* (11), 5595–5603.

(35) Vats, D.; Mukundan, L.; Odegaard, J. I.; Zhang, L.; Smith, K. L.; Morel, C. R.; Greaves, D. R.; Murray, P. J.; Chawla, A. Oxidative Metabolism and PGC-1β Attenuate Macrophage-Mediated Inflammation. *Cell Metab.* **2006**, *4* (1), 13–24.

(36) Namgaladze, D.; Brüne, B. Macrophage Fatty Acid Oxidation and Its Roles in Macrophage Polarization and Fatty Acid-Induced Inflammation. *Biochim. Biophys. Acta - Mol. Cell Biol. Lipids* **2016**, *1861* (11), 1796–1807.

(37) Brown, B. N.; Londono, R.; Tottey, S.; Zhang, L.; Kukla, K. A.; Wolf, M. T.; Daly, K. A.; Reing, J. E.; Badylak, S. F. Macrophage Phenotype as a Predictor of Constructive Remodeling Following the Implantation of Biologically Derived Surgical Mesh Materials. *Acta Biomater.* **2012**, *8* (3), 978–987.

(38) Badylak, S. F.; Valentin, J. E.; Ravindra, A. K.; McCabe, G. P.; Stewart-Akers, A. M. Macrophage Phenotype as a Determinant of Biologic Scaffold Remodeling. *Tissue Eng. Part A* **2008**, *14* (11), 1835–1842.

(39) Hetrick, E. M.; Prichard, H. L.; Klitzman, B.; Schoenfisch, M. H. Reduced Foreign Body Response at Nitric Oxide-Releasing Subcutaneous Implants. *Biomaterials*

2007, *28* (31), 4571–4580.

(40) Nichols, S. P.; Koh, A.; Brown, N. L.; Rose, M. B.; Sun, B.; Slomberg, D. L.; Riccio, D. A.; Klitzman, B.; Schoenfisch, M. H. The Effect of Nitric Oxide Surface Flux on the Foreign Body Response to Subcutaneous Implants. *Biomaterials* **2012**, *33* (27), 6305–6312.

(41) Soto, R. J.; Merricks, E. P.; Bellinger, D. A.; Nichols, T. C.; Schoenfisch, M. H. Influence of Diabetes on the Foreign Body Response to Nitric Oxide-Releasing Implants. *Biomaterials* **2018**, *157*, 76–85.

(42) Novak, M. T.; Yuan, F.; Reichert, W. M. Macrophage Embedded Fibrin Gels: An in Vitro Platform for Assessing Inflammation Effects on Implantable Glucose Sensors. *Biomaterials* **2014**, *35* (36), 9563–9572.

(43) Zou, C.; Wang, Y.; Shen, Z. 2-NBDG as a Fluorescent Indicator for Direct Glucose Uptake Measurement. *J. Biochem. Biophys. Methods* **2005**, *64* (3), 207–215.

(44) Tao, J.; Diaz, R. K.; Teixeira, C. R. V; Hackmann, T. J. Transport of a Fluorescent Analogue of Glucose (2-NBDG) versus Radiolabeled Sugars by Rumen Bacteria and Escherichia Coli. *Biochemistry* **2016**, *55* (18), 2578–2589.

(45) Yoshioka, K.; Takahashi, H.; Homma, T.; Saito, M.; Oh, K. B.; Nemoto, Y.; Matsuoka, H. A Novel Fluorescent Derivative of Glucose Applicable to the Assessment of Glucose Uptake Activity of Escherichia Coli. *Biochim. Biophys. Acta - Gen. Subj.* **1996**, *1289* (1), 5–9.

(46) Yamamoto, N.; Ueda-wakagi, M.; Sato, T.; Kawasaki, K.; Sawada, K.; Kawabata, K.; Akagawa, M. Measurement of Glucose Uptake in Cultured Cells. In *Current Protocols in Pharmacology*; 2015; pp 12.14.1-12.14.26.

(47) Chipinda, I.; Simoyi, R. H. Formation and Stability of a Nitric Oxide Donor: S-Nitroso-W- Acetylpenicillamine. *J. Phys. Chem. B* **2006**, *110* (10), 5052–5061.

(48) Bindra, D. S.; Zhang, Y.; Wilson, G. S.; Sternberg, R.; Thévenot, D. R.; Moatti, D.; Reach, G. Design and in Vitro Studies of a Needle-Type Glucose Sensor for Subcutaneous Monitoring. *Anal. Chem.* **1991**, *63* (17), 1692–1696.

(49) Koh, A.; Riccio, D. a.; Sun, B.; Carpenter, A. W.; Nichols, S. P.; Schoenfisch, M. H. Fabrication of Nitric Oxide-Releasing Polyurethane Glucose Sensor Membranes. *Biosens. Bioelectron.* **2011**, *28* (1), 17–24.

(50) Clarke, W. L.; Kovatchev, B. Continuous Glucose Sensors: Continuing Questions about Clinical Accuracy. *J. Diabetes Sci. Technol.* **2007**, *1* (5), 669–675.

(51) Novak, M. T.; Reichert, W. M. Modeling the Physiological Factors Affecting Glucose Sensor Function in Vivo. *J. Diabetes Sci. Technol.* **2015**, *9* (5), 993–998.

(52) Novak, M. T.; Yuan, F.; Reichert, W. M. Modeling the Relative Impact of Capsular Tissue Effects on Implanted Glucose Sensor Time Lag and Signal Attenuation. *Anal. Bioanal. Chem.* **2010**, *398* (4), 1695–1705.

(53) Lee, H. Y.; Lee, J. J.; Park, J.; Park, S. B. Development of Fluorescent Glucose Bioprobes and Their Application on Real-Time and Quantitative Monitoring of Glucose Uptake in Living Cells. *Chem. - A Eur. J.* **2011**, *17* (1), 143–150.

(54) Kim, W. H.; Lee, J.; Jung, D. W.; Williams, D. R. Visualizing Sweetness: Increasingly Diverse Applications for Fluorescent-Tagged Glucose Bioprobes and Their Recent Structural Modifications. *Sensors* **2012**, *12* (4), 5005–5027.

(55) Seo, J. Y.; Yu, J. H.; Lim, J. W.; Mukaida, N.; Kim, H. Nitric Oxide-Induced IL-8 Expression Is Mediated by NF-KappaB and AP-1 in Gastric Epithelial AGS Cells. *J. Physiol. Pharmacol.* **2009**, *60 Suppl 7* (26), 101–106.

(56) Suchyta, D. J.; Schoenfisch, M. H. Anticancer Potency of Nitric Oxide-Releasing Liposomes. *RSC Adv.* **2017**, *7* (84), 53236–53246.

CHAPTER 3 – ELUCIDATING BIOLOGICAL MECHANISMS OF IMPROVED HOST RESPONSE TO NITRIC OXIDE-RELEASING IMPLANTS

3.1. Introduction

Nitric oxide (NO) is a diatomic gasotransmitter with multiple endogenous roles, including the facilitation of intercellular communication, the regulation of inflammation, and a promotion of wound healing via in angiogenesis.[1–6] These characteristics have prompted the study of NO release to achieve anti-inflammatory and pro-wound healing outcomes an attractive area of research.[7–10] In particular, the active release of NO from the outer sensor membrane of glucose biosensors has been investigated as a means to improve sensor performance by mitigating the host response.[7–14] For transcutaneously implanted sensors, the improved sensor performance has been attributed to a reduced foreign body response (FBR).[11,15] The FBR induces cell infiltration over time to neutralize the implant, notably through the efflux of reactive oxygen and nitrogen in attempt to destroy the foreign object and later isolate it by collagenous encapsulation. Though many strategies exist for addressing the FBR,[11,15,16] NO release has unique advantages over most because sensor membranes need only modified via incorporation of NO donor.[9,17–20] Due to a short half-life (seconds) and travel distance (~200 μm),[21] NO has been shown to produce a uniquely localized effect.

The first studies concerning NO-releasing implantable glucose sensors employed a rat model in which these implants resulted in improved sensor accuracy, lower inflammatory cell infiltration and collagen capsule density, and increased markers of angiogenesis.[7,8,14] More recent in vivo work has transitioned to the use of porcine models due to greater similarity to between human tissue responses and blood flow, and the higher potential to study the impact

of diabetes.[22–24] These studies were shown to replicate similar behavior as seen in rats but at extended implant periods.[9,10,13] Literature has indicated that sustained NO release is necessary to stave off the inflammation response and promote favorable wound healing.[9,10,12] Though these studies support the utility of NO-releasing implantable sensors, the exact mechanisms through which exogenous NO acts on the surrounding tissue remain unclear. Elucidating these immune pathways may help identify strategies to refine NO payloads and release kinetics for optimal therapeutic efficacy. Herein, we present the first study examining the mechanisms that drive the host response from exogenous NO.

3.2. Materials and Methods

3.2.1 Materials

All materials were received as analytical grade and used as received unless otherwise noted. Sodium nitrite ($NaNO_2$), triethylamine, cetyltrimethylammonium bromide (CTAB), concen- trated hydrochloric acid (HCl), diethylenetriaminepentaacetic acid, and glutaraldehyde purchased from Sigma-Aldrich (St. Louis, MO). Ethanol (EtOH), methanol (MeOH), ammonium hydroxide (NH_4OH, 28 wt %), anhydrous N,N-dimethylformamide (DMF), anhydrous tetrahydrofuran (THF), RNAlater RNA Isolation Solution, and T-PER Protein Extraction Buffer were purchased from Fisher Scientific (Fair Lawn, NJ). Tetraethylorthosilicate (TEOS) and 3-mercaptopropyltrimethoxysilane (MPTMS) were obtained from Gelest (Morrisville, PA) and stored under nitrogen atmosphere. Polyurethanes HP93A and PC3585A were received as medical grade from Lubrizol (Cleveland, OH). Nitrogen (N_2) and nitric oxide (NO) calibration gas (25.87 ppm, balance N_2) were purchased from Airgas National Welders (Raleigh, NC). Water was purified using a Millipore water purification system (Bedford, MA) to a resistivity of 18.2 MΩ cm and a total organic content of < 6 ppb.

3.2.2 Particle Synthesis

Porous silica nanoparticles were synthesized as reported in previously published literature.[12,20] Briefly, a bolus of TEOS was injected to a solution of ethanol, water, NH_4Oh, and CTAB. Particles were washed with ethanol, isolated with centrifugation, and post-grafted with MPTMS, thiolating the interior and exterior of the particle. These particles were then nitrosated in a solution of acidified nitrite at 0 °C. Particles were synthesized and handled in the dark to prevent premature light-activated NO release. Non-releasing particles were synthesized in the same manner, omitting the nitrosation step.

3.2.3 In Vivo Protocol

All procedures and protocols were in accordance with institutional guidelines and approved by the Institutional Animal Care and Use Committee at the University of North Carolina in Chapel Hill. A single Sinclair piglet was included in this study and fed the Teklad Miniswine diet (7037; Teklad, Madison, WI).

In this work, we evaluated local immunological mechanisms using a euglycemic porcine model.[9,10,13] Briefly, mock sensors were coated with polyurethanes containing either NO-releasing or non-releasing nanoparticles. The mock sensor was designed to replicate the geometry and NO-release profile of an NO-releasing glucose biosensor, with an initial NO flux of roughly 6 pmol cm^{-2} s^{-1} that decreases to roughly 2 and 1 pmol cm^{-2} s^{-1} by day 7 and 14, respectively.[12,20] These sensors were fabricated in a biosafety cabinet by first sterilizing steel wire in 5% glutaraldehyde for 1 h, and loopcasting (i.e., 6.5 µL solution applied using a 2 mm steel wire loop) 10 coats of 25 mg mL^{-1} particles:25 mg mL^{-1} HP93A in 3:1 THF:DMF, with 4 min drying between each coat. A single loopcast of 3:1 PC3585A:HP93A in THF:DMF was applied, followed by a 30 min air dry. Implants were fabricated < 12 h prior to implantation and stored in centrifuge tubes contained in vacuum-sealed backs and kept at -20 °C until usage. Sensors were brought to room temperature ~ 2 min before implantation.

Three NO-releasing and non-releasing mock sensors (total of six) were implanted subcutaneously into the dorsum of a swine. The implants were explanted in a tissue block from the swine after either 7 or 14 days. The site of implantation was isolated from the explanted tissue using a biopsy punch. Biopsies were also obtained on day 0 (i.e., implantation day) and day 14 from an area without implants to serve as tissue-specific controls (i.e., no FBR influence). These three sample types are hereforward differentiated as NO-releasing, non-releasing, and control biopsy. Samples were vertically bisected along the sensor track, with each half is placed into either 0.6 mL of T-PER protein extraction buffer or 1 mL of RNAlater for protein and gene analysis respectively. The protein analysis samples are frozen immediately in a -80 °C freezer. The gene analysis samples are stored in a 4 °C fridge for < 1 week to promote full perfusion into the tissue. After perfusion, the gene analysis samples were moved to a -20 freezer for long term storage.

3.2.4 Cytokine Quantification

The tissue was homogenized in the T-PER and the homogenate was analyzed on the Luminex plate according to manufacturer protocol. Briefly, the Milliplex plate was filled with 25 µL of the bead suspension, 25 µL of buffer, and 25 µL of either the standard, control, or sample, in each well. These components were incubated overnight at 4 °C. Following the overnight incubation, the well plate was washed thrice with 200 µL of wash buffer per well, using a magnet to prevent loss of the magnetic beads during washing. After washing, 50 µL of the detection antibodies were added to each well and the plate was incubated for two hours. The plate was washed again after incubation and 50 µL of the included streptavidin-phycoerythrin solution was added for a 30 min incubation. Following a final 3X wash cycle, 100 µL of sheath fluid was added to resuspend the beads and the plate was run. Calibration standards for each of the target proteins were used to quantify the cytokine content of the porcine tissue. All cytokine concentrations are reported as the average of the three tissue

samples ± the standard error of the mean. P-values were assessed using two-tailed heteroscedastic t-tests.

3.2.5 Gene Expression Analysis

Utilizing Qiagen Tissuelyser II (Qiagen; Germantown, MD), tissue was homogenized in 2ml screw top tubes according to manufacturer instructions. The homogenized lysate was then processed with Qiagen RNeasy Fibrous Mini kit, including DNase I treatment, according to the included protocol. RNA was eluted from the column with 45 ul of nuclease-free water and frozen at -80 °C until further use. Before usage, the RNA was quantified using a Qubit fluorometer, according to standard protocol. The RNA was diluted to 1 ng/mL and 5 µL of the RNA solution was mixed with 8 µL Master Mix and 2 µL of the Capture Probe, both of which were provided in the kit. The mixture was left to hybridize on a Thermocycler at 65 °C overnight (~16-18 h). Following hybridization, the hybridized RNA was loaded onto the sample plate and run on a NanoString nCounter SPRINT Profiler. Both the predictive cell profiling and differential expression analyses were performed using NanoString's nSolver software.

3.3. Results and Discussion

3.3.1. Multiplex Protein Analysis

A porcine Luminex panel was used to assess the concentrations of immunomodulators within tissues surrounding NO-releasing implants and the non-releasing implants at 7- and 14-days post-implantation, and the FBR-free control biopsies (Figure 3.1). Using these three types of samples, we can compare soluble mediator expression between 1) native tissue and the FBR; 2) changes/shifts in the FBR-induced expression profile as a function of NO release; and, 3) the profile due to NO-releasing implants relative to native tissue. On day 14, IL-8

proved more abundant in the biopsy while TNFα, IL-1RA, IL-18, and IL-10 levels were greater in tissue having an FBR response (i.e., the non-releasing implants). The elevated cytokine levels are expected based on the increased immune signaling initiated by the FBR.[25–28] As a regular of granulocyte migration, IL-8 was decreased in the tissue surrounding the implant compared to the biopsy at day 7 and 14 because in a typical FBR timeline, granulocyte (i.e. neutrophil) infiltration resolves earlier (day 3).[26]

Several differences in soluble mediator profiles in tissues surrounding NO- and non-releasing sensors are apparent. None of the cytokines measured increased in concentration with NO release, suggesting that the sustained release of NO at the implant-tissue interface suppresses cytokine responses. Additionally, the cytokine levels surrounding the NO-releasing implants were unchanged between day 7 and day 14, with the exception of IL-18. At day 14 the tissues surrounding the NO-releasing implant had greater levels of TNFα and IL-1RA compared to control biopsies. All other cytokines concentrations associated with the NO-releasing sensor at day 14 were statistically indistinguishable from the 14-day biopsy, again with the exception of IL-18 which was reduced. The NO appears to stabilize cytokine levels, maintaining a wound environment that is not deleterious to sensor function, agreeing with prior studies showing greater FBR and concomitant deterioration of sensor performance and tissue integration.[9,10,13] These data support the unique therapeutic advantages of sustained NO release.

The trends in cytokine levels inform the inflammatory state. For example, TNFα, IFNγ, IL-1β, and IL-18 are each associated with increased inflammation.[29,30] In tissues surrounding the NO-releasing implants, TNFα and IL-18 were appreciably lower at days 7 and 14 while IFNγ was less only on day 7, compared to the non-releasing samples. This decrease in the inflammatory cytokines in the presence of the IL-1RA, an inhibitor to IL-1β, and the anti-inflammatory cytokine IL-10, suggests that NO is modulating the system away from a pro-inflammatory state. Curiously, the anti-inflammatory cytokine IL-10 was lower in tissues

experiencing NO release than those without. Others have reported IL-10 inhibiting the inducible nitric oxide synthase enzyme.[31,32] A negative feedback loop between IL-10 and NO may thus exist, wherein exogenous NO decreases IL-10 in a targeted and specific manner. Finally, both IL-8 and IL-6 are chemoattractants and are both decreased in concentration at day 7 specifically. This phenomenon implies that NO also acts to decrease leukocyte homing to the implantation site. In this manner, the lower leukocyte counts other studies have reported beyond day 7 may be attributed to NO-influenced chemokine reduction earlier in the FBR.[9,10,12,14]

The IL-1a, IL-2, IL-4, IL-12, and GM-CSF levels were each below the detection limit of the assay for each implant sample and timepoint. The absence of such cytokines was not surprising based on their cellular sources and/or functions that also enables a further understanding of FBR at 7- and 14-days post-implantation. Expressed most typically by mucosal cells, IL-1a is expected to be low in concentration in the subcutaneous tissue collected. Likewise, GM-CSF differentiates stem-cells coming out of the bone marrow and IL-2/ IL-12 expand and activate T cells populations, biology not anticipated to be a part of the FBR at the time-points studied.

3.3.2 Predictive Cell Profiling through Gene Expression

To expand upon these targeted analyses, predictive cell profiling and qualitative comparison of inflammation states between the NO-releasing sensor and the non-releasing sensor were evaluated through differential gene expression. A novel custom panel of 254 human genes with high porcine homology (>80%) was created to assess immunomodulation of known FBR and wound healing biomarkers, and to predict abundances of leukocyte types through the use of highly associated gene markers. All genetic data presented herein was analyzed by comparing fold changes as a function of FBR and NO release at either day 7 or

day 14. Without a day 7 control biopsy, all comparisons between the control biopsy and non-releasing sensor on day 7 use the day 0 control biopsy and the day 7 non-releasing sensor.

As part of the cell profiling, CD45, the pan-leukocyte marker, was used to infer inflammatory cell density at the implantation site, where greater expression of CD45 is indicative of a higher leukocyte density. As shown in Figure 3.2, the presence of an implant doubled the number of cells recruited to the implant site when compared to the control biopsy, perhaps expected given that the FBR induces cell recruitment to the implantation site. When examining the NO-releasing implant, the cell density was roughly half of the non-releasing implant. The decrease in cell densities are in close agreement with histological data published by Soto et al,[10] with the CD45 expression profile supporting NO's impact in reducing cellular migration towards the implant site.

In addition to CD45 expression, genes associated with a number of leukocytes (SI Table 1) were analyzed to infer the relative abundance of cell types present at the implantation site. As provided in Figure 3.3, it became clear that the NO release impacted the population of cells arriving to the implant site. Lower frequencies of T cells and macrophages were observed at day 14 compared to day 7, when comparing the NO-releasing sensor to the control sensors. Interestingly, B cells are among the most prominent cells found at both time points, even though NO release decreases the expression of many different leukocytes at day 14. Given the importance of B cells in wound reconstruction,[33,34] these results suggest the activity of B cells in response to exogenous NO is worthy of further investigation.

3.3.3 Differential Expression of Wound Healing Genes

Differential expression analysis was performed and we evaluated the 50 genes having the lowest p-values for the fold change between the control biopsy and non-releasing implants. Specifically, the modulation of such genes was evaluated as a function of NO release at 7- and 14-days post-implantation. In this comparison, genes activated by the FBR were

identified and analyzed with respect to NO's influence to identify how the addition of NO alters the base FBR response, as represented by the non-releasing implant.

A subset of the genes evaluated is provided in Figure 3.4, with genes grouped by class and color-coded for whether they were upregulated (red) or downregulated (blue) with NO release. Three genes that were affected by NO emerge from this analysis: CASP1, Blk, and MMP8. CASP1 can serve as an important marker of inflammation, as it regulates the IL-1 inflammation pathway.[29,30] While IL-1β, IL-1RA, and IL-18 each belong to that pathway, IL-18, in particular, responds to NO release (Figure 3.1). The downregulation of CASP1 on day 14 with NO again supports NO's role in mitigating pro-inflammatory activity. The discovery of Blk as a common gene suggests modulation of B cell infiltration in the presence of NO release, reinforcing the utility of further investigating B cell response in this system. As MMP-8 is perhaps the most abundant collagenase in both healing and non-healing wounds,[35,36] its modulation by NO suggests an active role in producing the thinner collagen capsule surrounding NO-releasing implants. The upregulation of CD163 with NO, a marker of anti-inflammatory macrophages, at day 7 and its disappearance at day 14 is also noteworthy. The presence of anti-inflammatory macrophages supports NO's mitigation of inflammation, but the results also agree with the cell profiling data (Figure 3.3), as with NO release, macrophages are more abundant on day 7 but become less present on day 14 with NO release, compared to the non-releasing implant samples.

More broadly, additional conclusions are drawn by analyzing gene changes on a class level. First, MMPs and chemokines are mostly downregulated at the NO-releasing implant site on both day 7 and day 14. This decrease in expression, due to their shared roles in chemokinesis, also supports the data found in the cell profiling. Specifically, the NO affects cell migration and the overall composition of cells at the implantation site. MMP2 and MMP9 were both downregulated by the NO, a finding previously reported by Matsunaga et al. who showed correlation between NO exposure, decrease in MMP2 and MMP9, and enhanced

angiogenesis.[5] The expressions of collagens was also decreased from days 7 to 14, in agreement with the lower collagen capsule density observed by Soto et al. at day 10 with NO release.[10] Among the cytokines, it is interesting to note that IL-18 and IL-1β were upregulated in the presence of NO release at day 7 relative to the non-releasing implant. These data conflict with the cytokine data in Figure 3.1, where all cytokines decreased in concentration with NO both at 7- and 14-days post-implantation. These data indicate reduced translation, inactivation, or depletion of these cytokines through another mechanism. Angiogenic markers VEGFB and TGFB2 were upregulated with NO on day 14, supporting NO's role as an angiogenic agent.

3.4. Conclusions

In conclusion, multiple biological mechanisms were elucidated regarding the effect of NO release on tissue reconstruction during the FBR. It was found NO promotes different proportions of cells and reduced chemokine expression and cell infiltration, each supportive of previously reported tissue histology. In regards to the different cell populations, this study may be expanded upon with immunohistochemistry or flow cytometry to identify the cell types are arriving at the implantation site, their spatial position relative to the implant, and their phenotypic changes. Biomarkers identified in this study should enable a systematic study of how modulating NO-release fluxes may provide more control over progression of the FBR. Ongoing research aims to expand this analysis to a hyperglycemic porcine model to elucidate mechanistic differences in NO's action in the diabetic FBR and guide development of more useful continuous glucose monitoring devices.[10,12,23]

3.5. Figures and Tables

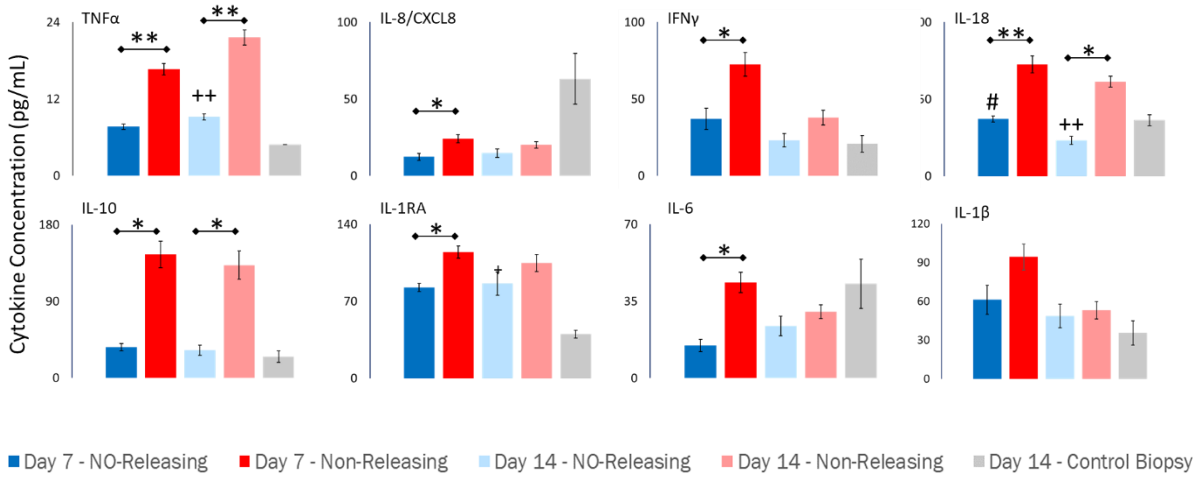

Figure 3.1. Cytokine concentrations calculated from explanted tissue using a Luminex multiplex assay. Bars represent the mean ± standard error of 3 unique implants. Symbols above individual bars denote statistical significance between NO-releasing and control biopsy at day 14 (+) or days 7 and 14 NO-releasing implants (#). (*) denotes statistical significance between NO-releasing and non-releasing samples. $p < 0.05$ for single symbols or $p < 0.005$ for double symbols. All statistical significance is determined through 2-tailed unpaired t-tests.

Table 3.1. Cell profiling analysis was performed using the listed genes as biomarkers of the interrogated cell types.

B Cells	CD45	$CD8^+$ Cells	Cytotoxic Cells	Dendritic Cells	Exhausted $CD8^+$ Cells	Macrophages	Mast Cells	Neutrophils	T Cells
Ms4a1	Ptprc	Cd8a	Prf1	Hsd11b1	Lag3	Cd84	Hdc	Fcgr4	Cd3e
Spib		Cd8b1	Gzmb	Ccl2	Eomes	Cd163	Cpa3	Fpr1	Cd3d
Cd19			Nkg7	Cd209e	Ptger4	Ms4a4a	Tpsb2	Ceacam3	Cd3g
Blk			Klrd		Cd44a	Cd68	Ms4a2	Csf3r	Trat1
Fcrlb			Ctsw				Tpsab1		Cd6
Tnfrsf17			Gzma						Sh2d1a
Pnoc			Klrk1						
Tcl1			Klrb1						

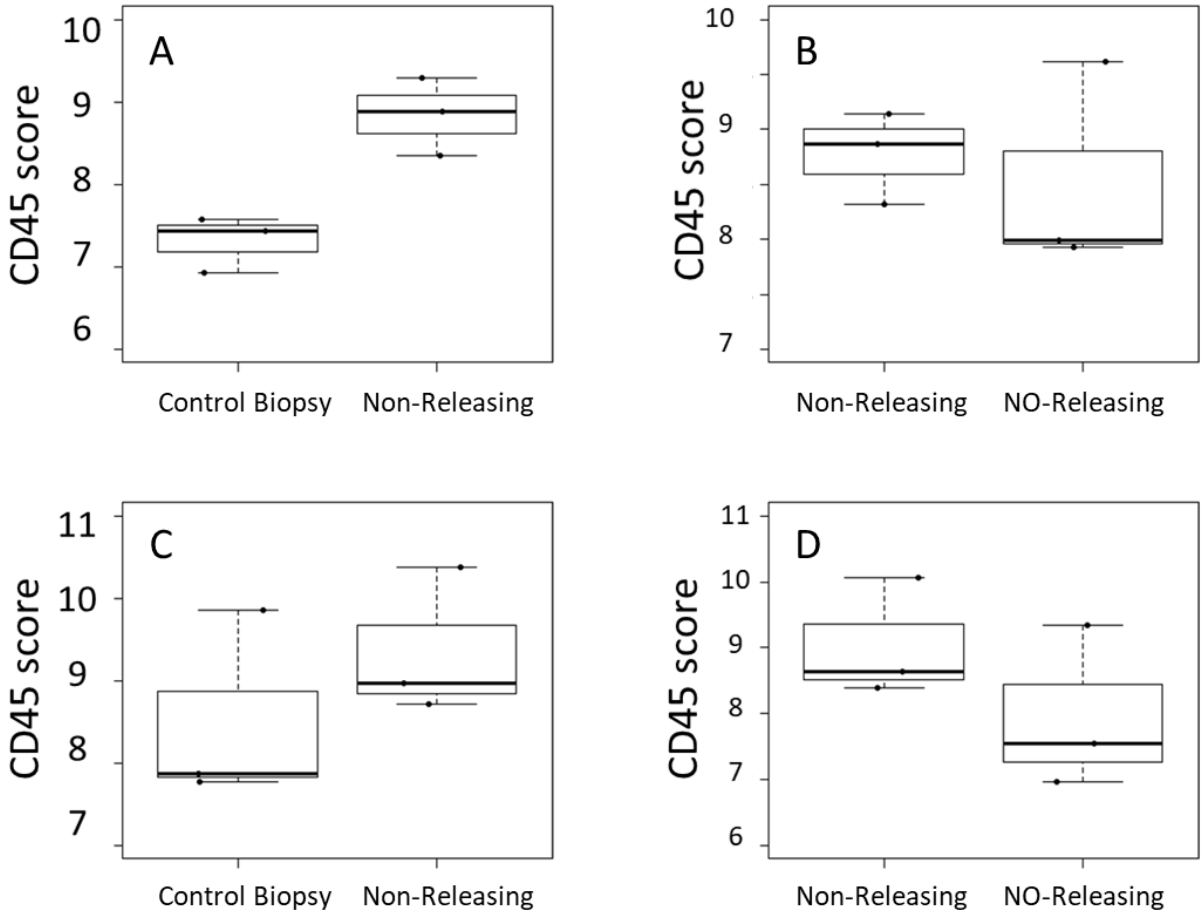

Figure 3.2. Box-and-whisker plots of CD45 expression scoring for A) day 7 control biopsy versus non-releasing sensor; (B) day 7 non-releasing sensor versus NO-releasing sensor; (C) day 14 control biopsy versus non-releasing sensor; (D) day 14 non-releasing sensor versus NO-releasing sensor. The y-axis, CD45 score, is on a log2 scale.

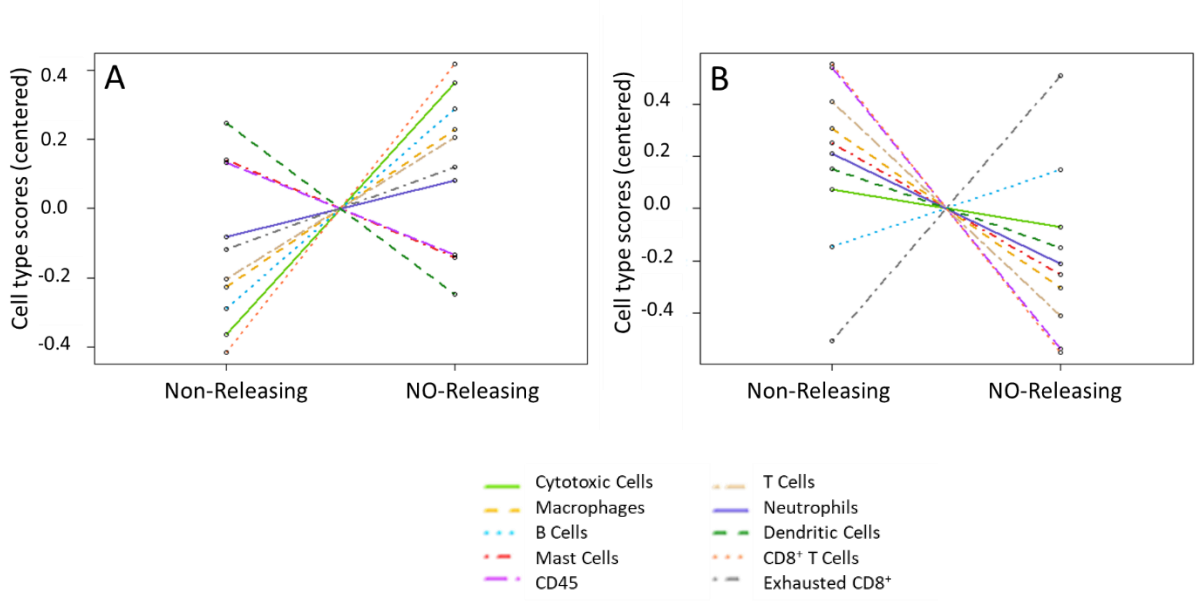

Figure 3.3. Relative changes in cell type abundance for A) day 7 non-releasing sensor versus NO-releasing sensor and B) day 14 non-releasing sensor versus NO-releasing sensor. Both the y-axes, cell type scores, are on a log2 scale.

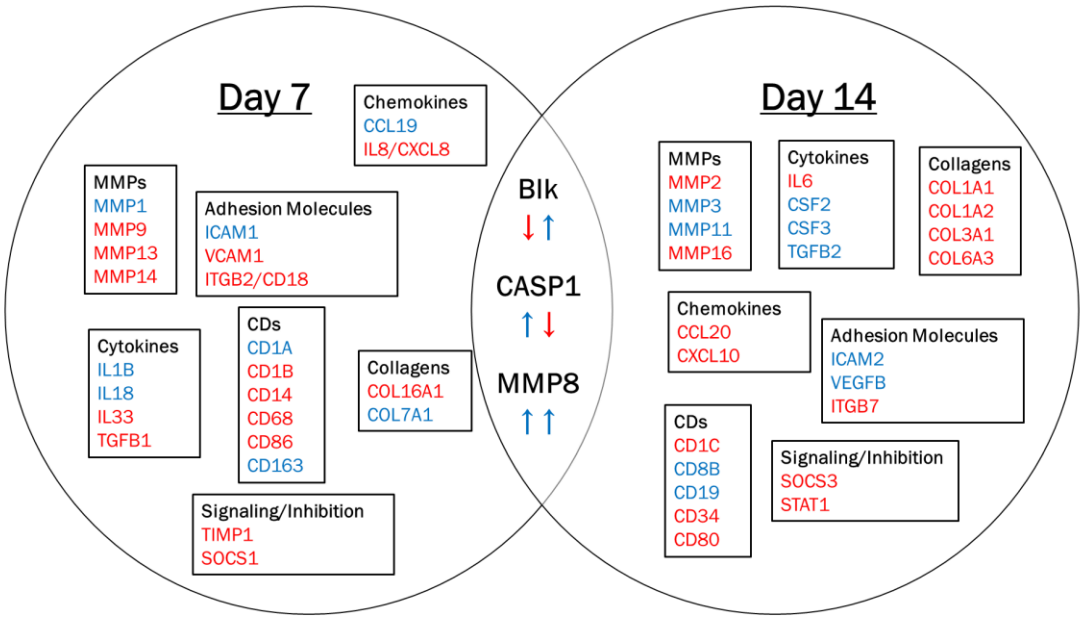

Figure 3.4. Subset of genes in Venn diagram identified in a differential expression analysis as statistically significant through the non-releasing versus control biopsy fold change, and that were detected in the non-releasing versus NO-releasing analysis. Genes are represented by their fold change in non-releasing versus NO-releasing analysis, wherein blue and red represent up- and downregulation respectively. Genes in the overlapping section are presented with fold change for the Day 7 comparison followed by the fold change for the Day 14 comparison.

REFERENCES

(1) Luo, J. D.; Chen, A. F. Nitric Oxide: A Newly Discovered Function on Wound Healing. *Acta Pharmacol. Sin.* **2005**, *26* (3), 259–264.

(2) Cooke, J. P.; Losordo, D. W. Nitric Oxide and Angiogenesis. *Circulation* **2002**, *105* (18), 2133–2135.

(3) Bogdan, C. Nitric Oxide and the Immune Response. *Nat. Immunol.* **2001**, *2* (10), 907–916.

(4) Frank, S.; Kämpfer, H.; Wetzler, C.; Pfeilschifter, J. Nitric Oxide Drives Skin Repair: Novel Functions of an Established Mediator. *Kidney Int.* **2002**, *61* (3), 882–888.

(5) Matsunaga, T.; Weihrauch, D. W.; Moniz, M. C.; Tessmer, J.; Warltier, D. C.; Chilian, W. M. Angiostatin Inhibits Coronary Angiogenesis during Impaired Production of Nitric Oxide. *Circulation* **2002**, *105* (18), 2185–2191.

(6) Napoli, C.; Paolisso, G.; Casamassimi, A.; Al-Omran, M.; Barbieri, M.; Sommese, L.; Infante, T.; Ignarro, L. J. Effects of Nitric Oxide on Cell Proliferation: Novel Insights. *J. Am. Coll. Cardiol.* **2013**, *62* (2), 89–95.

(7) Gifford, R.; Batchelor, M. M.; Lee, Y.; Gokulrangan, G.; Meyerhoff, M. E.; Wilson, G. S. Mediation of in Vivo Glucose Sensor Inflammatory Response via Nitric Oxide Release. *J. Biomed. Mater. Res. Part A* **2005**, *75A* (4), 755–766.

(8) Hetrick, E. M.; Prichard, H. L.; Klitzman, B.; Schoenfisch, M. H. Reduced Foreign Body Response at Nitric Oxide-Releasing Subcutaneous Implants. *Biomaterials* **2007**, *28* (31), 4571–4580.

(9) Nichols, S. P.; Koh, A.; Brown, N. L.; Rose, M. B.; Sun, B.; Slomberg, D. L.; Riccio, D. A.; Klitzman, B.; Schoenfisch, M. H. The Effect of Nitric Oxide Surface Flux on the Foreign Body Response to Subcutaneous Implants. *Biomaterials* **2012**, *33* (27), 6305–6312.

(10) Soto, R. J.; Merricks, E. P.; Bellinger, D. A.; Nichols, T. C.; Schoenfisch, M. H. Influence of Diabetes on the Foreign Body Response to Nitric Oxide-Releasing Implants. *Biomaterials* **2018**, *157*, 76–85.

(11) Soto, R. J.; Hall, J. R.; Brown, M. D.; Taylor, J. B.; Schoenfisch, M. H. In Vivo Chemical Sensors: Role of Biocompatibility on Performance and Utility. *Anal. Chem.* **2017**, *89* (1), 276–299.

(12) Malone-Povolny, M. J.; Merricks, E. P.; Wimsey, L. E.; Nichols, T. C.; Schoenfisch, M. H. Long-Term Accurate Continuous Glucose Biosensors via Extended Nitric Oxide Release. *ACS Sensors* **2019**, *4* (12), 3257–3264.

(13) Soto, R. J.; Privett, B. J.; Schoenfisch, M. H. In Vivo Analytical Performance of Nitric Oxide-Releasing Glucose Biosensors. *Anal. Chem.* **2014**, *86* (14), 7141–7149.

(14) Nichols, S. P.; Le, N. N.; Klitzman, B.; Schoenfisch, M. H. Increased In Vivo Glucose Recovery via Nitric Oxide Release. *Anal. Chem.* **2011**, *83* (4), 1180–1184.

(15) Nichols, S. P.; Koh, A.; Storm, W. L.; Shin, J. H.; Schoenfisch, M. H. Biocompatible Materials for Continuous Glucose Monitoring Devices. *Chem. Rev.* **2013**, *113* (4), 2528–2549.

(16) Vallejo-Heligon, S. G.; Klitzman, B.; Reichert, W. M. Characterization of Porous, Dexamethasone-Releasing Polyurethane Coatings for Glucose Sensors. *Acta Biomater.* **2014**, *10* (11), 4629–4638.

(17) Koh, A.; Riccio, D. a.; Sun, B.; Carpenter, A. W.; Nichols, S. P.; Schoenfisch, M. H. Fabrication of Nitric Oxide-Releasing Polyurethane Glucose Sensor Membranes. *Biosens. Bioelectron.* **2011**, *28* (1), 17–24.

(18) Soto, R. J.; Yang, L.; Schoenfisch, M. H. Functionalized Mesoporous Silica via an Aminosilane Surfactant Ion Exchange Reaction: Controlled Scaffold Design and Nitric Oxide Release. *ACS Appl. Mater. Interfaces* **2016**, *8* (3), 2220–2231.

(19) Soto, R. J.; Schofield, J. B.; Walter, S. E.; Malone-Povolny, M. J.; Schoenfisch, M. H. Design Considerations for Silica-Particle-Doped Nitric-Oxide-Releasing Polyurethane Glucose Biosensor Membranes. *ACS Sensors* **2017**, *2* (1), 140–150.

(20) Malone-Povolny, M. J.; Schoenfisch, M. H. Extended Nitric Oxide-Releasing Polyurethanes via S-Nitrosothiol-Modified Mesoporous Silica Nanoparticles. *ACS Appl. Mater. Interfaces* **2019**, *11* (13), 12216–12223.

(21) Lancaster, J. R. A Tutorial on the Diffusibility and Reactivity of Free Nitric Oxide. *Nitric Oxide* **1997**, *1* (1), 18–30.

(22) Soto, R. J.; Schoenfisch, M. H. Preclinical Performance Evaluation of Percutaneous Glucose Biosensors: Experimental Considerations and Recommendations. *J. Diabetes Sci. Technol.* **2015**, *9* (5), 978–984.

(23) Malone-Povolny, M. J.; Maloney, S. E.; Schoenfisch, M. H. Nitric Oxide Therapy for Diabetic Wound Healing. *Adv. Healthc. Mater.* **2019**, *8* (12), 1–18.

(24) Seaton, M.; Hocking, A.; Gibran, N. S. Porcine Models of Cutaneous Wound Healing. *ILAR J.* **2015**, *56* (1), 127–138.

(25) Anderson, J. M. Biological Responses to Materials. *Annu. Rev. Mater. Res.* **2001**, *31* (1), 81–110.

(26) Anderson, J. M.; Rodriguez, A.; Chang, D. T. Foreign Body Reaction to Biomaterials. *Semin. Immunol.* **2008**, *20* (2), 86–100.

(27) Chandorkar, Y.; Krishnamurthy, R.; Basu, B.; Ravikumar, K.; Basu, B. The Foreign Body Response Demystified. *ACS Biomater. Sci. Eng.* **2019**, *5* (1), 19–44.

(28) Sheikh, Z.; Brooks, P.; Barzilay, O.; Fine, N.; Glogauer, M. Macrophages, Foreign Body Giant Cells and Their Response to Implantable Biomaterials. *Materials (Basel).* **2015**, *8* (9), 5671–5701.

(29) Franchi, L.; Eigenbrod, T.; Muñoz-Planillo, R.; Nuñez, G. The Inflammasome: A Caspase-1-Activation Platform That Regulates Immune Responses and Disease Pathogenesis. *Nat. Immunol.* **2009**, *10* (3), 241–247.

(30) Denes, A.; Lopez-Castejon, G.; Brough, D. Caspase-1: Is IL-1 Just the Tip of the ICEberg? *Cell Death Dis.* **2012**, *3* (7), e338–e338.

(31) Goff, W. L.; Johnson, W. C.; Cluff, C. W. Babesia Bovis Immunity: In Vitro and in Vivo Evidence for IL-10 Regulation of IFN-γ and INOSa. *Ann. N. Y. Acad. Sci.* **1998**, *849* (1), 161–180.

(32) Yang, Z.; Zingarelli, B.; Szabó, C. Crucial Role of Endogenous Interleukin-10 Production in Myocardial Ischemia/Reperfusion Injury. *Circulation* **2000**, *101* (9), 1019–1026.

(33) Sîrbulescu, R. F.; Boehm, C. K.; Soon, E.; Wilks, M. Q.; Ilieş, I.; Yuan, H.; Maxner, B.; Chronos, N.; Kaittanis, C.; Normandin, M. D.; El Fakhri, G.; Orgill, D. P.; Sluder, A. E.; Poznansky, M. C. Mature B Cells Accelerate Wound Healing after Acute and Chronic Diabetic Skin Lesions. *Wound Repair Regen.* **2017**, *25* (5), 774–791.

(34) Iwata, Y.; Yoshizaki, A.; Komura, K.; Shimizu, K.; Ogawa, F.; Hara, T.; Muroi, E.; Bae, S.; Takenaka, M.; Yukami, T.; Hasegawa, M.; Fujimoto, M.; Tomita, Y.; Tedder, T. F.; Sato, S. CD19, a Response Regulator of B Lymphocytes, Regulates Wound Healing through Hyaluronan-Induced TLR4 Signaling. *Am. J. Pathol.* **2009**, *175* (2), 649–660.

(35) Gutiérrez-Fernández, A.; Inada, M.; Balbín, M.; Fueyo, A.; Pitiot, A. S.; Astudillo, A.; Hirose, K.; Hirata, M.; Shapiro, S. D.; Noël, A.; Werb, Z.; Krane, S. M.; López-Otín, C.; Puente, X. S. Increased Inflammation Delays Wound Healing in Mice Deficient in Collagenase-2 (MMP-8). *FASEB J.* **2007**, *21* (10), 2580–2591.

(36) Nwomeh, B. C.; Liang, H. X.; Cohen, I. K.; Yager, D. R. MMP-8 Is the Predominant Collagenase in Healing Wounds and Nonhealing Ulcers. *J. Surg. Res.* **1999**, *81* (2), 189–195.

CHAPTER 4 – MONITORING NITRIC OXIDE-AFFECTED MATRIX METALLOPROTEINASE ACTIVITY IN INFLAMMATORY CONDITIONS

4.1. Introduction

The foreign body response (FBR) is an adverse host response towards an implanted object.[1–3] The FBR is comprised of a cascading series of inflammatory events, such as the infiltration of inflammatory cells (e.g., neutrophils, macrophages, foreign body giant cells), the production of high levels of reactive oxygen and nitrogen species, and the release of various inflammatory mediators such as eicosanoids and cytokines, with the goal of degrading the implant or foreign object. The host response resolves with the isolation of the implant in a collagenous capsule, which is uniquely deleterious to the analytical performance of in vivo biosensors due to impedance of analyte transport through the tortuous collagen capsule. Emerging biomaterials employ strategies to lessen the FBR response.[1,2,4,5] These techniques broadly aim to reduce inflammation or to improve wound healing by promoting wound healing through either the use of intricately designed implant topographies for passive modulation of cell behavior or the active release of physiological mediators (i.e., anti-inflammatory steroids, growth factors) directly from the implant surface.[3,4,6]

An emerging class of biomaterials with promise for promoting longterm implant biocompatibility is nitric oxide (NO)-releasing materials. An endogenously produced diatomic gasotransmitter,[7,8] NO modulates physiological processes relevant to controlling the FBR such as angiogenesis,[9,10] cell proliferation,[11,12] and collagen deposition.[13–15] Through the use of NO donors, molecular scaffolds that controllably release NO, implantable devices have been developed that release exogenous NO to mitigate adverse reactions at the implant surface. These include glucose biosensors,[16–18] vascular grafts,[19] and both urinary track and venous

catheters,[20–23], and all of these models have demonstrated the therapeutic benefits of in situ NO release.

Though much promise surrounds NO-releasing biomaterials, many unanswered questions remain concerning the wound healing pathways and mediators immunomodulated by exogenous NO. These questions are of vital importance for the rational tuning of optimal NO dosage and release kinetics to further improve the biocompatibility conferred by NO release. An important class of wound-healing mediators is the matrix metalloproteinases (MMPs), a class of proteinases with a Zn^{2+} core.[24–28] These proteinases are synthesized with a prodomain, fully blocking the active site and preventing enzymatic activity. Once the prodomain is removed via another protease, MMPs regulate biological events by processing extracellular matrix components and structural proteins, such as collagen and elastin. Importantly, MMPs are receiving more interest due to their role in protein regulation (e.g., chemokines, growth factors, other MMPs), through cleaving their prodomains or releasing them from the extracellular matrix.[24–28] Characterizing the functions of various MMPs in the FBR would help deepen the understanding of FBR regulation. Analyzing this class of mediators is particularly attractive as the FBR depends heavily on collagen deposition and chemokinesis of inflammatory cells, both of which, as aforementioned, are regulated by MMP activity.

Due to their numerous biological functions, MMPs have been explored for their roles in inflammation. Chronic wounds and inflammation are characterized in part by increased concentration of MMPs and MMP activity has increasingly been explored in inflammation models. Bozkurt et al. observed rising MMP expression in gingival fibroblasts when exposed to increasing endotoxin concentrations.[29] Ploeger et al. exposed human dermal fibroblasts to conditioned media from either pro- or anti-inflammatory macrophages.[30] The expression of different chemokines was quantified via PCR, and it was found that the expression of pro-inflammatory chemokines increased when the fibroblasts were incubated with media from

pro-inflammatory macrophages and vice versa. Plasticity was observed in this effect, meaning that fibroblasts previously exposed to pro-inflammatory media would see decreases in the expressions of MMPs and inflammatory cytokines when exposed to anti-inflammatory media.[30] Given the established link between MMPs and inflammation, researchers have investigated the effects of MMPs on the FBR. For example, Jones et al. grew primary human macrophages on polymer surfaces and discovered that MMP concentration is material dependent. Furthermore, macrophage activity (e.g., fusion to polymorphonuclear cells, surface adhesion) could be modulated with MMP inhibiting drugs.[27] These results show the potential of MMPs as markers of FBR severity.

To date, there remains a limited understanding of how NO-releasing biomaterials affect MMPs at the implantation site. Herein, MMP activity of macrophages and fibroblasts were investigated as a function of NO release and inflammatory state. Both are MMP-producing cells that control much of the inflammatory cascade and deposit the collagenous capsule towards the resolution of the FBR, respectively.[2,31] By examining MMP activity as a function of both inflammation and NO dosage, NO's effect on this critical class of mediators in the wound healing process was investigated.

4.2. Materials and Methods

4.2.1 Materials

All materials were analytical grade and used as received unless otherwise noted. Lipopolysaccharides derived from *E. coli* 055:B5 (LPS), Brij-35, diethylenetriamine (DETA), bis(3-aminopropyl)amine (DPTA), HEPES sodium salt, concentrated hydrochloric acid (HCl), and fetal bovine serum (FBS) were obtained from MilliporeSigma. Calcium chloride dihydrate and the LDH CyQuant Kits were obtained from Thermo Fisher. 2-mercaptoethanol (55 mM; βME) and penicillin-streptomycin were obtained from Gibco. Poly-L-lysine (0.01%; PLL) was obtained from R&D Systems. [Ethylenedinitrilo]-tetraacetic acid disodium salt (EDTA) was

obtained from Mallinkrodt and diluted to a 50 mM solution in 10 mM PBS at pH 7.4. DETA/NO and DPTA/NO were obtained from Cayman Chemical. The fluorogenic probe BML-P126 and phorbol 12-myristate 13-acetate (PMA) were obtained from Enzo Scientific. Methanol was purchased from VWR and 200 proof ethanol was purchased from Decon Labs. 1X RPMI-1640 was purchased from Corning.

4.2.2 Chemiluminescent Measurement of NO Release

For both DPTA/NO and DETA/NO, NO-release profiles were measured in 30 mL PBS (pH 7.4, 37 °C) with a Zysense model 280i chemiluminescence Nitric Oxide Analyzer. Approximately 1 mg of NO donor was added to 30 mL of deoxygenated PBS, sparged with 200 mL min^{-1} nitrogen. Analysis was terminated when NO concentration fell below 100 ppb mg^{-1}. The instrument was calibrated with a NO zero filter and 25.87 ppm NO gas (nitrogen balance).

4.2.3 Cell Culture Protocol

Human gingival fibroblasts and complete fibroblast medium were obtained from Sciencell, and cells were grown according to manufacturer instructions. Human monocytes (THP-1) were obtained from the UNC Tissue Culture Facility. Monocytes were grown in complete macrophage media prepared from RMPI supplemented with 20% FBS, 1 % Penstrep, and 0.05 mM βME according to supplier protocols. All cells were stored in an incubator at 37 °C and 5% CO_2. For cell experiments, fibroblasts were seeded in a 96-well plate and incubated overnight. Monocytes were similarly plated in 96-well plates, with 200 nM PMA supplemented to the complete monocyte media, and incubated for 24 h prior to experimentation. The addition of PMA induces monocyte differentiation into macrophages. All well plates were precoated with PLL before experimentation through a 30 min incubation with the PLL solution followed by a wash with sterile PBS.

Following cell attachment, media was aspirated from cells plated in wells and was replaced with media containing 0.02-2 mg/mL DETA/NO or DPTA/NO and 0-5 μg/mL LPS. This allowed for a co-incubation of an inflammatory stimulant (i.e., LPS) and an NO donor. The non-NO-releasing DETA and DPTA were used as control amines against their NO-releasing counterparts (DETA/NO and DPTA/NO, respectively). Of note, macrophage studies were done using the aforementioned complete media with only 10% FBS to reduce MMP background. Solutions were titrated to neutral pH using 5 N HCl before addition to wells. The well plates were placed into the incubator for 24 h, after which 10 μL of 10X Lysis Buffer (from the LDH CyQUANT Kit) was introduced into the well to lyse cells, and 10 μL of deionized water were added to the unlysed wells.

4.2.4 NO-Releasing Wire Fabrication

Mock sensors were created to serve as an NO source, adapting previously published work.[18,32–34] Briefly, mesoporous nanoparticles were synthesized through the bolus addition of TEOS to a solution of ethanol, water, ammonium hydroxide, and the liquid crystal template (CTAB).[18,34] Particles were washed with ethanol, collected via centrifugation, and post-grafted with MPTMS to provide exterior and intraporous thiols. These particles were suspended in a chilled solution of 4 mL of 5 N HCl and 4 mL of methanol, stirring and shielded from light. A solution of acidified nitrite (400 mg $NaNO_2$ in 2 mL water) was added to the particle suspension, nitrosating the free thiols to NO-releasing S-nitrosothiol moieties. Particles were stored at -20 °C until use and were handled in the dark to mitigate premature NO release from light exposure.

Nitrosated particles were suspended in a 2 mL polyurethane casting solution with 50 mg/mL HP93A and 25 mg/mL nitrosated particles, in 3:1 THF:DMF. Ten layers of the casting solution were applied to a steel wire using 6.5 μL pipetted onto a 2 mm steel wire loop and passed over the wire serving as a single layer. Five minutes of drying time were used between

each coat. After the ten layers were deposited to the wire, the same method was used to apply a single top coat of 3:1 PC3585:HP93A in 3:1 THF:DMF. Wires were then left to dry for 30 min and used immediately after.

4.2.5 Validating Fluorogenic Measurement of MMP Activity

The fluorogenic measurement protocol was adapted from Ploeger et al.[30] Briefly, a 1 mg/mL solution of BML-P126 was prepared in methanol and was diluted to make the final fluorophore solution (15 nM BML-P126, 0.1% (w/v) Brij-35, 20 mM $CaCl_2$, 0.1 M HEPES; adjusted to pH 7). A 1 mL test solution was made by combining 500 µL of fluorophore solution and 500 µL of 10% FBS in PBS or 10% FBS and 50 mM EDTA in PBS and allowed to incubate for 20 h, shielded from light at 37 °C. The fluorogenic probe is activated after procession by MMPs native to FBS and after incubation, aliquots were measured on a Molecular Devices SpectraMax M2e Spectrophotometer (excitation: 328 nm; emission: 393 nm). Background fluorescence was recorded by omitting BML-P126 from the fluorophore solution. The effect of NO release on MMP activity was assessed by incubating an NO-releasing wire in the 1 mL test solution for either 5, 10, or 20 h. Aliquots were taken from the test solution for indirect quantification of NO via the Griess assay, wherein 50 µL of the test solution was combined with 50 µL of sulfanilamide and 50 µL NED, incubated in the dark for 30-45 min, and absorbance was measured at 540 nm.[35,36]

4.2.6 Viability Testing and Fluorogenic Measurement of Cellular MMP Activity

Supernatant from the aforementioned well plates was divided, with 50 µL going to a 96-well plate for the fluorogenic measurement and another 50 µL to a 96-well plate for the colorimetric LDH quantification. The fluorogenic measurement protocol was adapted from Ploeger et al.[30] To every well, 50 µL of the fluorophore solution were added, and then the well plate was incubated for 20 h. After incubation, the plate fluorescence was measured on a

Molecular Devices SpectraMax M2e (excitation: 328 nm; emission: 393 nm). All fluorescence signals were background-subtracted using the wells containing 50 μL complete cell media and 50 μL of the fluorophore solution without BML-P126.

Viability measurements were performed according to manufacturer instructions on the LDH CyQuant kit. Briefly, 50 μL of the LDH reaction mixture was added to 50 μL of the cell supernatant, and the plate was incubated in the dark at room temperature for 30 min. Absorbance measurements were recorded using the plate reader at a wavelength of 490 nm. All LDH signals were background-subtracted using the signal from blank culture media incubated with the LDH reagent. The percent killing was calculated as the ratio between the unlysed LDH signal and lysed LDH signal for every condition.

4.3. Results and Discussion

4.3.1 Characterization of NO-Release Profiles

Both DPTA/NO and DETA/NO were characterized with regards to the NO released and the associated kinetics over 24 h to ascertain what NO-release conditions the cells would be exposed to over the course of the cell experiments (Table 4.1). The two NO donors confer NO payloads over the 24-h-incubation period, despite both liberating 2 mol NO per mol donor via hydrolysis, due to their release kinetics, with reported half-lives of 3 and 20 h for DPTA/NO and DETA/NO, respectively. Due to faster decomposition, DPTA/NO liberates NO at a quicker pace and thus has a nearly 4-fold max flux compared to DETA/NO, which degrades/releases NO much slower. During the 24-h exposure duration, the DPTA/NO system delivers nearly double the mol NO per mg as DETA/NO.

Additionally, NO measurements were replicated in a solution containing 0.05 mM 2-mercaptoethanol, simulating the concentration found in the complete macrophage media. As 2-mercaptoethanol is a potent reducing agent, it was critical to identify potential variations in NO release with βME exposure. No significant changes in NO release were observed with

DETA/NO in βME, likely due to the donor's high stability as reflected by its longer half-life. However, DPTA/NO was shown to release slightly more NO with βME, with a ~20% increase in total μmol mg^{-1} and a ~30% increase in max flux. In this case, the reducing agent likely contributes to the decomposition of the NO-releasing diazeniumdiolate moiety, given that DPTA/NO is less stable than DETA/NO.

4.3.2 MMP Activity Assay Validation

The assay employed made use of the fluorogenic substrate BML-P126 as a measure of MMP activity. This substrate is selectively cleaved by MMPs and becomes fluorescently active, allowing for correlation of increased fluorescence to increased MMP activity. Using MMPs native to FBS and background subtraction by the solution with no fluorophore, a strong fluorescence signal was observed (Figure 4.1). To validate this assay further, 50 mM EDTA was used to chelate the MMPs' Zn^{2+} active site to facilitate deactivation, which resulted in fluorescence attenuation by several orders of magnitude. This relationship demonstrates that this assay is indeed selective to metalloproteinases.

The acquired fluorescence signal, importantly, is a measurement pertaining strictly to MMPs that have had their prodomains removed, as they are unable to activate the fluorophore while inactive.[25,37,38] As prior literature has shown that oxidative and nitrosative stress may remove the prodomain,[25,37,39] NO-releasing wires were employed as removable NO sources to investigate NO's influence on the measurements. No significant change in signal between the control and a sample incubated with an NO-releasing wire for 20 h (~0.44 mM NO released), indicating that permanent removal of prodomains does not occur solely from exogenous NO exposure. These data are in agreement with work by Owens et al., who observed that peroxynitrite, formed on reaction between NO and superoxide, is critical in NO's regulation of MMPs with NO alone not able to achieve any significant effect.[37] This assay can thus be used with biologically representative levels of superoxide to predict MMP activity surrounding an

NO-releasing implant in future studies to examine the dose-dependent influence NO release exerts on MMPs and elucidate possible mechanisms of MMP activity in promoting or hindering wound healing. Curiously, the MMP activity at 5 and 10 h were both significantly lower than the FBS control, despite the lower NO doses delivered (~0.26 and ~0.36 mM, respectively). This result is promising for the tuning of NO-releasing implants for promoting of wound healing by reducing the local MMP burden. Future studies should employ increased temporal resolution of NO exposure to better characterize this decrease.

4.3.3 MMP Activity and Viability of Stimulated Cells

Results from the combined well-plate assays are provided in Figures 4.2-4.5, grouped by the cell type and NO donor used. Before assessing the MMP activity, it was critical to identify the effect of the combination of endotoxin and NO donor on cell viability. By analyzing the effect of endotoxin concentration without the addition of NO donors or control amines, it was found that cell viability is not dramatically affected between 0-5 μg/mL LPS, with the percent killing limited to ~40%. While DETA was well tolerated by both cell lines up to 2 mg/mL (Figures 4.2 and 4.4), DPTA resulted in > 80% cell killing at 2 mg/mL and < 50% killing at all other concentrations (Figures 4.3 and 4.5). For the NO-releasing scaffolds, DETA/NO and DPTA/NO both resulted in < 50% killing at 0.2 and 0.02 mg/mL, but ~100% killing at 2 mg/mL (Figures 4.2-4.5). Due to the high cell death observed at 2 mg/mL DPTA, DETA/NO, and DPTA/NO, MMP activities are not reported for 2 mg/mL NO donor or control amine.

In examining MMP activity in response to endotoxin concentration, no significant difference was observed for fibroblasts at any level of LPS (Figures 4.2-4.3). For macrophages, the measured activity did not have an observable dose dependence even though MMP activity was raised with the addition of LPS (Figures 4.4-4.5). Importantly, macrophages are known to release superoxide with exposure to inflammatory stimulants.[40–42] Thus, peroxynitrite

production is likely causing an increase in MMP activity. Fibroblasts were associated with less MMP activity when compared to macrophages, implying that targeting MMPs produced by macrophages may be of greater therapeutic interest. In addition, the MMP activity from the NO-affected population did not differ significantly from the activity of the control for most samples. Despite the lack of significant differences, the divergence between NO release and the control was greater for the macrophages than the fibroblasts. Of note, the macrophages stimulated with DPTA/NO and LPS produced a significant difference between NO release and the non-releasing control, with the exception of 0.2 mg/mL DPTA/NO at 5 μg/mL LPS (Figure 4.5). In examining the DPTA/NO-stimulated macrophages, the NO-associated MMP activity was consistently greater than that of the control, implying that treatment with NO is increasing MMP activity, and without NO, the native amine itself depresses MMP activity. When comparing to baseline (i.e., treated only with LPS), using 0.02 mg/mL DPTA/NO led to a significant increase in MMP activity at LPS concentrations ≥ 2.5 μg/mL. Though the NO concentrations differ, it is important to note that while lower levels of NO reduced MMP activity in the FBS solution, the use of lower concentrations of NO donor led to the opposite effect. Further investigation into the NO-release kinetics, NO-dose dependence, and environmental differences (e.g., superoxide production) driving these diverging results will be key in elucidating the role of exogenous NO in MMP regulation.

4.4. Conclusions and Future Directions

Through the use of this fluorescence assay, we have begun to elucidate NO's effect on MMP activity. Initial results indicate that larger levels of NO have no independent lasting effect on local MMP activity; low level NO exposure can lower MMP activity in the absence of superoxide or raise MMP activity in its presence; fibroblast MMP activity is independent of endotoxin concentration; and, the major contributors to MMP activity are macrophages. These results may be vital to the rational development of NO-releasing implants. Both tuning

the NO release to lower local MMP activity and targeting macrophages to stunt their MMP production may enable less inflammation and promote wound healing with concomitant extensions of implant lifetime.

Ongoing studies are underway to quantify MMP concentration in the samples analyzed using immunoabsorption assays such as ELISA or Luminex. While the MMP activity is a possible measure of how much protein processing is occurring at a site of inflammation, the MMP concentration is important to elucidate whether NO exposure results in more or less MMP translation or activation, and how MMP activity is changed independently of MMP concentration. It is also important to note that both NO and amines may quench fluorescence and thus skew reported MMP activities down,[43–45] raising the possibility that the NO masks its own catalytic action on MMPs, or that the amine scaffolds are disguising increased or unchanged MMP activity. Nevertheless, quenching studies should be performed with NO donors and the control amines. Through the Stern-Volmer equation, a Stern-Volmer constant can be derived, allowing for quantitation of the true fluorescence and MMP activity.

4.4. Figures and Tables

Table 4.1. The 24-h NO-release characteristics of DETA/NO and DPTA/NO

NO Donor	In 10 mM PBS		In 10 mM PBS + 5 mM 2-mercaptoethanol	
	$[NO]_{max}$ (pmol mg^{-1} s^{-1})	Total $[NO]_{24\ h}$ (µmol mg^{-1})	$[NO]_{max}$ (pmol mg^{-1} s^{-1})	Total $[NO]_{24\ h}$ (µmol mg^{-1})
DETA/NO	55.8 ± 8.2	0.79 ± 0.01	50.7 ± 10.5	0.68 ± 0.05
DPTA/NO	205.7 ± 13.0	1.67 ± 0.04	288.0 ± 13.0	2.18 ± 0.02

$[NO]_{max}$ – Maximum NO flux obtained
Total $[NO]_{24h}$ – Total amount of NO liberated in 24 hours

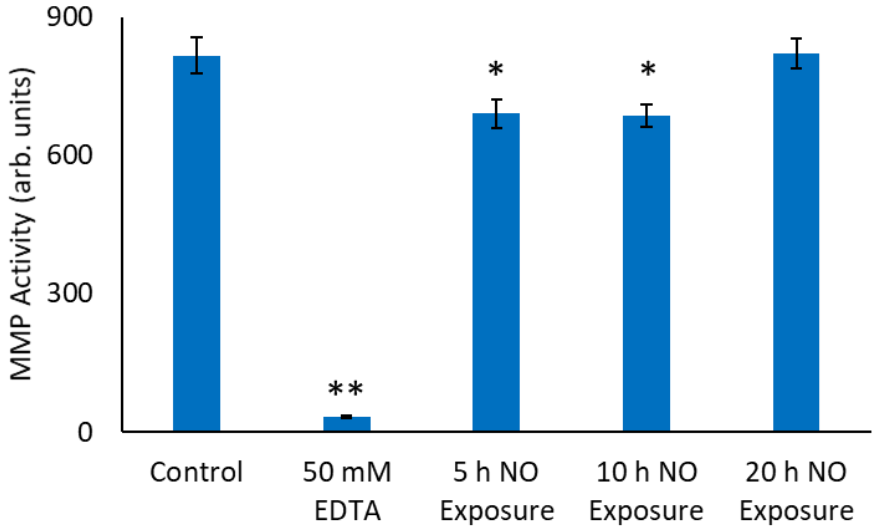

Figure 4.1. MMP activity of 10% FBS in PBS (control) was analyzed with either the addition of EDTA to deactivate MMPs or incubation with NO-releasing wires to determine whether NO can activate MMPs in solution. Significance levels were calculated against control, * $p < 0.05$, ** $p < 0.0000005$

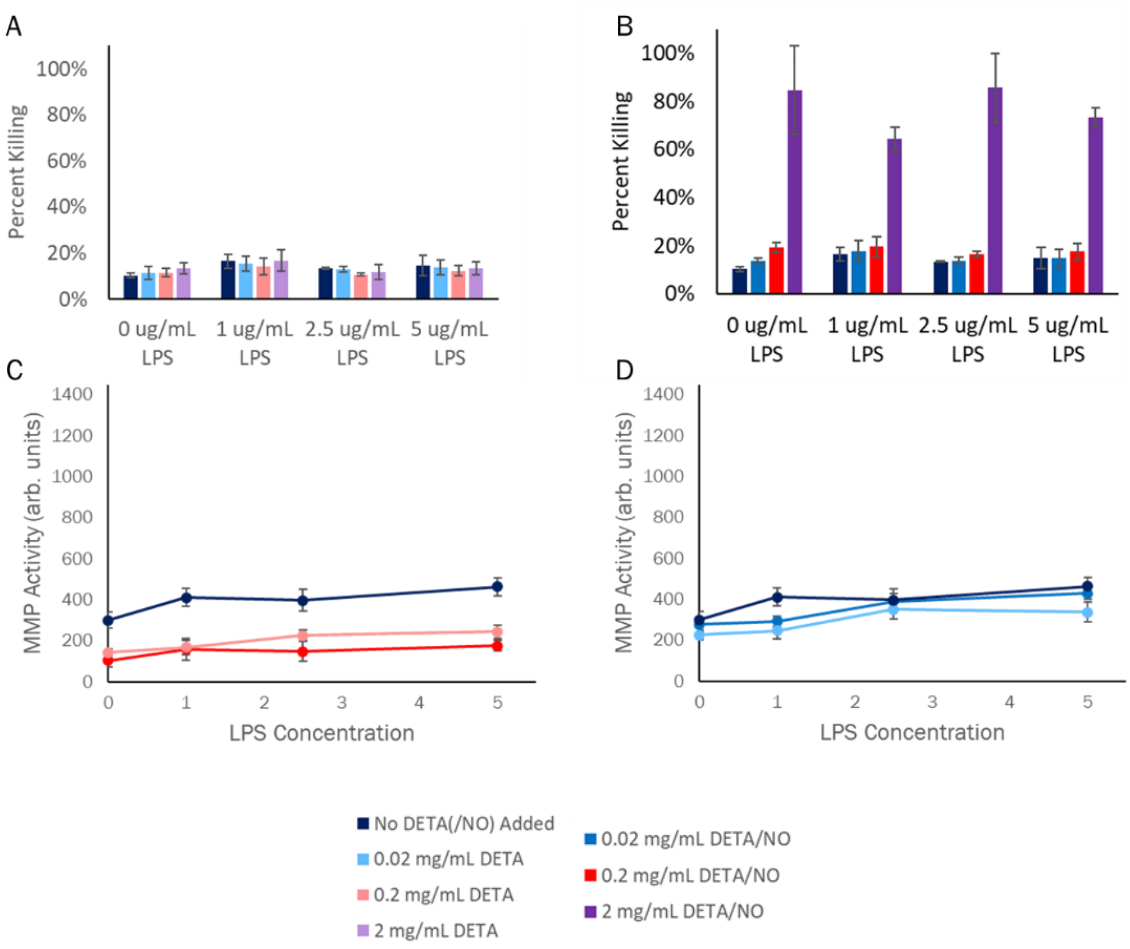

Figure 4.2. MMP activity and cell viability for human gingival fibroblasts exposed to DETA and DETA/NO. A) viability data for fibroblasts exposed to DETA; B) viability data for fibroblasts exposed to DETA/NO; C) MMP activity for fibroblasts exposed to 0.2 mg/mL DETA and 0.2 mg/mL DETA/NO; and, D) MMP activity for fibroblasts exposed to 0.02 mg/mL DETA and 0.02 mg/mL DETA/NO.

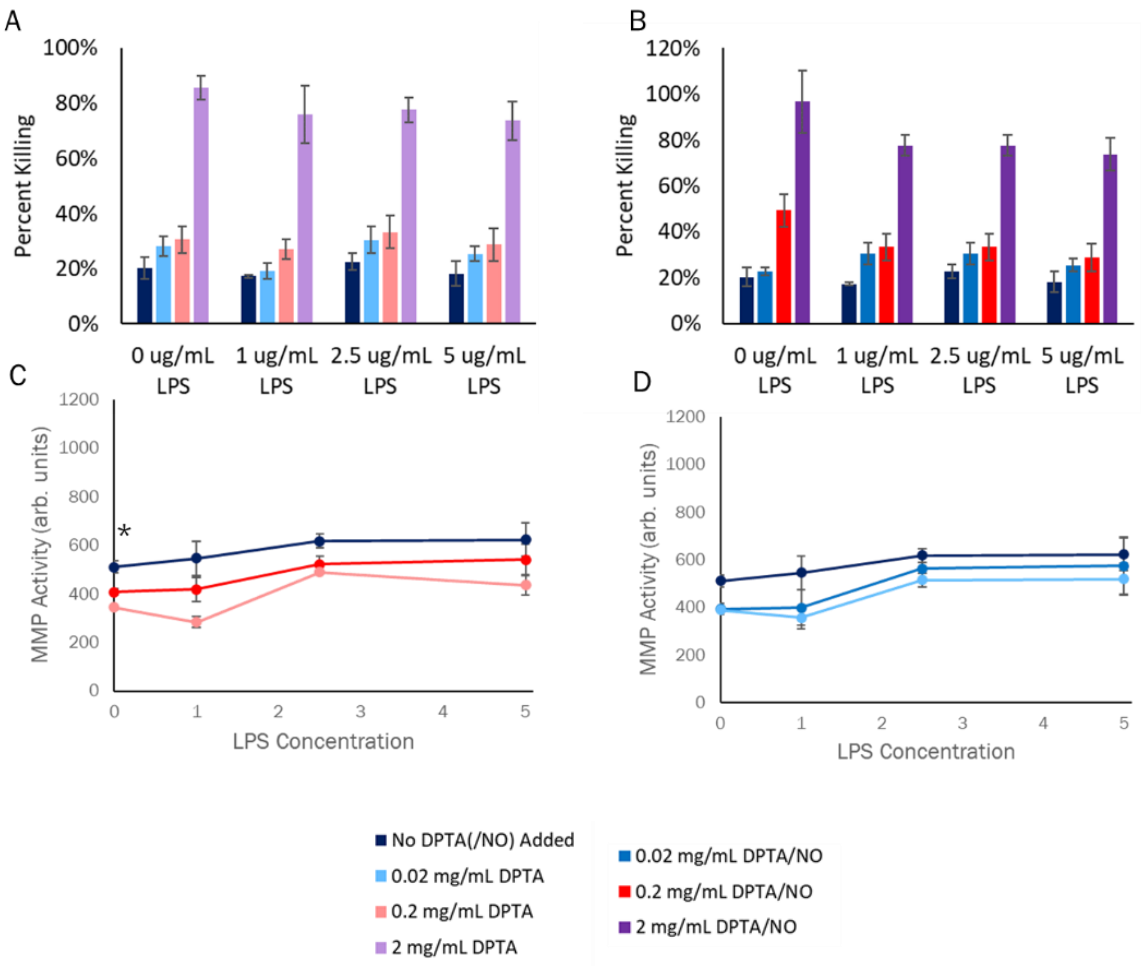

Figure 4.3. MMP activity and cell viability for human gingival fibroblasts exposed to DPTA and DPTA/NO. A) viability data for fibroblasts exposed to DPTA; B) viability data for fibroblasts exposed to DPTA/NO; C) MMP activity for fibroblasts exposed to 0.2 mg/mL DPTA and 0.2 mg/mL DPTA/NO; and, D) MMP activity for fibroblasts exposed to 0.02 mg/mL DPTA and 0.02 mg/mL DPTA/NO. * $p < 0.05$, comparing MMP activity of DPTA and DPTA/NO.

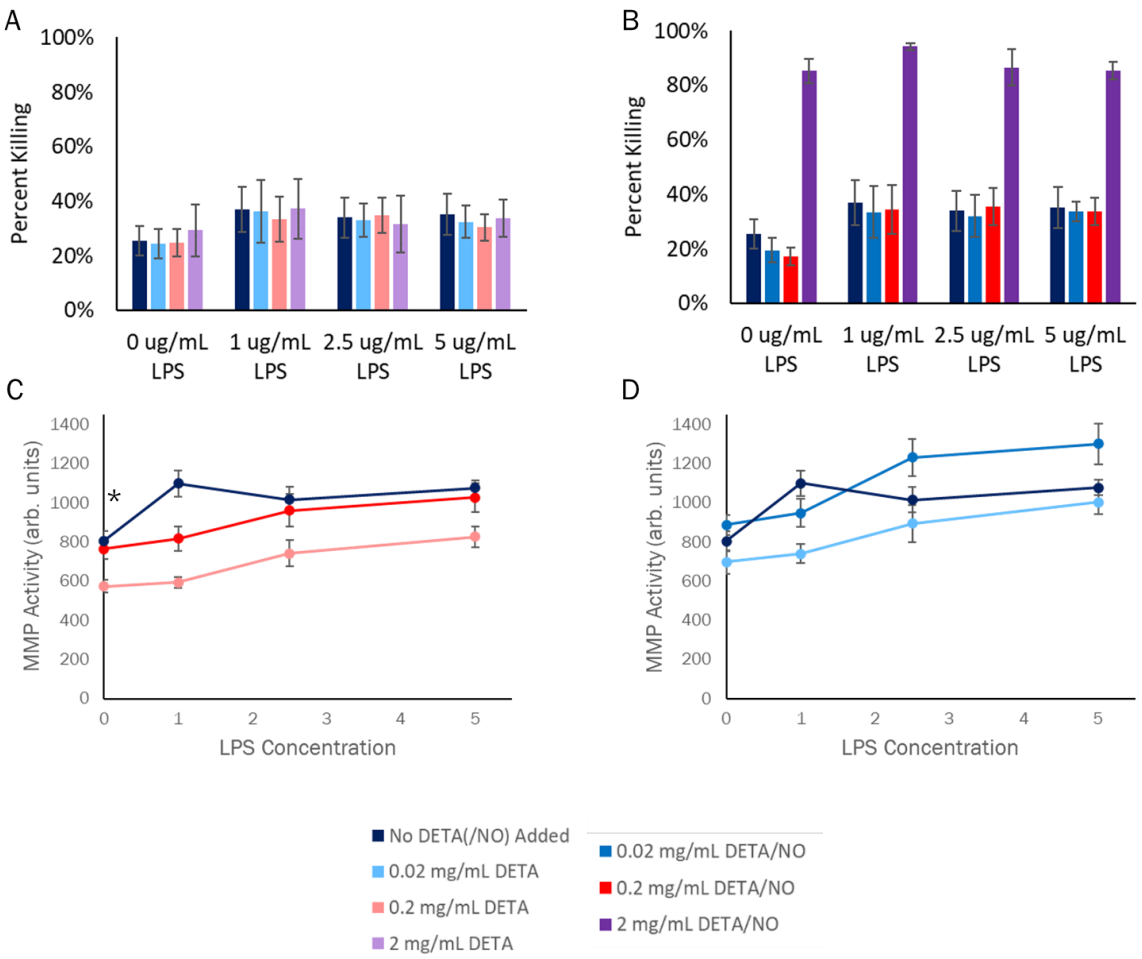

Figure 4.4. MMP activity and cell viability for human macrophages exposed to DETA and DETA/NO. A) viability data for macrophages exposed to DETA; B) viability data for macrophages exposed to DETA/NO; C) MMP activity for macrophages exposed to 0.2 mg/mL DETA and 0.2 mg/mL DETA/NO; and, D) MMP activity for macrophages exposed to 0.02 mg/mL DETA and 0.02 mg/mL DETA/NO. * $p < 0.05$, comparing MMP activity of DETA and DETA/NO.

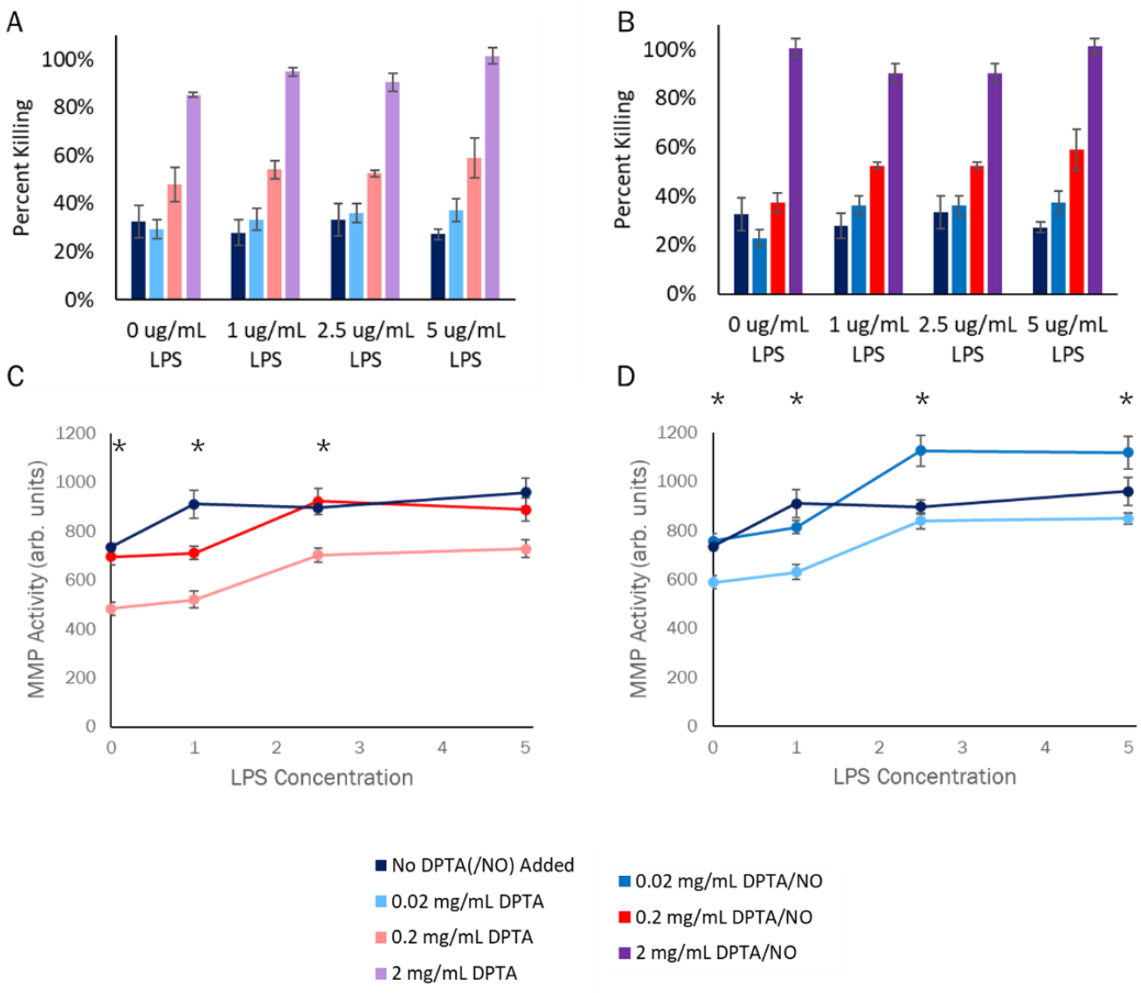

Figure 4.5. MMP activity and cell viability for human macrophages exposed to DPTA and DPTA/NO. A) viability data for macrophages exposed to DPTA; B) viability data for macrophages exposed to DPTA/NO; C) MMP activity for macrophages exposed to 0.2 mg/mL DPTA and 0.2 mg/mL DPTA/NO; and, D) MMP activity for macrophages exposed to 0.02 mg/mL DPTA and 0.02 mg/mL DPTA/NO. * $p < 0.05$, comparing MMP activity of DPTA and DPTA/NO.

REFERENCES

(1) Anderson, J. M. Biological Responses to Materials. *Annu. Rev. Mater. Res.* **2001**, *31* (1), 81–110.

(2) Anderson, J. M.; Rodriguez, A.; Chang, D. T. Foreign Body Reaction to Biomaterials. *Semin. Immunol.* **2008**, *20* (2), 86–100.

(3) Grainger, D. W. All Charged up about Implanted Biomaterials. *Nat. Biotechnol.* **2013**, *31* (6), 507–509.

(4) Soto, R. J.; Hall, J. R.; Brown, M. D.; Taylor, J. B.; Schoenfisch, M. H. In Vivo Chemical Sensors: Role of Biocompatibility on Performance and Utility. *Anal. Chem.* **2017**, *89* (1), 276–299.

(5) Chandorkar, Y.; Krishnamurthy, R.; Basu, B.; Ravikumar, K.; Basu, B. The Foreign Body Response Demystified. *ACS Biomater. Sci. Eng.* **2019**, *5* (1), 19–44.

(6) Nichols, S. P.; Koh, A.; Storm, W. L.; Shin, J. H.; Schoenfisch, M. H. Biocompatible Materials for Continuous Glucose Monitoring Devices. *Chem. Rev.* **2013**, *113* (4), 2528–2549.

(7) Ignarro, L. J.; Buga, G. M.; Wood, K. S.; Byrns, R. E.; Chaudhuri, G. Endothelium-Derived Relaxing Factor Produced and Released from Artery and Vein Is Nitric Oxide. *Proc. Natl. Acad. Sci.* **1987**, *84* (24), 9265–9269.

(8) Bogdan, C. Nitric Oxide and the Immune Response. *Nat. Immunol.* **2001**, *2* (10), 907–916.

(9) Cooke, J. P.; Losordo, D. W. Nitric Oxide and Angiogenesis. *Circulation* **2002**, *105* (18), 2133–2135.

(10) Matsunaga, T.; Weihrauch, D. W.; Moniz, M. C.; Tessmer, J.; Warltier, D. C.; Chilian, W. M. Angiostatin Inhibits Coronary Angiogenesis during Impaired Production of Nitric Oxide. *Circulation* **2002**, *105* (18), 2185–2191.

(11) Villalobo, A. Nitric Oxide and Cell Proliferation. *FEBS J.* **2006**, *273* (11), 2329–2344.

(12) Luo, J. D.; Chen, A. F. Nitric Oxide: A Newly Discovered Function on Wound Healing. *Acta Pharmacol. Sin.* **2005**, *26* (3), 259–264.

(13) Shukla, A.; Rasik, A. M.; Shankar, R. Nitric Oxide Inhibits Wound Collagen Synthesis. *Mol. Cell. Biochem.* **1999**, *200*, 27–33.

(14) Cao, M.; Westerhausen-Larson, A.; Niyibizi, C.; Kavalkovich, K.; Georgescu, H. I.; Rizzo, C. F.; Hebda, P. A.; Stefanovic-Racic, M.; Evans, C. H. Nitric Oxide Inhibits the Synthesis of Type-II Collagen without Altering Col2A1 MRNA Abundance: Prolyl Hydroxylase as a Possible Target. *Biochem. J.* **1997**, *324* (1), 305–310.

(15) Park, J. E.; Abrams, M. J.; Efron, P. A.; Barbul, A. Excessive Nitric Oxide Impairs

Wound Collagen Accumulation. *J. Surg. Res.* **2013**, *183* (1), 487–492.

(16) Gifford, R.; Batchelor, M. M.; Lee, Y.; Gokulrangan, G.; Meyerhoff, M. E.; Wilson, G. S. Mediation of in Vivo Glucose Sensor Inflammatory Response via Nitric Oxide Release. *J. Biomed. Mater. Res. Part A* **2005**, *75A* (4), 755–766.

(17) Soto, R. J.; Privett, B. J.; Schoenfisch, M. H. In Vivo Analytical Performance of Nitric Oxide-Releasing Glucose Biosensors. *Anal. Chem.* **2014**, *86* (14), 7141–7149.

(18) Malone-Povolny, M. J.; Merricks, E. P.; Wimsey, L. E.; Nichols, T. C.; Schoenfisch, M. H. Long-Term Accurate Continuous Glucose Biosensors via Extended Nitric Oxide Release. *ACS Sensors* **2019**, *4* (12), 3257–3264.

(19) Kabirian, F.; Brouki Milan, P.; Zamanian, A.; Heying, R.; Mozafari, M. Nitric Oxide-Releasing Vascular Grafts: A Therapeutic Strategy to Promote Angiogenic Activity and Endothelium Regeneration. *Acta Biomater.* **2019**, *92*, 82–91.

(20) Hofler, L.; Koley, D.; Wu, J.; Xi, C.; Meyerhoff, M. E. Electromodulated Release of Nitric Oxide through Polymer Material from Reservoir of Inorganic Nitrite Salt. *RSC Adv.* **2012**, *2*, 6765–6767.

(21) Ren, H.; Colletta, A.; Koley, D.; Wu, J.; Xi, C.; Major, T. C.; Bartlett, R. H.; Meyerhoff, M. E. Thromboresistant/Anti-Biofilm Catheters via Electrochemically Modulated Nitric Oxide Release. *Bioelectrochemistry* **2015**, *104*, 10–16.

(22) Pant, J.; Goudie, M. J.; Chaji, S. M.; Johnson, B. W.; Handa, H. Nitric Oxide Releasing Vascular Catheters for Eradicating Bacterial Infection. *J. Biomed. Mater. Res. Part B Appl. Biomater.* **2018**, *106* (8), 2849–2857.

(23) Homeyer, K. H.; Goudie, M. J.; Singha, P.; Handa, H. Liquid-Infused Nitric-Oxide-Releasing Silicone Foley Urinary Catheters for Prevention of Catheter-Associated Urinary Tract Infections. *ACS Biomater. Sci. Eng.* **2019**, *5* (4), 2021–2029.

(24) Caley, M. P.; Martins, V. L. C.; O'Toole, E. A. Metalloproteinases and Wound Healing. *Adv. Wound Care* **2015**, *4* (4), 225–234.

(25) Gill, S. E.; Parks, W. C. Metalloproteinases and Their Inhibitors: Regulators of Wound Healing. *Int. J. Biochem. Cell Biol.* **2008**, *40* (6–7), 1334–1347.

(26) Gu, Z.; Kaul, M.; Yan, B.; Kridel, S. J.; Cui, J.; Strongin, A.; Smith, J. W.; Liddington, R. C.; Lipton, S. A. S-Nitrosylation of Matrix Metalloproteinases: Signaling Pathway to Neuronal Cell Death. *Science (80-.).* **2002**, *297* (5584), 1186–1190.

(27) Jones, J. A.; Mcnally, A. K.; Chang, D. T.; Qin, L. A.; Meyerson, H.; Colton, E.; Kwon, I. L. K.; Matsuda, T.; Anderson, J. M. Matrix Metalloproteinases and Their Inhibitors in the Foreign Body Reaction on Biomaterials. *J. Biomed. Mater. Res. - Part A* **2008**, *84* (1), 158–166.

(28) Van Wart, H. E.; Birkedal-Hansen, H. The Cysteine Switch: A Principle of Regulation of Metalloproteinase Activity with Potential Applicability to the Entire Matrix Metalloproteinase Gene Family. *Proc. Natl. Acad. Sci. U. S. A.* **1990**, *87* (14), 5578–5582.

(29) Bozkurt, S. B.; Hakki, S. S.; Hakki, E. E.; Durak, Y.; Kantarci, A. Porphyromonas Gingivalis Lipopolysaccharide Induces a Pro-Inflammatory Human Gingival Fibroblast Phenotype. *Inflammation* **2017**, *40* (1), 144–153.

(30) Ploeger, D. T. A.; Hosper, N. A.; Schipper, M.; Koerts, J. A.; Rond, S. De; Bank, R. A. Cell Plasticity in Wound Healing : Paracrine Factors of M1 / M2 Polarized Macrophages Influence the Phenotypical State of Dermal Fibroblasts. *Cell Commun. Signal.* **2013**, *11* (29), 1–17.

(31) Witherel, C. E.; Abebayehu, D.; Barker, T. H.; Spiller, K. L. Macrophage and Fibroblast Interactions in Biomaterial-Mediated Fibrosis. *Adv. Healthc. Mater.* **2019**, *8* (4), 1–16.

(32) Soto, R. J.; Yang, L.; Schoenfisch, M. H. Functionalized Mesoporous Silica via an Aminosilane Surfactant Ion Exchange Reaction: Controlled Scaffold Design and Nitric Oxide Release. *ACS Appl. Mater. Interfaces* **2016**, *8* (3), 2220–2231.

(33) Soto, R. J.; Schofield, J. B.; Walter, S. E.; Malone-Povolny, M. J.; Schoenfisch, M. H. Design Considerations for Silica-Particle-Doped Nitric-Oxide-Releasing Polyurethane Glucose Biosensor Membranes. *ACS Sensors* **2017**, *2* (1), 140–150.

(34) Malone-Povolny, M. J.; Schoenfisch, M. H. Extended Nitric Oxide-Releasing Polyurethanes via S-Nitrosothiol-Modified Mesoporous Silica Nanoparticles. *ACS Appl. Mater. Interfaces* **2019**, *11* (13), 12216–12223.

(35) Griess, P. On a New Series of Bodies in Which Nitrogen Is Substituted for Hydrogen. *Philos. Trans. R. Soc. London* **1864**, *154* (1864), 667–731.

(36) Hetrick, E. M.; Schoenfisch, M. H. Analytical Chemistry of Nitric Oxide. *Annu. Rev. Anal. Chem. (Palo Alto. Calif).* **2009**, *2*, 409–433.

(37) Owens, M. W.; Milligan, S. A.; Jourd'Heuil, D.; Grisham, M. B. Effects of Reactive Metabolites of Oxygen and Nitrogen on Gelatinase A Activity. *Am. J. Physiol. - Lung Cell. Mol. Physiol.* **1997**, *273* (2 17-2), 445–450.

(38) Ra, H. J.; Parks, W. C. Control of Matrix Metalloproteinase Catalytic Activity. *Matrix Biol.* **2007**, *26* (8), 587–596.

(39) Siwik, D. A.; Colucci, W. S. Regulation of Matrix Metalloproteinases by Cytokines and Reactive Oxygen/Nitrogen Species in the Myocardium. *Heart Fail. Rev.* **2004**, *9* (1), 43–51.

(40) Nathan, C. F.; Murray, H. W.; Wlebe, I. E.; Rubin, B. Y. Identification of Interferon-γ, as the Lymphokine That Activates Human Macrophage Oxidative Metabolism and Antimicrobial Activity. *J. Exp. Med.* **1983**, *158* (3), 670–689.

(41) Adams, D. O.; Hamilton, T. a. The Cell Biology of Macrophage Activation. *Annu. Rev. Immunol.* **1984**, *2*, 283–318.

(42) Koh, T. J.; DiPietro, L. A. Inflammation and Wound Healing: The Role of the Macrophage. *Expert Rev. Mol. Med.* **2011**, *13* (e23).

(43) Weil-Malherbe, H.; Weiss, J. Quenching of Fluorescence by Nitric Oxide. *Nature* **1943**, *151* (3833), 449.

(44) van Shui-Pong, S.; Hammond, G. S. Amine Quenching of Aromatic Fluorescence and Fluorescent Exciplexes. *J. Am. Chem. Soc.* **1978**, *100* (12), 3895–3902.

(45) Schoenfisch, M. H.; Zhang, H.; Frost, M. C.; Meyerhoff, M. E. Nitric Oxide-Releasing Fluorescence-Based Oxygen Sensing Polymeric Films. *Anal. Chem.* **2002**, *74* (23), 5937–5941.

CHAPTER 5 – SUMMARY AND FUTURE DIRECTIONS

5.1 Summary of Research

This dissertation work sought to use both novel and existing in vivo and in vitro bioassays to analyze the effect of nitric oxide (NO) on the foreign body response (FBR). Published reports of histological outcomes and sensor performance have both supported the use of NO-release sensor membrane coatings to boost the analytical biocompatibility of implantable glucose monitors, leading to stronger performance for an extended timespan versus controls.[1–7] However, NO's mechanism of action in this context had remained uninvestigated. My dissertation research served to explore these two questions to correlate the exogenous NO dose necessary for improved sensor performance with wound-healing pathways and biomarkers immunomodulated by NO. Understanding biological mechanisms will allow future work to investigate the rational design of NO-releasing glucose sensors and perhaps how NO release might be tuned to achieve a desired outcome.

The introductory chapter to this dissertation explored the health benefits of continuous glucose monitoring (CGM)[8–14] and the impact of the foreign body response (FBR) on implanted glucose monitor lifetime.[15–18] With a complex cascade of cells to the sensor surface, the FBR causes to sensor damage and decreased sensitivity through various mechanisms including the release of damaging reactive oxygen and nitrogen species, an interfering glucose depletion by local inflammatory cells, and the eventual isolation of the sensor in a collagen capsule. Though there are many different mechanisms to lessen the FBR and inflammatory response, such as surface texturing of the sensor and the active release of

anti-inflammatory agents such as dexamethasone,[17,19–22] Chapter 1 focused on the unique advantages of NO as an active release anti-inflammatory agent. The biological effects of NO have been explored since its identification as the endothelium-derived relaxing factor, both through modulation of its endogenous production[23,24] or via the addition of NO-releasing molecules.[25,26] In particular, NO has been implicated in modulating cell proliferation,[27,28] in promoting angiogenesis,[24,29] and in altering collagen formation.[23,30,31] These effects of NO have also been observed in the in vivo reports on NO-releasing glucose sensors.[1–7] Recent studies have focused on sensor investigations in euglycemic and hyperglycemic porcine. Both Soto et al. and Malone-Povolny et al. reported that the use of NO-release coatings led to a longer retention of sensor accuracy, reduced cell infiltration, and increased angiogenesis.[2–4] Importantly, these results persisted for as long as the NO was being released: once the NO supply was exhausted, the NO-releasing sensor's performance gradually reversed towards the performance of the non-releasing controls, highlighting the importance of sustained NO release in preserving this improved performance[2,4]

Chapter 2 described the use of glucose measurements to assess macrophage response to NO. As macrophages are cells that are vital to the regulation of the FBR, it is important to supplement the data on NO's therapeutic effect on the FBR with studies of how that NO flux may affect macrophages directly. Of particular relevance to glucose sensors, macrophages can be influenced across a polarization gradient by environmental stimuli, shifting reversibly between pro-inflammatory (M1) and anti-inflammatory (M2) phenotypes.[32–34] Concerning the proper implementation of implantable glucose sensors, it is vital to minimize interfering glucose consumption, particularly that by macrophages, to maintain sensor accuracy because macrophages consume more glucose than other cell types[35] and because glucose consumption is increased when macrophages are in an M1 phenotype.[36–39] Two orthogonal techniques were implemented to analyze the glucose consumption by RAW 264.7 macrophages: 1) use of a fluorescent tracer (2-NBDG) to model glucose consumption, and 2) embedding macrophages

in a 3D-cell scaffold to monitor their bulk glucose consumption using an intrascaffold electrochemical glucose sensor. Flow cytometry studies involving 2-NBDG showed modulation of glucose consumption in response to small molecule NO donors, including DETA/NO and SNAP.

The mechanisms of NO's effect on FBR were detailed in Chapter 3. A euglycemic porcine model was employed to compare both cytokine and gene expression in the tissue surrounding NO-releasing implants, non-releasing implants, and control biopsies. This investigation sought specifically to elucidate the NO-induced immunomodulation responsible for enhanced analytical biocompatibility. The cytokine concentration showed that NO both lowers chemokine concentration and is associated with a less pro-inflammatory tissue response when compared to non-releasing implants. Interestingly, it was also observed that NO release from the sensor led to cytokine loads closer to the native tissue compared to non-releasing controls. A custom 254-gene panel was created for the analysis of differential gene expression across different samples as well as predictive profiling of the abundances of various cell types. Through cell profiling, it was noted that NO release halves the expression of the pan-leukocyte marker CD45 compared to non-releasing sensors, implying lower leukocyte infiltration as a result of exogenous NO. Additionally, NO was shown to unequivocally affect the composition of the cell population present at the site of insult. When comparing the two sensor types, expression of collagens and chemokines decreased collagen production with NO, compared to the non-releasing sensor. On day 14, angiogenic markers TGFB and VEGFB were upregulated with NO. Finally, Blk, MMP8, and CASP1 were immunomodulated by both the non-releasing and NO-releasing implants, and thus identified as biomarkers for monitoring NO's effect on the FBR. Taken together, these findings both substantiated previously published investigations into NO-releasing sensors and enabled identification of new biomarkers and immune pathways modulated with NO release.

The aforementioned differential expression analyses also demonstrated the immunomodulation of matrix metalloproteinases (MMPs) as a result of FBR, with that immunomodulation altering under exposure to NO. Given the role of MMPs in both protein regulation (e.g., chemokines, other MMPs) and in degradation of extracellular matrix components such as collagen, Chapter 4 detailed the exploration of NO's effect on MMP activity. Due to their prominent roles in the wound healing process, macrophages and fibroblasts were interrogated with increasing concentrations of lipolysaccharides (LPS), serving as an inflammatory stressor, and varying levels of either DPTA/NO or DETA/NO. While fibroblast MMP activity had minimal differences between the NO donor and its respective control scaffold (DPTA or DETA, respectively), MMP activity in macrophages was found to be increased by NO using 0.02 mg/mL DPTA/NO. No significant changes in MMP activity were observed in macrophages using 0.2 mg/mL DPTA/NO, nor with 0.02 or 0.2 mg/mL DETA/NO, implying a narrow window of NO dosage creating quantifiable effects on MMP activity. Exposing a solution of fetal bovine serum to low levels of NO from an NO-releasing wire (0.26-0.36 mM) was also shown to reduce MMP activity in vitro, contrasted with 0.42 mM NO producing no significant effect, demonstrated the potential of NO release to reduce MMP activity an NO-releasing sensor implantation site.

5.2 Future Directions

The work completed in this dissertation serves as a foundation for exploring the basic science of NO's mediation of the foreign body response (FBR). Below, future experiments are proposed to further this effort in three orthogonal directions. One direction is the development of a device on which NO could be released in a controlled manner, allowing interrogation of NO's effect on cell biology without needing to rely on an NO donor, as the scaffold may possess independent physiological effects that may disguise or alter the response to NO. Second, data from a pilot study examining changes in the lipid profile of polarized

macrophages exposed to NO suggest that lipids are a potential biomarker for monitoring the FBR. Lastly, to complement in vivo investigations, strategies for developing more informative and representative in vitro and ex vivo models are discussed to facilitate systematic study of NO-release conditions on cell and tissue biology.

5.2.1 Utilizing Modular NO Release for Direct Cell Interrogation

To best explore the effects of NO-release kinetics on cell function, it is critical to have both a reliable source of NO and a tunable NO-release profile. Thus far, we have explored using NO donors to expose cells to NO fluxes. However, this method is not without complications. Though we can run control experiments against non-releasing scaffolds, the scaffold itself still may be affecting the cellular phenotype, as has been reported previously with silica nanoparticles and polyamines systems.[40–42] Due to the effect of the scaffold, deconvoluting the role of NO may not be possible. Further, due to the diversity in macromolecular scaffolds, if the identity of the scaffold has any effect, disparate, scaffold-dependent phenotypes may be observed. An additional concern involves limitations with the NO donors themselves, as only NO fluxes from readily available or synthesizable NO donors can be tested.

To address these challenges, in situ generation of NO would obviate the need for macromolecular scaffolds without reintroducing any of the disadvantages of NO gas cylinder usage, such as poor NO availability in solution.[43] Electrogeneration of nitric oxide requires the electrochemical reduction of nitrite from solution and has been reported previously by the Meyerhoff lab, via NO-releasing catheters.[44,45] These catheters were made with silicone tubing filled with an electrogeneration solution (i.e., 1 M $NaNO_2$, 0.30 M NaCl, 0.02 M EDTA, 1 M phosphate buffer; pH 7.05), a copper working electrode, and an Ag|AgCl reference electrode. Using a function generator to control the applied potential and corresponding evolution of NO, the system was shown to have reproducible control over the resultant NO flux through

modulation of the cathodic potential, releasing fluxes of up to 1.5 x 10^{-10} mol min^{-1} cm^{-2} at -1.4 V.[44] This cathodic step is paired with an anodic pulse for regeneration of the copper electrode surface, and cycling between the cathodic and anodic steps at high frequencies provides the reproducible evolution of NO.[44,45] When implanted in mice, these NO-producing catheters prevented thrombosis, platelet adhesion, and biofilm growth in comparison to a non-releasing control.[44,45]

Translation of this platform to cell culture would facilitate precise and hands-free control of the NO flux, as the necessary waveform can be accurately applied with a function generator. A minimum viable product, as prototyped in Figure 5.1, could be designed with a static well plate design holding 9-96 wells with working volumes of 100 μL, similar to a standard 96-well plate. A chamber at the bottom of the device would contain the electrogeneration solution, counter and reference electrodes, and copper electrodes set directly beneath each well, allowing for NO to diffuse to the cells from the bottom. Importantly, these copper electrodes would be connected to a function generator, likely from the bottom. A semipermeable film of silicone or fluorosilicone would be positioned between the wells and the electrogeneration chamber, simultaneously permitting the diffusion of NO to the wells and preventing the transport of the hypertonic electrogeneration solution into the cell medium. Cells would be seeded on top of the film, which could then be coated with fibrin, poly-L-lysine, or similar substrate to promote cell adhesion. While electrodes could be connected to a common function generator, the use of multiple function generators would allow different waveforms to be cast to each, allowing for novel experiments pertaining to NO gradients (Figure 5.2.), such as a preliminary exploration into chemotaxis along nitric oxide gradients.

The electrogeneration of NO from copper is fairly well-characterized, so the main obstacle for this platform would be determining the extent to which NO reaches the cells. Doing so would require two separate steps: determining the NO yield from the copper

electrode and assessing what portion reaches the cells. Characterizing the copper electrode may be performed using a nitric oxide analyzer (NOA). By placing the copper, reference, and counter electrodes in the NOA reaction vessel, filled with the electrogeneration solution, different waveforms can be applied to the electrode and the evolution of NO can be monitored in real-time. For assessing NO transport to the cells, the fluorophore DAF-FM can be used to monitor NO's transit into the well via confocal microscopy. As the fluorophore is detectable only after reaction with NO, DAF-FM will serve as a selective indicator for monitoring and quantifying the NO reaching the wells.[46] Kinetic studies can also be performed by removing timepoint aliquots from the wells and measuring their fluorescence intensity, which would allow for comparison with the NO flux profile generated by the electrode in the NOA. Identifying discrepancies will inform adjustments to the device's design, such as changing the depth of the solution chamber at the bottom or increasing the flux of NO produced at the bottom to achieve proper levels of NO in the well.

This platform would streamline several biological assays currently performed in the NO research community, through the obviation of an NO donor. Applying a desired NO flux would become simply a matter of applying the correct waveform. The effects of NO flux kinetics in various studies including cell proliferation, cytokine production, cytotoxicity and biocidal activity, the aforementioned chemotaxis across an NO gradient, and morphological changes, could all be explored without requiring the independent synthesis of an appropriate donor. Indeed, this system would allow studies to surpass the current limitations of NO donors, including scaffold toxicity concerns and ceilings on the total release duration.

5.2.2 Lipidomic Analysis of Cellular Markers

My dissertation research relied on various markers of cellular polarization in response to NO, such as gene expression to cytokine profiles to glucose consumption, to interrogate aspects of the FBR. The role of lipid markers, however, remains a largely untapped frontier in

the full characterization of the foreign body response. Lipids are an important energy source and structural unit for the cell (e.g., phospholipids forming the cellular membrane), but lipid metabolism and using metabolized lipids as novel markers for differentiating healthy and diseased physiologies remains quite novel. The presence or absence of different lipids has been well characterized in wound healing, inflammation, and macrophage polarization.[47] For example, the fatty acid arachidonic acid, released from phospholipids by phospholipase A_2, is a precursor to many pro-inflammatory mediators, notably prostaglandins.[48,49] Prostaglandin expression and phospholipase A_2 activity have been linked to inflammatory phenomena, including increased cellular glucose consumption and the onset of cytokine storms.[50] Lipid processing has also been linked to NO production, as phospholipase A_2 activity is positively correlated to the expression of the inducible nitric oxide synthase (iNOS)[51,52] and phospholipase A_2 was downregulated when NO synthesis is inhibited.[53] Thus, lipids have the potential to serve as biomarkers for monitoring the wound healing response towards the FBR and how it is altered by NO release.

Lipidomic analysis of a cell system's full lipid profile, or lipidome, can identify and quantify changes in lipid expression as a complement to traditional phenotyping techniques. However, various characteristics of lipids make their identification and quantification difficult, including a large number of existing lipids (at least 30,000 identified, while the total count of naturally occurring lipids is estimated to be on the order of 10^5), the prevalence of isobars and isomers, and low-abundance lipid species. Despite the difficulty in lipid identification, a universal nomenclature system has been developed and is used herein. Using PC(16:0e_20:5) as an example, the leading letter code identifies the lipid headgroup and thus the subclass the lipid belongs to, in this case, is phosphatidylcholine. The underscore separates the different fatty acid (FA) chains and also denotes that there is no known steric information regarding those chains (e.g., a forward slash separating the fatty acids would mean those fatty acids are ordered based on their positions on the phospholipid's glycerol backbone). And

finally, the fatty acid is coded as the number of carbon atoms in the chain on the left of the colon and the number of double bonds on the right of the colon. The lowercase 'e' denotes an ether linkage in the chain. For this example, PC(16:0e_20:5) identifies a phosphatidylcholine with two FA chains: one with 16 carbons, an ether linkage, no double bonds, and a 20 carbon chain containing 5 double bonds.

Techniques for identifying lipids include thin-layer chromatography (TLC) and NMR. A new promising technique is ultrahigh-pressure liquid chromatography (UHPLC). The high pressure in addition to a packed capillary column allows effective resolution of a large number of lipids. Lee et al. used UHPLC to probe polarization of RAW 264.7 macrophages at increasing concentrations of LPS (i.e., increasing inflammation). They observed dose-dependent increases of LPS upregulated 11 classes of lipids, including phosphatidylinositol (PI), phosphatidylserine (PS), and phosphatidylethanolamine (PE); while downregulating cholesterol, phosphatidylcholine (PC), and lysophosphatidic acid (LyPA).[54] Inspired by this literature, I initiated a pilot study to interrogate macrophage polarization in response to NO using lipidomic analysis in collaboration with Dr. Kelsey Miller of the Jorgenson lab at UNC.

Briefly, RAW 264.7 macrophages were plated on T-75 culture flasks and either left untreated (unstimulated; M(-)) or co-stimulated with either 1 μg/mL LPS or 0.1 μM dexamethasone and either 5 or 500 μg/mL DETA/NO. The negative control, DETA, was used in place of DETA/NO to confirm that the NO release had an independent effect on the cells from the scaffold. After 24 hours, stimulated macrophages were scraped from the flask, pelleted, and the lipids were extracted for analysis using UHPLC, paired with a mass spectrometer for analysis (UHPLC-MS). Biological duplicates of each sample were run and lipids were identified using LipidSearch 4.2.21 (Thermo Fisher, CA). Peak areas were normalized to both the mass of lipid run and to one of three controls: M(-) to compare M(LPS) and M(DEX), M(LPS) for the pro-inflammatory macrophages, and M(DEX) for the anti-inflammatory macrophages. Peak areas were used for partial least squares-discriminate

analysis (PLS-DA) allowing comparison between the common lipids found in different macrophage populations.

Comparison between M(-), M(LPS), and M(DEX) cells did not present a clear biomarker differentiating an M1 phenotype from an M2 phenotype. The 25 most prominent lipids of the 386 unique lipids identified, as determined using variable importance in projection (VIP) scoring, were present in all 3 samples. The VIP score used a partial least squares regression to identify the most influential targets in the model, where a higher VIP score increases the likelihood of the target being a potential biomarker. Those 25 lipids were plotted on a heatmap based on their fold change in expression, relative to M(-) (Figure 5.3). Minute differences between M(LPS) and M(DEX) were observed, such as more severe downregulation of various PI lipids and PC (18:1_18:1), suggesting possible utility in lipidomics-based phenotype differentiation, despite the lack of biomarker.

The effect of NO on the lipid profile of polarized macrophages was also examined through the co-culturing of macrophages with either 5 or 500 μg/mL DETA/NO alongside either 1 μg/mL LPS for M1 macrophages (LPS Control), or 0.1 μM dexamethasone for M2 macrophages (DEX Control). Serving as a control, 5 and 500 μg/mL DETA were also tested to isolate the effects of NO from the scaffold. For both pro- and anti-inflammatory macrophages, 422 and 463 unique lipids were identified, respectively. Again, a comparison for the top 25 lipids was accomplished through VIP scoring for both data sets, relative to either the M1 or the M2 control (Figures 5.4 and 5.5). For M1 macrophages, 500 μg/mL DETA/NO effectively downregulated a number of PIs, PEs, and PCs, including PI(18:0_16:1), PE(16:1e_20:4), and PC(14:0_14:0). Conversely, the 5 μg/mL dose of DETA/NO led to upregulation of some PCs and PEs, including PC(16:0_12:1), PC(18:0_12:1), and PE(18:0_20:1), highlighting the dose-dependent and diverse nature of NO. For anti-inflammatory macrophages, NO elicited more subtle differences, such as the slight downregulation of PCs, PEs, and PSs, including PS(18:0_22:6), PE(16.1e_22:6), PC(14:0_20:4), when treated at 500 μg/mL DETA/NO.

This pilot study demonstrated that even though there was not necessarily a strong biomarker to differentiate M(LPS) from M(DEX), NO did induce measurable changes in the lipid profiles of inflammatory cells at two concentrations. The lipid profiles from the NO donors also differed significantly from the lipid profiles of the bare DETA scaffold, supporting that NO itself is eliciting at least part of the biological change. In conclusion, lipidomics remains an unexplored tool for understanding the foreign body response in relation to NO exposure. Expansion of this study should focus on a deeper characterization of the macrophages, such as comparison to cytokine and gene expression data, modulation of NO exposure (i.e., altering NO donors used, NO dosage, and NO release profiles), and using more sophisticated biostatistics to identify trends and possible biomarkers. Additionally, the use of higher than conventional UHPLC pressures (~35 kpsi) and a custom packed capillary has been reported for lipidomic analysis and will likely resolve phospholipids at a higher resolution was obtained in this study.[55]

5.2.3 Exploring NO-affected Inflammation in Advanced Tissue Models

In Chapter 4, the relationship between inflammation and NO dose was assessed in monocultures of macrophages and fibroblasts. As NO was shown to affect these cells and their inflammatory states, research should continue in addressing this and similar questions of phenotypical change using more reliable models. In particular, a move towards more representative cell culture models would improve the power and predictive ability of the aforementioned assay, and better aid identification of the optimal exogenous NO flux to be used with implantable glucose monitors. Of note, in vivo models can also be used to explore NO's effects on the FBR, as demonstrated in Chapter 3. Though less complex and physiologically representative, in vitro and ex vivo models are amenable to systematic studies of design properties of an NO-releasing sensor, where, due to their cost and relative simplicity, testing large numbers of parameters would be advantageous. Here, I will focus specifically on

new in vitro and ex vivo models that can be used for either preliminary inquiries preceding in vivo studies or in expanding on the findings of in vivo experiments.

One improvement to the monocultures explored in this dissertation would be a transition to cellular co-cultures. A co-culture model allows for some level of intercellular communication between different cell types, either as a paracrine (i.e., indirect) co-culture, relying on using conditioned media to introduce cell signals from one cell line to another, or a juxtacrine (i.e., direct) co-culture, growing at least two distinct cell lines in concert. Given that the foreign body response is predicated on interactions between different cells, co-cultures are a natural way to study the FBR. Indeed, there is already evidence that these cells influence the inflammatory phenotype of one another. Ploeger et al. reported that paracrine factors (i.e., conditioned media) from either pro- or anti-inflammatory macrophages could alter the phenotype of fibroblasts, including their rates of extracellular matrix formation, matrix metalloproteinase (MMP) activity, and chemokine expression.[56] An expansion of the work presented in Chapter 4 could employ conditioned media from one cell type exposed to another cell type to determine if the different cytokine profiles alter NO's effect on MMP activity. Additionally, either of these co-culture models facilitates the elucidation of how NO treatment alongside intercellular communication affects cell proliferation, phenotypic polarization, and chemokine gradients. As NO is implicated in cell-cell communication,[57] investigating exogenous NO in a co-culture model would allow for the elucidation of how the addition of another intercellular signal affects the foreign body response.

Another improvement could be made by employing three-dimensional cell scaffolds. Despite the ubiquity of the two-dimensional cell culture in biomedical research, its shortcomings have been well-characterized. In general, two-dimensional cultures lack the complexity of tissue or an actual wound bed whereas three-dimensional culture has been linked to cell morphologies, growth, and migration, and intercellular interactions more akin to an in vivo model.[58,59] Multiple types of 3D cell cultures exist, including gels,[36,60]

microfluidics,[61,62] and paper-based scaffolds.[63–65] Of particular interest to this dissertation work is the gel model, such as the one developed by Novak et al. and adapted for the studies in Chapter 2.[36] Briefly, that model embedded macrophages in a fibrin gel, generating a 3D culture of cells in a biological scaffold at a macrophage density comparable to a site of insult. The gel was then pierced with a glucose sensor to monitor the glucose consumption of the cells over time. This model is particularly attractive for exploring FBR interactions, as it allows for the introduction of an implant. A mock glucose sensor (i.e., wire) may be coated with an NO-releasing polyurethane membrane and implanted, producing an NO point source from which physiological effects can be characterized. Immunofluorescence facilitates phenotypic assessment but could also afford new spatial information (i.e., resolving the relationship between distance from NO source and polarization state). Importantly, 3D cell cultures are not limited to monocultures and are amenable to both types of co-culture. In fact, performing a juxtacrine co-culture in a 3D scaffold results in an in vitro system most closely approaching the layout of cells in their native in vivo environment, mimicking both the intercellular communication and spatial orientation found in vivo. Using immunofluorescence allows for analyses of inflammatory markers, but also identification of and discrimination between different cell types as a function of NO release.

Lastly, the use of a new ex vivo or tissue model could be explored to examine the effects of NO. For example, the Mattek EpiDerm FT features a full-thickness human tissue sample consisting of primary fibroblasts and keratinocytes. This tissue has been used in several studies, including observing the inflammatory effects of mustard compounds and assessing ionic liquids for delivering antibiotics to transdermal biofilms.[66–68] Many of the aforementioned analyses, such as cytokine profiling and gene expression, may be employed using this model. The platform also lends itself to histological and immunohistochemical queries, adding new routes of interrogation. Similar to the gel cell scaffold, this tissue sample could be wounded with a mock glucose sensor serving as an NO source, emulating an NO-

releasing sensor implanted in the subcutaneous layer of skin. As the scaffold is a tissue, additional sensor elements affecting tissue reintegration may be analyzed without the use of an in vivo model. For example, Malone-Povolny et al. found NO-releasing sensors could be combined with passive FBR mitigation (i.e., pores and electrospun fibers on the sensor surface) for improvements in the FBR mitigation, outperforming either strategy in isolation. The Mattek platform would allow for systematic testing to determine the optimal NO-release profiles and pore sizes required for an enhanced wound healing response in a more cost-effective manner than using animals.

5.3 Conclusions

Given that the FBR is a major impediment to longterm continuous glucose monitoring, investigations into FBR-reducing implants are critical in improving diabetic healthcare. Active release of exogenous NO has emerged as a powerful strategy for improving the analytical biocompatibility of CGM technology. My research sought to elucidate the mechanisms through which NO promoted these therapeutic effects. In using both traditional and novel biological assays, it was discovered that NO does indeed have influences on the concentrations of proteins at the site of insult, on the immunomodulation of various wound-healing genes, in the activity of MMPs, and potentially in the glucose consumption of polarized macrophages. The effects of NO-release kinetics and NO dose were also explored in vitro, showing that MMP activity can be modulated in a narrow window of NO exposure, both in acellular and cellular testing conditions. Though much work exploring the physiological outcomes of NO-releasing glucose sensors exists, the observations made in my research will serve as a foundation for further bioassay development towards a systematic study of how those outcomes are achieved. Expanding investigations into NO's mechanisms of action, as well as the NO doses and the release kinetics required to drive the desired wound healing pathways, may facilitate the

rational design of NO-releasing glucose sensors, allowing for development of more beneficial CGM technology for diabetes treatment.

5.4 Figures and Tables

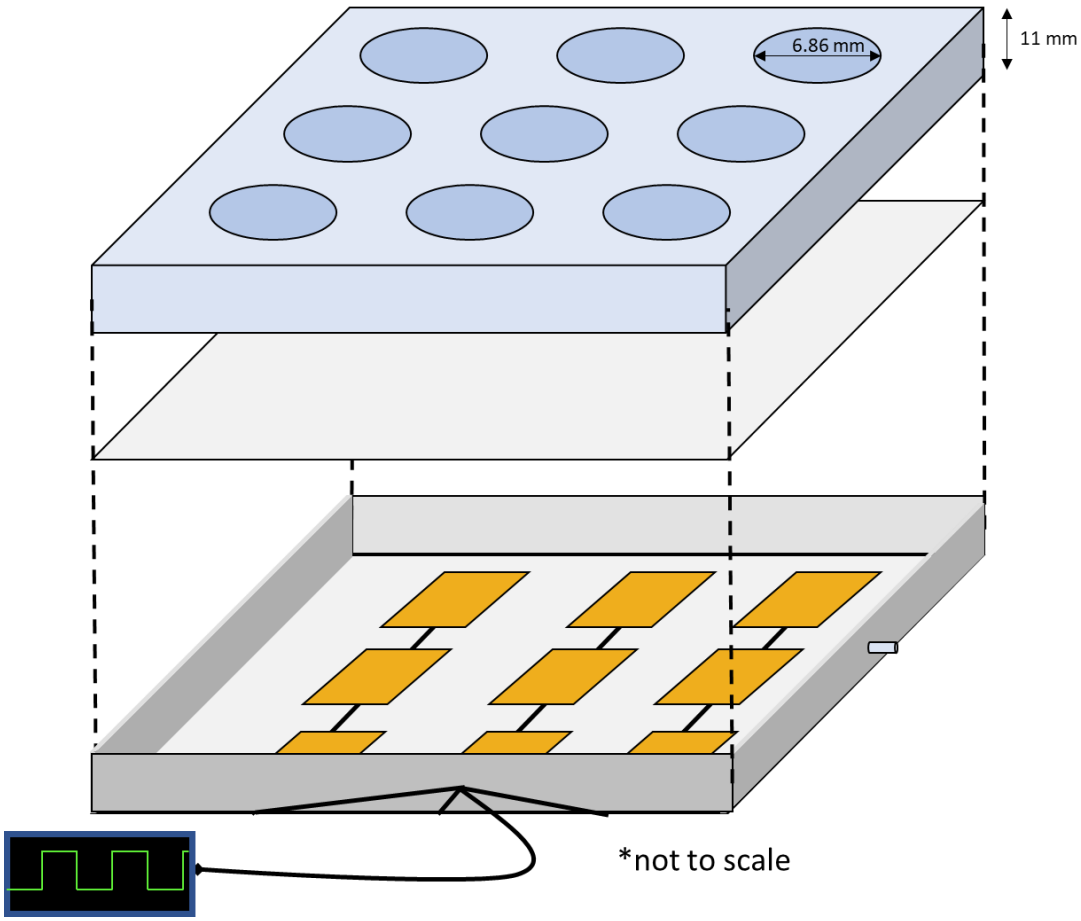

Figure 5.1. A nitric oxide-generating well plate prototype. The top layer features a well plate molded from PDMS and cast to dimensions analogous to a 96 well plate. Cells will be seeded on top of the middle layer, a thin film of silicone rubber or fluorosilicone, which are gas-permeable to allow transport of NO and solution-impermeable to prevent leaking of the hypertonic electrogeneration solution. The bottom chamber contains the electrogeneration solution and copper electrodes positioned below each well, NO evolution to the seeded cells. The electrodes will be connected to a function generator to apply custom waveforms via computer control. Reference and counter electrodes not shown.

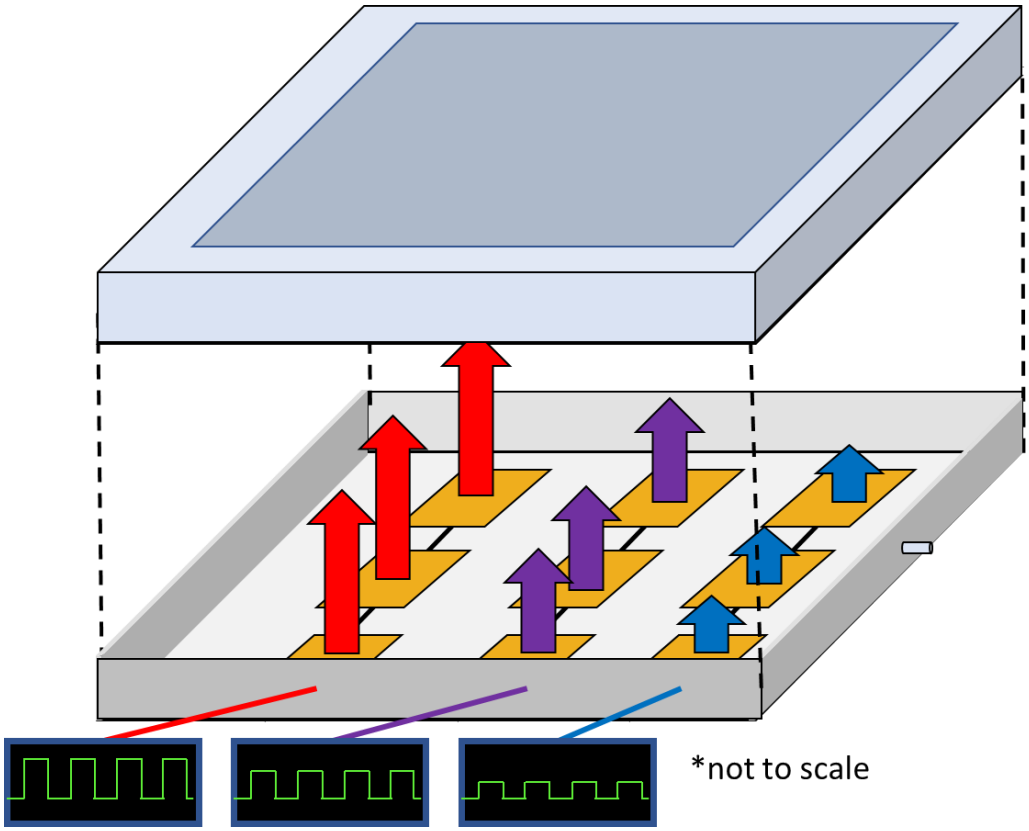

Figure 5.2. An alternative model of the nitric oxide-generating well plate. Different waveforms can be applied to each column of electrodes, producing a different flux of NO at each electrode. Using a larger seeding area will allow cells to receive a NO on a concentration gradient and migrate along the well for chemotaxis experiments. Middle silicone layer, counter electrode, and reference electrode are not shown.

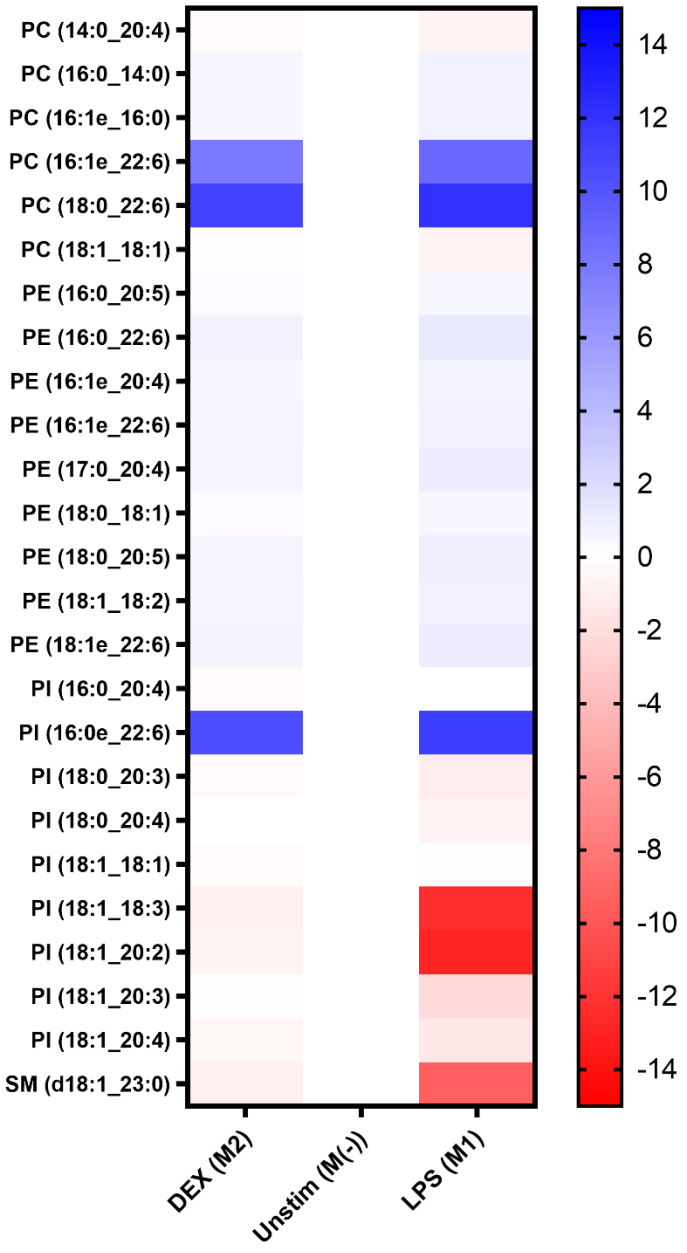

Figure 5.3. Fold change heat map of lipids with the top 25 VIP scores, comparing M(-) with M1 (i.e., M(LPS)) and M2 (i.e., M(DEX)). Fold change is normalized to the M(-) lipidome. PI = phosphatidylinositol, PE = phosphatidylethanolamine, PC = phosphatidylcholine, SM = sphingomyelin

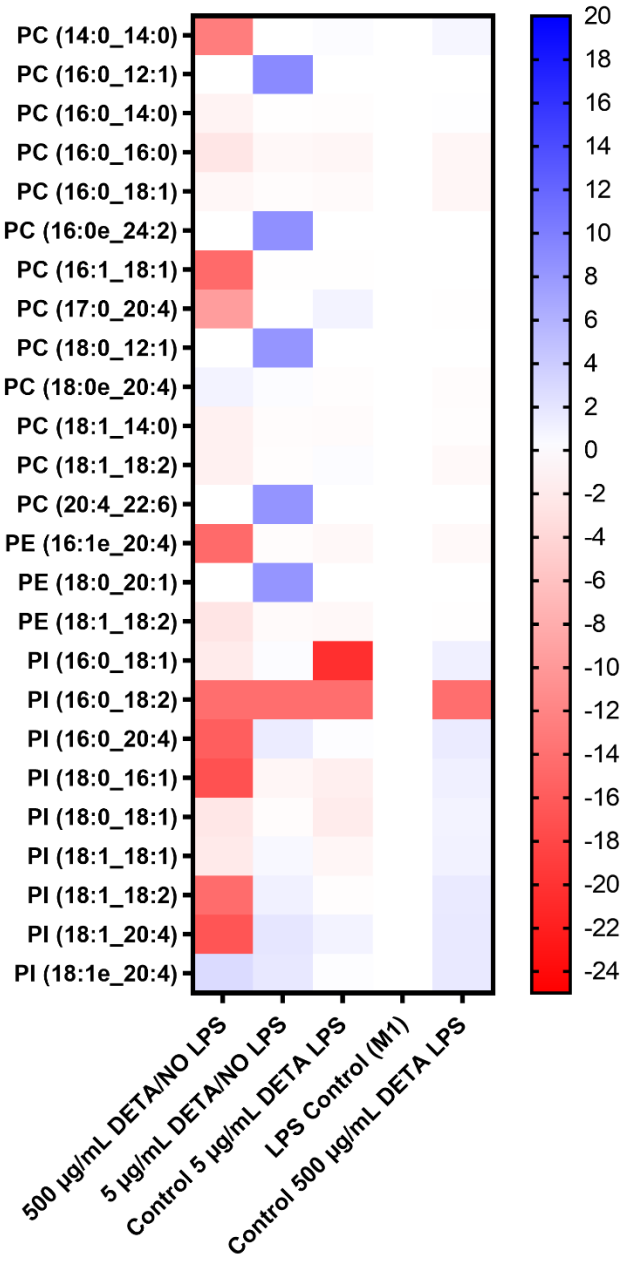

Figure 5.4. Fold change heat map of lipids with the top 25 VIP scores, comparing pro-inflammatory macrophages exposed to DETA/NO or DETA at 5 or 500 µg/mL. Fold change is normalized to the LPS Control lipidome. PI = phosphatidylinositol, PE = phosphatidylethanolamine, PC = phosphatidylcholine

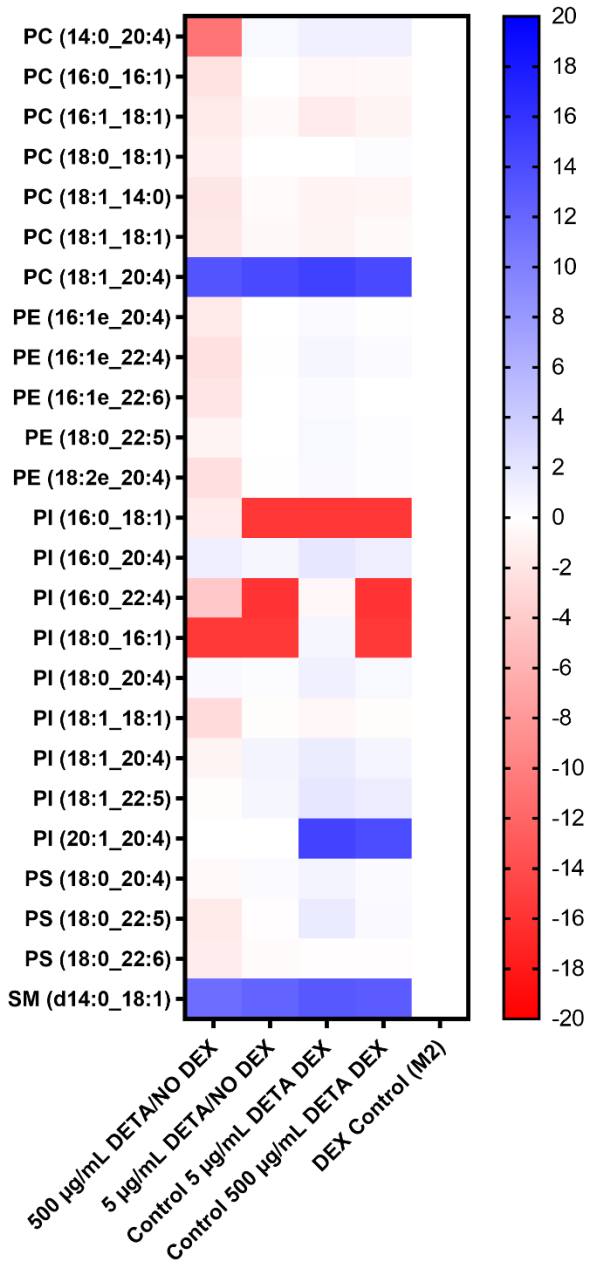

Figure 5.5. Fold change heat map of lipids with the top 25 VIP scores, comparing anti-inflammatory macrophages exposed to DETA/NO or DETA at 5 or 500 µg/mL. Fold change is normalized to the DEX Control lipidome. PI = phosphatidylinositol, PE = phosphatidylethanolamine, PC = phosphatidylcholine, PS = phosphatidylserine, SM = sphingomyelin

REFERENCES

(1) Gifford, R.; Batchelor, M. M.; Lee, Y.; Gokulrangan, G.; Meyerhoff, M. E.; Wilson, G. S. Mediation of in Vivo Glucose Sensor Inflammatory Response via Nitric Oxide Release. *J. Biomed. Mater. Res. Part A* **2005**, *75A* (4), 755–766.

(2) Soto, R. J.; Merricks, E. P.; Bellinger, D. A.; Nichols, T. C.; Schoenfisch, M. H. Influence of Diabetes on the Foreign Body Response to Nitric Oxide-Releasing Implants. *Biomaterials* **2018**, *157*, 76–85.

(3) Soto, R. J.; Privett, B. J.; Schoenfisch, M. H. In Vivo Analytical Performance of Nitric Oxide-Releasing Glucose Biosensors. *Anal. Chem.* **2014**, *86* (14), 7141–7149.

(4) Malone-Povolny, M. J.; Merricks, E. P.; Wimsey, L. E.; Nichols, T. C.; Schoenfisch, M. H. Long-Term Accurate Continuous Glucose Biosensors via Extended Nitric Oxide Release. *ACS Sensors* **2019**, *4* (12), 3257–3264.

(5) Hetrick, E. M.; Prichard, H. L.; Klitzman, B.; Schoenfisch, M. H. Reduced Foreign Body Response at Nitric Oxide-Releasing Subcutaneous Implants. *Biomaterials* **2007**, *28* (31), 4571–4580.

(6) Nichols, S. P.; Koh, A.; Brown, N. L.; Rose, M. B.; Sun, B.; Slomberg, D. L.; Riccio, D. A.; Klitzman, B.; Schoenfisch, M. H. The Effect of Nitric Oxide Surface Flux on the Foreign Body Response to Subcutaneous Implants. *Biomaterials* **2012**, *33* (27), 6305–6312.

(7) Nichols, S. P.; Le, N. N.; Klitzman, B.; Schoenfisch, M. H. Increased In Vivo Glucose Recovery via Nitric Oxide Release. *Anal. Chem.* **2011**, *83* (4), 1180–1184.

(8) Farmer, A.; Balman, E.; Gadsby, R.; Moffatt, J.; Cradock, S.; McEwen, L.; Jameson, K. Frequency of Self-Monitoring of Blood Glucose in Patients with Type 2 Diabetes: Association with Hypoglycaemic Events. *Curr. Med. Res. Opin.* **2008**, *24* (11), 3097–3104.

(9) O'Connell, M. A.; Donath, S.; O'Neal, D. N.; Colman, P. G.; Ambler, G. R.; Jones, T. W.; Davis, E. A.; Cameron, F. J. Glycaemic Impact of Patient-Led Use of Sensor-Guided Pump Therapy in Type 1 Diabetes: A Randomised Controlled Trial. *Diabetologia* **2009**, *52* (7), 1250–1257.

(10) Miller, K. M.; Beck, R. W.; Bergenstal, R. M.; Goland, R. S.; Haller, M. J.; McGill, J. B.; Rodriguez, H.; Simmons, J. H.; Hirsch, I. B. Evidence of a Strong Association between Frequency of Self-Monitoringof Blood Glucose and Hemoglobin A1c Levels in T1D Exchange Clinic Registry Participants. *Diabetes Care* **2013**, *36* (7), 2009–2014.

(11) Deiss, D.; Bolinder, J.; Riveline, J. P.; Battelino, T.; Bosi, E.; Tubiana-Rufi, N.; Kerr, D.; Phillip, M. Improved Glycemic Control in Poorly Controlled Patients with Type 1 Diabetes Using Real-Time Continuous Glucose Monitoring. *Diabetes Care* **2006**, *29* (12), 2730–2732.

(12) Beck, R. W. Sustained Benefit of Continuous Glucose Monitoring on A1C, Glucose Profiles, and Hypoglycemia in Adults With Type 1 Diabetes. *Diabetes Care* **2009**, *32* (11), 2047–2049.

(13) Beck, R. W.; Hirsch, I. B.; Laffel, L.; Tamborlane, W. V; Bode, B. W.; Buckingham, B.; Chase, P.; Clemons, R.; Fiallo-Scharer, R.; Fox, L. A.; Gilliam, L. K.; Huang, E. S.; Kollman, C.; Kowalski, A. J.; Lawrence, J. M.; Lee, J.; Mauras, N.; O'Grady, M.; Ruedy, K. J.; Tansey, M.; Tsalikian, E.; Weinzimer, S. A.; Wilson, D. M.; Wolpert, H.; Wysocki, T.; Xing, D. The Effect of Continuous Glucose Monitoring in Well-Controlled Type 1 Diabetes. *Diabetes Care* **2009**, *32* (8), 1378–1383.

(14) Peters, A. L.; Ahmann, A. J.; Battelino, T.; Evert, A.; Hirsch, I. B.; Murad, M. H.; Winter, W. E.; Wolpert, H. Diabetes Technology—Continuous Subcutaneous Insulin Infusion Therapy and Continuous Glucose Monitoring in Adults: An Endocrine Society Clinical Practice Guideline. *J. Clin. Endocrinol. Metab.* **2016**, *101* (11), 3922–3937.

(15) Anderson, J. M. Biological Responses to Materials. *Annu. Rev. Mater. Res.* **2001**, *31* (1), 81–110.

(16) Grainger, D. W. All Charged up about Implanted Biomaterials. *Nat. Biotechnol.* **2013**, *31* (6), 507–509.

(17) Nichols, S. P.; Koh, A.; Storm, W. L.; Shin, J. H.; Schoenfisch, M. H. Biocompatible Materials for Continuous Glucose Monitoring Devices. *Chem. Rev.* **2013**, *113* (4), 2528–2549.

(18) Soto, R. J.; Hall, J. R.; Brown, M. D.; Taylor, J. B.; Schoenfisch, M. H. In Vivo Chemical Sensors: Role of Biocompatibility on Performance and Utility. *Anal. Chem.* **2017**, *89* (1), 276–299.

(19) Keeler, G. D.; Durdik, J. M.; Stenken, J. A. Localized Delivery of Dexamethasone-21-Phosphate via Microdialysis Implants in Rat Induces M(GC) Macrophage Polarization and Alters CCL2 Concentrations. *Acta Biomater.* **2015**, *12* (1), 11–20.

(20) Keeler, G. D.; Durdik, J. M.; Stenken, J. A. Effects of Delayed Delivery of Dexamethasone-21-Phosphate via Subcutaneous Microdialysis Implants on Macrophage Activation in Rats. *Acta Biomater.* **2015**, *23*, 27–37.

(21) Abraham, A. A.; Means, A. K.; Clubb, F. J.; Fei, R.; Locke, A. K.; Gacasan, E. G.; Coté, G. L.; Grunlan, M. A. Foreign Body Reaction to a Subcutaneously Implanted Self-Cleaning, Thermoresponsive Hydrogel Membrane for Glucose Biosensors. *ACS Biomater. Sci. Eng.* **2018**.

(22) Bota, P. C. S.; Collie, A. M. B.; Puolakkainen, P.; Vernon, R. B.; Sage, E. H.; Ratner, B. D.; Stayton, P. S. Biomaterial Topography Alters Healing in Vivo and Monocyte/Macrophage Activation in Vitro. *J. Biomed. Mater. Res. - Part A* **2010**, *95 A* (2), 649–657.

(23) Shukla, A.; Rasik, A. M.; Shankar, R. Nitric Oxide Inhibits Wound Collagen Synthesis. *Mol. Cell. Biochem.* **1999**, *200*, 27–33.

(24) Matsunaga, T.; Weihrauch, D. W.; Moniz, M. C.; Tessmer, J.; Warltier, D. C.; Chilian, W. M. Angiostatin Inhibits Coronary Angiogenesis during Impaired Production of Nitric Oxide. *Circulation* **2002**, *105* (18), 2185–2191.

(25) Seo, J. Y.; Yu, J. H.; Lim, J. W.; Mukaida, N.; Kim, H. Nitric Oxide-Induced IL-8 Expression Is Mediated by NF-KappaB and AP-1 in Gastric Epithelial AGS Cells. *J. Physiol. Pharmacol.* **2009**, *60 Suppl 7* (26), 101–106.

(26) Suchyta, D. J.; Schoenfisch, M. H. Anticancer Potency of Nitric Oxide-Releasing Liposomes. *RSC Adv.* **2017**, *7* (84), 53236–53246.

(27) Villalobo, A. Nitric Oxide and Cell Proliferation. *FEBS J.* **2006**, *273* (11), 2329–2344.

(28) Luo, J. D.; Chen, A. F. Nitric Oxide: A Newly Discovered Function on Wound Healing. *Acta Pharmacol. Sin.* **2005**, *26* (3), 259–264.

(29) Cooke, J. P.; Losordo, D. W. Nitric Oxide and Angiogenesis. *Circulation* **2002**, *105* (18), 2133–2135.

(30) Cao, M.; Westerhausen-Larson, A.; Niyibizi, C.; Kavalkovich, K.; Georgescu, H. I.; Rizzo, C. F.; Hebda, P. A.; Stefanovic-Racic, M.; Evans, C. H. Nitric Oxide Inhibits the Synthesis of Type-II Collagen without Altering Col2A1 MRNA Abundance: Prolyl Hydroxylase as a Possible Target. *Biochem. J.* **1997**, *324* (1), 305–310.

(31) Park, J. E.; Abrams, M. J.; Efron, P. A.; Barbul, A. Excessive Nitric Oxide Impairs Wound Collagen Accumulation. *J. Surg. Res.* **2013**, *183* (1), 487–492.

(32) Murray, P. J.; Allen, J. E.; Biswas, S. K.; Fisher, E. A.; Gilroy, D. W.; Goerdt, S.; Gordon, S.; Hamilton, J. A.; Ivashkiv, L. B.; Lawrence, T.; Locati, M.; Mantovani, A.; Martinez, F. O.; Mege, J.-L.; Mosser, D. M.; Natoli, G.; Saeij, J. P.; Schultze, J. L.; Shirey, K.; Sica, A.; Suttles, J.; Udalova, I.; van Ginderachter, J. A.; Vogel, S. N.; Wynn, T. A. Macrophage Activation and Polarization: Nomenclature and Experimental Guidelines. *Immunity* **2014**, *41* (1), 14–20.

(33) Sica, A.; Mantovani, A. Macrophage Plasticity and Polarization: In Vivo Veritas. *J. Clin. Invest.* **2012**, *122* (3), 787–795.

(34) Mosser, D. M.; Edwards, J. P. Exploring the Full Spectrum of Macrophage Activation. *Nat. Rev. Immunol.* **2008**, *8* (12), 958–969.

(35) Novak, M. T.; Yuan, F.; Reichert, W. M. Predicting Glucose Sensor Behavior in Blood Using Transport Modeling: Relative Impacts of Protein Biofouling and Cellular Metabolic Effects. *J. Diabetes Sci. Technol.* **2013**, *7* (6), 1547–1560.

(36) Novak, M. T.; Yuan, F.; Reichert, W. M. Macrophage Embedded Fibrin Gels: An in Vitro Platform for Assessing Inflammation Effects on Implantable Glucose Sensors. *Biomaterials* **2014**, *35* (36), 9563–9572.

(37) Vats, D.; Mukundan, L.; Odegaard, J. I.; Zhang, L.; Smith, K. L.; Morel, C. R.; Greaves, D. R.; Murray, P. J.; Chawla, A. Oxidative Metabolism and PGC-1β Attenuate Macrophage-Mediated Inflammation. *Cell Metab.* **2006**, *4* (1), 13–24.

(38) Palmer, C. S.; Anzinger, J. J.; Zhou, J.; Gouillou, M.; Landay, A.; Jaworowski, A.; McCune, J. M.; Crowe, S. M. Glucose Transporter 1–Expressing Proinflammatory Monocytes Are Elevated in Combination Antiretroviral Therapy–Treated and Untreated HIV+ Subjects. *J. Immunol.* **2014**, *193* (11), 5595–5603.

(39) Freemerman, A. J.; Johnson, A. R.; Sacks, G. N.; Milner, J. J.; Kirk, E. L.; Troester, M. A.; Macintyre, A. N.; Goraksha-Hicks, P.; Rathmell, J. C.; Makowski, L. Metabolic Reprogramming of Macrophages: Glucose Transporter 1 (GLUT1)-Mediated Glucose Metabolism Drives a Proinflammatory Phenotype. *J. Biol. Chem.* **2014**, *289* (11), 7884–7896.

(40) Caracciolo, G.; Palchetti, S.; Colapicchioni, V.; Digiacomo, L.; Pozzi, D.; Capriotti, A. L.; La Barbera, G.; Lagan??, A. Stealth Effect of Biomolecular Corona on Nanoparticle Uptake by Immune Cells. *Langmuir* **2015**, *31* (39), 10764–10773.

(41) Walkey, C. D.; Olsen, J. B.; Guo, H.; Emili, A.; Chan, W. C. W. Nanoparticle Size and Surface Chemistry Determine Serum Protein Adsorption and Macrophage Uptake. *J. Am. Chem. Soc.* **2012**, *134* (4), 2139–2147.

(42) Monopoli, M. P.; Walczyk, D.; Campbell, A.; Elia, G.; Lynch, I.; Baldelli Bombelli, F.; Dawson, K. A. Physical-Chemical Aspects of Protein Corona: Relevance to in Vitro and in Vivo Biological Impacts of Nanoparticles. *J. Am. Chem. Soc.* **2011**, *133* (8), 2525–2534.

(43) Hall, J. R.; Rouillard, K. R.; Suchyta, D. J.; Brown, M. D.; Ahonen, M. J. R.; Schoenfisch, M. H. Mode of Nitric Oxide Delivery Affects Antibacterial Action. *ACS Biomater. Sci. Eng.* **2020**, *6* (1), 433–441.

(44) Ren, H.; Colletta, A.; Koley, D.; Wu, J.; Xi, C.; Major, T. C.; Bartlett, R. H.; Meyerhoff, M. E. Thromboresistant/Anti-Biofilm Catheters via Electrochemically Modulated Nitric Oxide Release. *Bioelectrochemistry* **2015**, *104*, 10–16.

(45) Hofler, L.; Koley, D.; Wu, J.; Xi, C.; Meyerhoff, M. E. Electromodulated Release of Nitric Oxide through Polymer Material from Reservoir of Inorganic Nitrite Salt. *RSC Adv.* **2012**, *2*, 6765–6767.

(46) Kojima, H.; Nagano, T. Fluorescent Indicators for Nitric Oxide. *Adv. Mater.* **2000**, *12* (10), 763–765.

(47) Quehenberger, O.; Armando, A.; Dumlao, D.; Stephens, D. L.; Dennis, E. A. Lipidomics Analysis of Essential Fatty Acids in Macrophages. *Prostaglandins Leukot. Essent. Fat. Acids* **2008**, *79* (3–5), 123–129.

(48) Lehr, M. Phospholipase A2 Inhibitors in Inflammation. *Expert Opin. Ther. Pat.* **2001**, *11* (7), 1123–1136.

(49) Gilroy, D. W.; Newson, J.; Sawmynaden, P.; Willoughby, D. A.; Croxtall, J. D. A Novel Role for Phospholipase A2 Isoforms in the Checkpoint Control of Acute Inflammation. *FASEB J.* **2004**, *18* (3), 489–498.

(50) Dennis, E. A.; Norris, P. C. Eicosanoid Storm in Infection and Inflammation. *Nat. Rev. Immunol.* **2015**, *15* (8), 511–523.

(51) Tsukahara, Y.; Morisaki, T.; Horita, Y.; Torisu, M.; Tanaka, M. Phospholipase A2 Mediates Nitric Oxide Production by Alveolar Macrophages and Acute Lung Injury in Pancreatitis. *Ann. Surg.* **1999**, *229* (3), 385–392.

(52) Salvemini, D.; Settle, S. L.; Masferrer, J. L.; Seibert, K.; Currie, M. G.; Needleman, P. Regulation of Prostaglandin Production by Nitric Oxide; an in Vivo Analysis. *Br. J. Pharmacol.* **1995**, *114* (6), 1171–1178.

(53) Wang, G.; Daniel, B. M.; DeCoster, M. A. Role of Nitric Oxide in Regulating Secreted Phospholipase A2 Release from Astrocytes. *Neuroreport* **2005**, *16* (12), 1345–1350.

(54) Lee, J. W.; Mok, H. J.; Lee, D. Y.; Park, S. C.; Kim, G. S.; Lee, S. E.; Lee, Y. S.; Kim, K. P.; Kim, H. D. UPLC-QqQ/MS-Based Lipidomics Approach to Characterize Lipid Alterations in Inflammatory Macrophages. *J. Proteome Res.* **2017**, *16* (4), 1460–1469.

(55) Sorensen, M. J.; Miller, K. E.; Jorgenson, J. W.; Kennedy, R. T. Ultrahigh-Performance Capillary Liquid Chromatography-Mass Spectrometry at 35 Kpsi for Separation of Lipids. *J. Chromatogr. A* **2020**, *1611*, 460575.

(56) Ploeger, D. T. A.; Hosper, N. A.; Schipper, M.; Koerts, J. A.; Rond, S. De; Bank, R. A. Cell Plasticity in Wound Healing : Paracrine Factors of M1 / M2 Polarized Macrophages Influence the Phenotypical State of Dermal Fibroblasts. *Cell Commun. Signal.* **2013**, *11* (29), 1–17.

(57) Bogdan, C. Nitric Oxide and the Immune Response. *Nat. Immunol.* **2001**, *2* (10), 907–916.

(58) Anton, D.; Burckel, H.; Josset, E.; Noel, G. Three-Dimensional Cell Culture: A Breakthrough in Vivo. *Int. J. Mol. Sci.* **2015**, *16* (3), 5517–5527.

(59) Breslin, S.; O'Driscoll, L. Three-Dimensional Cell Culture: The Missing Link in Drug Discovery. *Drug Discov. Today* **2013**, *18* (5–6), 240–249.

(60) Chen, Z.; Yang, J.; Wu, B.; Tawil, B. A Novel Three-Dimensional Wound Healing Model. *J. Dev. Biol.* **2014**, *2* (4), 198–209.

(61) Haessler, U.; Kalinin, Y.; Swartz, M. A.; Wu, M. An Agarose-Based Microfluidic Platform with a Gradient Buffer for 3D Chemotaxis Studies. *Biomed. Microdevices* **2009**, *11* (4), 827–835.

(62) Kim, B. J.; Wu, M. Microfluidics for Mammalian Cell Chemotaxis. *Ann. Biomed. Eng.* **2012**, *40* (6), 1316–1327.

(63) Mosadegh, B.; Dabiri, B. E.; Lockett, M. R.; Derda, R.; Campbell, P.; Parker, K. K.; Whitesides, G. M. Three-Dimensional Paper-Based Model for Cardiac Ischemia. *Adv. Healthc. Mater.* **2014**, *3* (7), 1036–1043.

(64) Boyce, M. W.; Kenney, R. M.; Truong, A. S.; Lockett, M. R. Quantifying Oxygen in Paper-Based Cell Cultures with Luminescent Thin Film Sensors Young Investigators in Analytical and Bioanalytical Science. *Anal. Bioanal. Chem.* **2016**, *408* (11), 2985–2992.

(65) Kenney, R. M.; Lloyd, C. C.; Whitman, N. A.; Lockett, M. R. 3D Cellular Invasion Platforms: How Do Paper-Based Cultures Stack Up? *Chem. Commun.* **2017**, *53* (53), 7194–7210.

(66) Zakrewsky, M.; Lovejoy, K. S.; Kern, T. L.; Miller, T. E.; Le, V.; Nagy, A.; Goumas, A. M.; Iyer, R. S.; DelSesto, R. E.; Koppisch, A. T.; Fox, D. T.; Mitragotri, S. Ionic Liquids as a Class of Materials for Transdermal Delivery and Pathogen Neutralization. *Proc. Natl. Acad. Sci. U. S. A.* **2014**, *111* (37), 13313–13318.

(67) Black, A. T.; Hayden, P. J.; Casillas, R. P.; Heck, D. E.; Gerecke, D. R.; Sinko, P. J.; Laskin, D. L.; Laskin, J. D. Regulation of Hsp27 and Hsp70 Expression in Human and Mouse Skin Construct Models by Caveolae Following Exposure to the Model Sulfur Mustard Vesicant, 2-Chloroethyl Ethyl Sulfide. *Toxicol. Appl. Pharmacol.* **2011**, *253* (2), 112–120.

(68) Black, A. T.; Hayden, P. J.; Casillas, R. P.; Heck, D. E.; Gerecke, D. R.; Sinko, P. J.; Laskin, D. L.; Laskin, J. D. Expression of Proliferative and Inflammatory Markers in a Full-Thickness Human Skin Equivalent Following Exposure to the Model Sulfur Mustard Vesicant, 2-Chloroethyl Ethyl Sulfide. *Toxicol. Appl. Pharmacol.* **2010**, *249* (2), 178–187.